ROYAL SOCIETY
OF CHEMISTRY

REVIEW

Check for updates

Quantitative framework development for understanding the relationship between doping and photoelectrochemical energy conversion of TiO$_2$†

Aparna Markose, [ID] Debanita Das and Prasanth Ravindran [ID] *

Efficient energy harvesting devices are required to achieve sustainable development goals. Titania is a semiconductor that has attracted substantial research attention in pursuit of energy independence since it is an abundant, stable, toxin-free, and energy-prospective substance. Careful tailoring of morphological and electronic properties is required to address the poor conductivity of TiO$_2$ to achieve competitive Power Conversion Efficiency (PCE). Adding an optimum amount of impurity to TiO$_2$ is one of the prominent methods to increase its conductivity. This review critically analyzes doping of TiO$_2$ in light of the power conversion efficiencies of various electrochemical cells. This review suggests an alternative quantitative framework for developing and establishing the relationship between doping and photoelectrochemical energy conversion in TiO$_2$-based devices. It offers an alternative for accurate data reporting after a careful analysis of the PCE data in research articles and data reporting processes now in use. This study provides information on data analysis, visualization, and contemporary techniques for doping TiO$_2$.

1. Introduction

Titanium dioxide (titania, TiO$_2$) is a semiconductor with diverse applications in solar cells, catalysts, sunscreens, medicine, inks, wastewater treatment, water splitting, energy storage,

Nano Photonics Laboratory, Department of Green Energy Technology, UNESCO Madanjeet School of Green Energy Technologies, Pondicherry University, Pondicherry, 605014, India. E-mail: prasanth.ravindran@gmail.com

† Electronic supplementary information (ESI) available. See DOI: **https://doi.org/10.1039/d3ma00059a**

and electrochemical cells[1-4] (Fig. 1). The properties of titanium dioxide such as its wide bandgap, charge injection, extraction-favored band edge alignments, long excited electron lifetime, abundance, chemical inertness, and resistance to photocorrosion make it an excellent material for photovoltaic applications. TiO$_2$ has three natural polymorphs: anatase, rutile, and brookite (Fig. 2). Anatase and rutile have the same tetragonal structure, while brookite is orthorhombic. Even though brookite is the most stable form, anatase exhibits low recombination and superior charge transfer properties.[5-8] Employing

Aparna Markose received her Master of Physics degree from the University of Calicut, Kerala, in 2014 and received a Master of Green Energy Technology from Pondicherry University in 2019 with Distinction. She is now a Research Scholar at Madanjeet School of Green Energy Technologies, Pondicherry University. Her research interests are designing and developing hetero-structures, one-dimensional and zero-dimensional nano-systems for energy conversion.

Aparna Markose

Debanita Das is pursuing her PhD from the Indian Institute of Technology Bombay (IITB) – Monash University Joint Research Academy. She is currently studying the impact of plasmonic structures on optical sensing-based applications. She is working under the joint supervision of Prof. Anshuman Kumar (IITB) and Prof. Alison Funston (Monash University). She had completed her Master's in Green Energy Technology from Pondicherry University and graduated as a gold medalist.
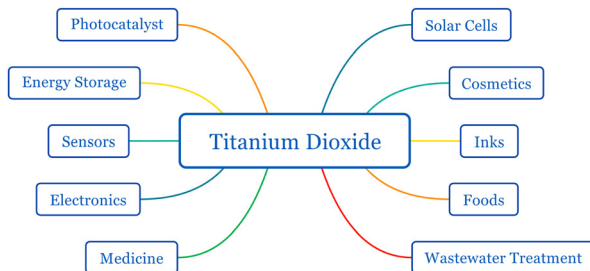
Debanita Das

Fig. 1   Applications of titanium dioxide.

titanium dioxide for photoelectrochemical conversion became a milestone in the history of dye-sensitized solar cells (DSSCs).[9] Until the discovery of Grätzel cells, DSSCs performed poorly due to their low photon absorption.[10] Other wide bandgap semiconductors such as ZnO, SnO_2, and Nb_2O_5 have been used in DSSCs instead of TiO_2.[11,12] The abundance, stable and trouble-free production of mesoporous particles, non-toxicity, stability, and apposite band alignment with popular dye N719 made TiO_2 the most suitable electrode material for DSSCs.[12]

The limitations of other organic-based solar cells have been an ongoing focus of DSSC research due to the explosive growth of the perovskite solar cell industry over the past five years. Whereas the majority of PV technologies fail to succeed, humidity, oxygen conditions, and an easy production process are favorable for DSSCs.[13] One significant benefit of DSSCs is their exceptional power production in all lighting circumstances, even indoor lighting. It has been found that under diffused or dim sunlight conditions silicon based solar cells do not perform well.[13–15] This requirement gap is satisfied by DSSCs in an efficient and competitive way. Indoor light harvesting using DSSCs even surpassed 30 percentage without co-sensitizers. For wireless sensor nodes, consumer electronics, wearable technology, and smart meters, DSSCs can be implemented indoors as portable electronic modules.[16] The potential to scale up and that to minimize production costs are key game changers in DSSC research. Because of their potential for indoor lighting, DSSCs can maximize energy efficiency while minimizing their carbon footprint.

Prasanth Ravindran

Dr. Prasanth Ravindran is professor at Madanjeet School of Green Energy Technologies, Pondicherry University. He received his PhD from the Eindhoven University of Technology, Netherlands, for the thesis entitled "Photonic switching in III–V nanostructures." He pursued his post-doctoral research at the Peter Debye Institute at Utrecht University. His current research interest is developing one-dimensional and zero-dimensional nano-systems for energy conversion.

In DSSCs, the current is generated when a dye molecule absorbs a photon and injects an electron into the semiconductor's conduction band. The circuit is completed when the dye is degenerated by the electrolyte's redox species. This electrolyte is then reduced at the counter electrode, which is usually platinum. A monolayer dye absorbs approximately 1% of the incident monochromatic light. In order to increase the photon absorption, Grätzel cells were equipped with stable dyes and high surface area TiO_2 films. These transparent, nonporous titanium dioxide films increased the absorption of incident solar energy to 46%.[18] According to Henry J. Snaith, it is possible to attain a maximum efficiency of 20.25 percent in DSSCs. Photovoltaic loss in a DSSC originates from the following (Fig. 3): (a) incomplete light harvesting, (b) inefficient electron transfer, where absorbed photons are diverted to non-injecting channels, (c) heterogeneity of dye and the semiconductor band alignment, which results in an "overpotential" to unify the electron transfer, (d) energy loss when dye relaxation causes a conformational change in the dye structure (this change causes electrons to diffuse into the oxide with lower energy), and (e) dye regeneration which causes a potential drop of around 0.3 eV, eventually leading to the most significant single loss in the DSSC. Considering these, reducing the difference between the optical bandgap of the absorber and the open circuit voltage increases the Power Conversion Efficiency (PCE).

By lowering the bandgap between the semiconductor and sensitizer, it is possible to reduce the loss in potential by a factor of 0.2 eV. When the dye is strongly coupled to TiO_2, it broadens the absorption width and rearranges the optical bandgap of the DSSC. Hence the DSSC's optical bandgap cannot be determined from the sensitizer's absorption alone. Furthermore, the optical bandgap can be estimated only from the sensitized electrode's absorption onset values.[19]

Fundamental quantities that affect the PCE are the open circuit voltage (V_{oc}), short circuit current (J_{sc}), and fill factor (FF) of DSSCs. J_{sc} depends on the charge collection efficiency of TiO_2 and the light absorption efficiency of dye. The open circuit voltage depends on the valence band (VB) of the hole transport material (HTM), the band configuration of TiO_2, and recombination inside the DSSC. The fill factor accounts for the resistive losses in the DSSC circuit. The more sophisticated and vigilant the architecture, the better the FF. It is essential to engineer the CB of TiO_2 and the CB/lowest unoccupied molecular orbital (LUMO) of the hole transport material for higher V_{oc} and improved electron injection to enhance PCE.

Device power output is determined by the TiO_2/dye/electrolyte interface's charge separation and collection. According to the detailed energetics, forward kinetic processes are light absorption, electron injection, dye regeneration and charge transport.[21–26] The thermodynamically downhill loss pathways are excited state decay to the ground state, electron recombination to dye and electron recombination to electrolyte (Fig. 3(b)). The appreciable point in here is that the efficiency of electron injection in DSSCs depends on the magnitude of these injection kinetics relative to excited state decay to the ground state. It is also noteworthy to
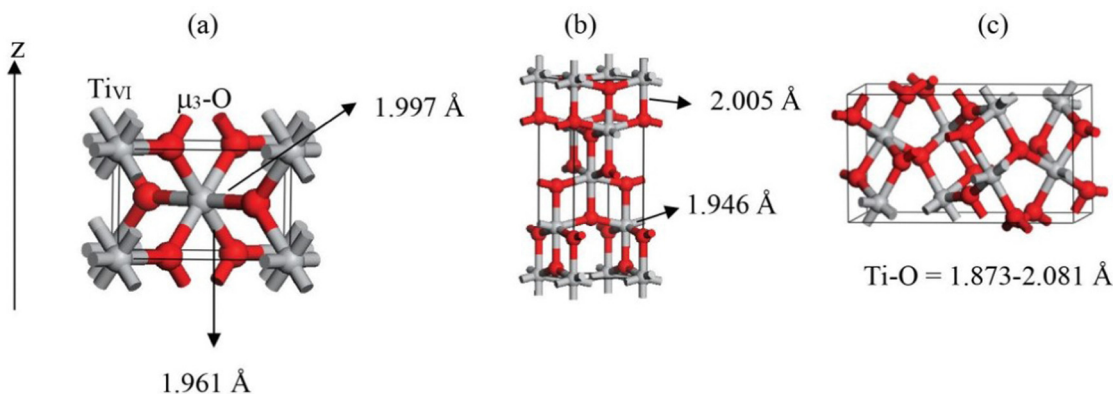
Fig. 2 Structures of TiO$_2$ natural polymorphs: (a) rutile, (b) anatase and (c) brookite.[17]
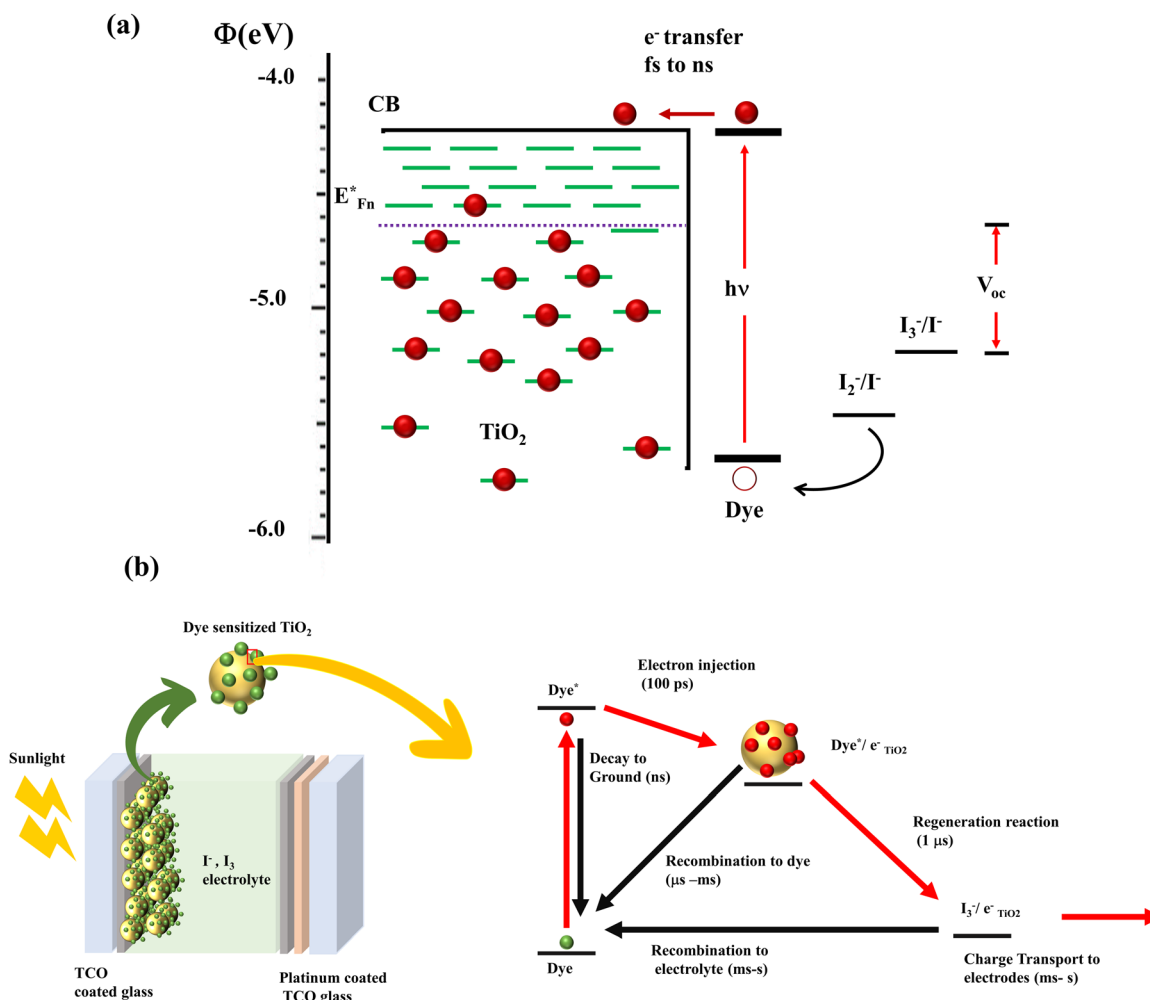

Fig. 3 (a) Illustration of the energy level of the DSSC.[20] (b) Charge transfer and recombination mechanisms involved in the DSSC.[27]

mention that fast electron injection dynamics requires strong electronic coupling of the dye LUMO to the metal oxide conduction-band states and energetically accessible TiO$_2$ density of states from the excited state of the dye. The key to achieving maximum efficiency devices lies in minimizing free energy losses, while maintaining high quantum efficiencies.[27]

The electron injection rate (k_{inj}) can be expressed as the sum of all electron transfer processes as follows:

$$k_{inj} = A \int V^2 (1 - f(E, E_F)) \rho(E) \times \exp\left\{ \frac{-\left(E^*_{-E_{ox}} + \lambda\right)^2}{4\pi\lambda k_B T} \right\} dE$$

where E is the absolute energy relative to NHE of the semiconductor acceptor state, E_{ox}^* is the redox potential of the dye excited state, $\rho(E)$ is the density of semiconductor acceptor states at energy E relative to NHE, V is the average electronic coupling between the dye excited state and different states in the semiconductor with the same energy E, $f(E,E_F)$ is the Fermi occupancy factor for each semiconductor acceptor state which can be determined from the semiconductor electron Fermi level E_F and λ is the total reorganization energy for electron injection.[28] The TiO$_2$ conduction band density of states increases exponentially in the presence of electrolyte. This exponentially increasing density is explained by the localized intraband states corresponding to the Ti^{4+} sites which reduce to Ti^{3+} when subjected to oxygen vacancies or in the presence of more electronegative impurities. The exponentially increasing DOS originates from an inhomogeneous distribution of conduction band edge energies. An example of this type of system is nanoparticle crystals showing inhomogeneous surfaces and charge.[29]

Doping plays a significant role in PCE by affecting the morphology and particle size of TiO$_2$ and changing the conduction band edge DOS. These intentional changes induced *via* doping influence the TiO$_2$–dye interaction and determine the energetics. If the doping favors the injection dynamics, the PCE increases. If the acceptor DOS potential (Semiconductor, TiO$_2$) and injection state energy (Dye excitation) potential match, there will be a three-fold increase in the injection kinetics (k_{inj}).[30–35] Surprisingly, the importance of electron injection and its influence on PCE is not considered widely. One of the reasons for this neglect is the early model systems which indicated an increase in photocurrent with increased proton/lithium concentration. The studies employing ultrafast transient absorption spectroscopy showed that the injection dynamics in N719 sensitized TiO$_2$ films was two orders of magnitude slower in the presence of typical redox electrolyte.[36–44] However, recent studies have employed time correlated single photon counting to measure injection kinetics and correlated these measurements with photocurrent. In these cases, a correlation was observed between the efficiency of electron injection and photocurrent density. These studies are in perfect agreement with IPCE data, and transient kinetic studies.[34,35,45–49]

TiO$_2$ is a natural n-type semiconductor with a 3.2 eV bandgap and an electrical resistivity of 10^{13}–10^{18} Ohm cm.[50,51] According to DOS calculations, the extreme upper end of the valence band is dominated by O 2p$_\pi$ orbitals, and the bottom of the conduction band consists of isolated Ti 3d$_{xy}$ orbitals.[52] Decreasing the resistivity of TiO$_2$ is the key to increasing the efficiency of DSSCs. Once the electron is injected, two highly undesirable yet unavoidable reactions occur in DSSCs. Injected photo-induced electrons (i) recombine with oxidized dye molecules and (ii) react with the electrolyte to produce iodide. This recombination reduces the number of electrons traveling through the designated pathways to complete the DSSC circuit; consequently, the PCE is reduced.[53] We can resolve these issues by increasing the conductivity of TiO$_2$, by improving the dye–TiO$_2$ interaction by refining the band alignment and increasing the surface area of TiO$_2$ to increase the dye loading.

The most crucial property in increasing the efficiency of a DSSC, the conductivity of TiO$_2$, depends on its carrier concentration, carrier separation, charge collection efficiency, and charge transport efficiency.[54–57] Conductivity is directly proportional to charge mobility and carrier concentration. Charge mobility indicates a carrier's ability to move through the material under an electric field. This is linked with charge transport and collection efficiency. Oxygen vacancies, titanium interstitials, and the presence of impurities and defects in the structures can improve the conductivity.[50,52,58] Introducing elements into the TiO$_2$ lattice disturbs the conduction band and forms subbands below the CB. These can be either from the formation of Ti^{3+} or from the impurity which replaced Ti^{4+}. These n type defects can increase the carrier concentration and boost the conductivity. Moreover, if electrons from deep trap states which lie in the DOS tail are freed, they will also promote conductivity.[59]

HTM and TiO$_2$ share a delicate interface in DSSCs. This heterojunction creates a space charge region, indicating an energy level difference between the CB of TiO$_2$ and HTM, causing a band bending. An external voltage that cancels out this band bending is called the flat band potential (V_{fb}). Negative shift in the existing V_{fb} will result in an upward shift of the CB and Fermi level and *vice versa*. The upward shift in the CB reduces the efficiency of electron injection. Nevertheless, an intentional impurity causing a downward shift in the CB by introducing defects makes electron injection efficient.[60] Throughout the discussion, doping is identifiable as a trivial method for increasing the conductivity of TiO$_2$, hence improving the PCE of DSSCs.

Electrodes require higher sunlight harvesting efficiency, photoelectron injection efficiency, and electron collection efficiency in order to increase PCE. The surface area and absorption coefficient of TiO$_2$ determine how effectively sunlight is captured. If doping changes the morphology and increases the surface area without altering the active TiO$_2$ mass, it can enhance PCE through light absorption. Photoelectron injection efficiency kinetics is dependent on the density of states in the conduction band. The photocurrent density fluctuates as a result of how the flat band potential influences the conduction band density. Electron collection efficiency is determined by electron transport, electron transfer resistance and electron recombination. The crystallite size of doped TiO$_2$ is connected to the density of states and electron kinetics. Throughout the review, with available data, we explain how doping affects the flat band potential and PCE. The bandgap too plays an influencing role in recombination dynamics. All the recombination pathways are connected to conduction band and surface states. Three major charge recombination pathways are direct transfer from the conduction band to electrolyte, indirect transfer from monoenergetic deep surface states, and indirect transfer from the distribution of bandgap surface states. Understanding how the bandgap changes with doping is the primary step in tackling the recombination.

Doping is an incredible way to engineer the electronic properties of materials. Since the first report of TiO$_2$ photovoltaic properties, there has been a growing trend in the research industry to
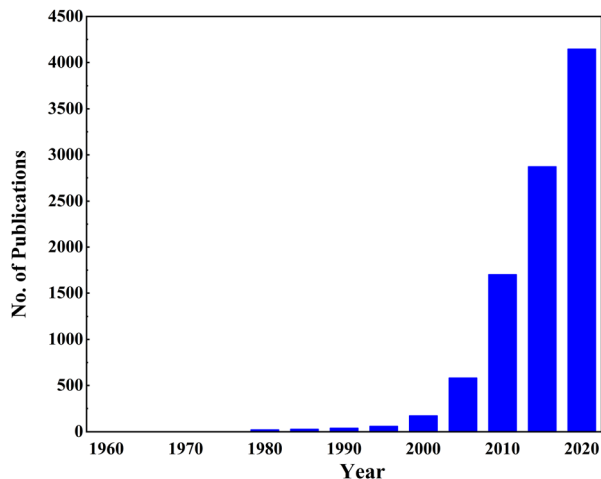
Fig. 4 Growing trend of TiO$_2$ doping (Articles published from 1960 to 2020 using the keywords "TiO$_2$" and "Doping" on the ScienceDirect website, scrutinized by checking their relevance).

increase the conductivity of TiO$_2$. Fig. 4 shows conclusive evidence for ongoing and booming research in doping TiO$_2$. Doping TiO$_2$ for improving the physical and morphological properties is well-known in solar cell research. In DSSCs, TiO$_2$ acts as a photoanode that facilitates electron transportation from the dye to the conductive oxides. This anode requires high absorbance, a reduced bandgap, and a low recombination rate for better performance. Doping affects all these properties by altering the morphology and structural properties. For example, Ag and Ni doping make TiO$_2$ more porous, and the size and shape of big particles become irregular. Also, doping creates a sponge-like structure, increasing the surface area and the efficiency of light absorption. Single doping, co-doping, doping into a composite, and growing delicate designs with doped TiO$_2$ have been tried for efficiency enhancement in DSSCs.[61]

Although TiO$_2$ is the most suitable candidate as a photoanode material in terms of abundance and non-toxicity, it is a poor conductor. Generations of researchers have doped TiO$_2$ with various elements in the periodic table. A comprehensive view is essential to understanding doping and its effect on materials properties to engineer a new material. Many reviews have been published based on doping in TiO$_2$ since the beginning of interest. There are reviews about doping of TiO$_2$ to increase the efficiency of DSSCs, the fundamental mechanisms and properties of TiO$_2$ photoanodes, and different TiO$_2$ fabrication methods.[1,62–64] In doped TiO$_2$, the cell efficiency varied with the doping strategy. Hence, this review creates a framework for analyzing the effect of doping by normalizing the increase in efficiency. Up until this point, doping has been reported as changing the DSSC output if there is a change in efficiency. However, there are errors involved in this type of analysis. When the preparation method is sophisticated, we get higher efficiency solar cells for undoped TiO$_2$.[65] Different researchers have reported different efficiencies for bare TiO$_2$-based DSSCs. This ambiguity in bare DSSCs' efficiency makes it difficult to find the effect of doping. There are undoped TiO$_2$-based DSSCs with less than 1% efficiency and above 5%.[65,66]

The efficiency of DSSCs based on undoped TiO$_2$ changed between 0.019 and 9.05%.[65–75] To understand how a dopant affects the performance of DSSCs, we need to reframe the understanding of how the Power Conversion Efficiency (PCE) changes when we add a tiny amount of dopant into TiO$_2$. This review provides a detailed summary of the effect of doping of TiO$_2$ on its photoconversion efficiency based on the performance of the DSSC. However, the trends predicted with this analysis help optimize TiO$_2$-based thin-film heterojunction solar cells and PEC hydrogen production.

Alkali metals, alkaline earth metals, transition metals, lanthanoids, post-transition metals, metalloids, non-metals, and halogen were doped into TiO$_2$ to increase the efficiency of electrochemical cells.[76–84] Elements doped into TiO$_2$ for electrochemical applications are marked in Fig. 5. This review is structured to discuss doping and co-doping separately in different electrochemical systems. Single elemental doping will be discussed based on the periodic element group-wise. Codoping is categorized into three main sections: metal doping, non-metal doping, and metal–non-metal doping. A detailed discussion of bandgap tuning, size effects with doping, and different preparation methods of doped TiO$_2$ is included. The review structure is illustrated in Fig. 6.

2. Framework for analyzing the impact of dopants in DSSCs

The impact of a dopant on the efficiency of a DSSC is estimated from the percentage increase/decrease in efficiency calculated using eqn (1):

$$\text{Enhancement of PCE} = \frac{\eta_d - \eta_b}{\eta_b} \times 100\% \qquad (1)$$

where η_d is the efficiency of the doped TiO$_2$ electrode-based DSSC/QDSSC, and η_b is the efficiency of the bare TiO$_2$-based DSSC (control cell).

Fig. 8 is obtained after calculating the percentage increase in PCE on doping TiO$_2$ with alkali and alkaline earth metal dopants using eqn (1). The analysis shows that among all the alkali and alkaline earth metals explored to date, Sr dopant has the maximum impact on the efficiency enhancement of the bare TiO$_2$ photoanode when treated with TiCl$_4$, and a scattering layer is introduced. However, if we consider only the impact of the dopant alone on a bare TiO$_2$ photoanode, then Mg and Na are the potential dopants.

3. Single elemental doping

Doping a semiconductor increases the conductivity and tunes its optical properties. Metal dopants block recombination and enhance the driving force for electron injection. They also form complexes that enhance dye binding on the surface of TiO$_2$. Hence the overall power conversion efficiency can be enhanced. TiO$_2$ is doped with various elements in the periodic table to adjust its optical and electrical characteristics. This section discusses single elemental doping on TiO$_2$ in groups. Alkali
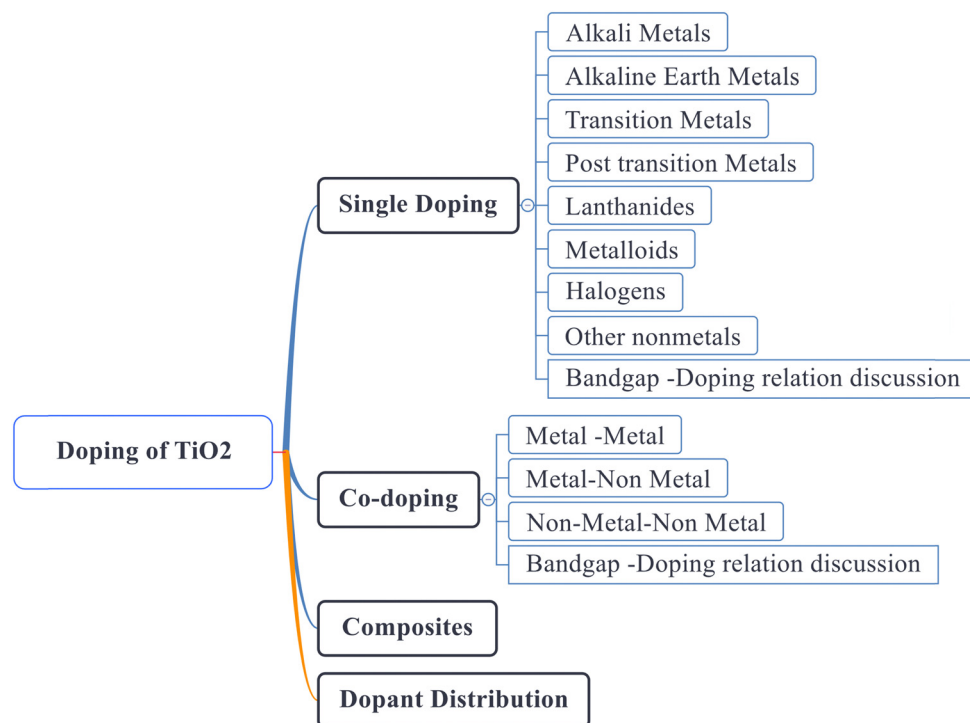
Fig. 5 Elements doped into TiO_2 included in this review.

Fig. 6 Structure of this review.

metals, alkaline earth metals, transition metals, and post-transition metals are all thoroughly discussed. Lanthanoids, metalloids, halogens, and other non-metals are also extensively investigated for doping TiO_2. The link between doping and the bandgap is examined using presented bandgap data.

3.1. Alkali metals

The alkali metal group consists of lithium, sodium, potassium, rubidium, cesium, and francium. All the elements in this group have their outermost electron in the s-orbital. Usually, these metals are all shiny, soft, and highly reactive. Among alkali

metals, sodium and lithium were doped into TiO_2 to enhance the PCE of solar cells. Table 1 lists the most recent J_{sc}, V_{oc}, and PCE data of alkali metals.

Sodium (Na). When Na is doped into the TiO_2 lattice structure, then the Ti^{4+} ions are substituted by Na^+ ions. Such substitution leads to the generation of oxygen vacancies and electrons. As a result, the electron concentration increases, increasing the conductivity. Another impact of Na dopant is that it positively shifts the flat band potential, leading to a high band gap and driving force resulting from incident photons. The enhanced device performance can also be attributed to the large surface area. However, optimizing the dopant concentration is necessary as an excess of dopant can lead to the generation of deep dopant levels or electron–hole recombination centers. Thus, it is clear that excessive dopant can increase the recombination rate, which will be the reason for the reduced percentage absorption and poor performance of the device.[68] Fig. 7(a) and (b) and Table 1 explain the position of sodium among dopants in alkali–alkaline metals.

Lithium (Li). Electron transport in liquid electrolyte is defined based on carrier diffusion due to the absence of a sizeable electronic field. This can be associated with the formation of traps. When electrons spend more transient time in traps, it will cause slow diffusion. The population of traps has a direct relation to surface area. High concentrations of Li^+ in the lattice can change the trap population and electron diffusion as well.[85] Li ions adsorbed onto TiO_2 can intercalate into the interstitial sites and result in the shifting of the TiO_2 conduction band.[86] Li doping does not increase the effectiveness of the DSSC, despite the fact that it aids in our understanding of structures and processes. A DSSC prepared with Li doped into TiO_2 performed 40% less effectively than a P25-based DSSC.[87]

3.2. Alkaline earth metals

Elements with an oxidation state of +2 and having a full outer s-orbital belong to alkaline earth metals. They have a shiny, silvery appearance. These elements usually exhibit low density, melting point, and boiling point values. Magnesium, calcium, and strontium are some potential dopant candidates that can enhance the photocurrent and efficiency of DSSCs by modifying TiO_2 electrode properties.

Magnesium (Mg). Mg is a readily available, low-cost metal dopant that can enhance the photoanode's performance. Due to the comparable atomic radii of Mg^{2+} (0.72 Å) and the Ti cation (0.64 Å), Mg^{2+} ions occupy quadrivalent Ti^{4+} sites via substitutional doping.[88] This results in a reduced e^-/h^+ pair recombination rate and an increased electrical conductivity of the Mg-doped TiO_2 photoelectrode due to the increased excited state electron injection or generation of donor levels.[88,89] Mg doping also positively impacts the flat band potential, which improves the driving force for electrons injected from the LUMO of the dye into the conduction band (CB) of TiO_2.[89] The enlarged energy difference between the LUMO of the dye and the CB of TiO_2 also plays a vital role in enhancing the short circuit current of the device. Mg doping also shifts the

Table 1 Current statistics of alkali and alkaline metal doping in TiO_2

| S. no.	Dopant	Treatment/coating	Structure	Synthesis method	V_{oc} (V)	Photocurrent density (mA cm^{-2})	FF	PCE (%)	Enhancement in PCE (%)	Bandgap (eV)	Application	Sensitizer/dye	Ref.
1	Lithium (Li)		Nanoparticles	Hydrothermal	0.655	9.81	0.358	2.5	362.96		DSSC	N719	76
2	Sodium (Na)		Nanorods	Hydrothermal	0.55	5.5	0.545	1.65	79.35		DSSC	Extract from petals of Hibiscus sabdariffa (Roselle)	68
3	Calcium (Ca)		Nanorods	Hydrothermal	0.649	19.2	0.67	8.35	13.92		DSSC	N3	96
4	Magnesium (Mg)		Thin films	Aerosol assisted chemical vapor deposition	0.74	11.99	0.67	6.1	81.55	2.8	DSSC	N719	97
5	Magnesium (Mg)		Thin films	Dip coating	0.83	3.02	0.668	1.68	12.13	2.98	DSSC	N719	90
6	Magnesium (Mg)		Nanoparticles	Hydrothermal	0.615	19.1	0.605	7.12	12.13		DSSC	N3	89
7	Magnesium (Mg)		Nanoparticles	Solvothermal	1.21	1.8	0.55	1.2	66.67		DSSC	Alkoxysilyl-coumarin dye	91
8	Magnesium (Mg)		Nanoparticles	Solvothermal microwave irradiation (SMI) technique	0.6435	16.536	0.692	7.36	190.91	3.638	DSSC	N3	88
9	Strontium (Sr)	$TiCl_4$	Nanoparticles	Chemical hydrolysis	0.78	18.53	0.66	9.57	249.27		DSSC	N719	98
10	Strontium (Sr)		Nanoparticles	Hydrothermal	0.728	17.43	0.62	7.88	12.73	3.05	DSSC		99
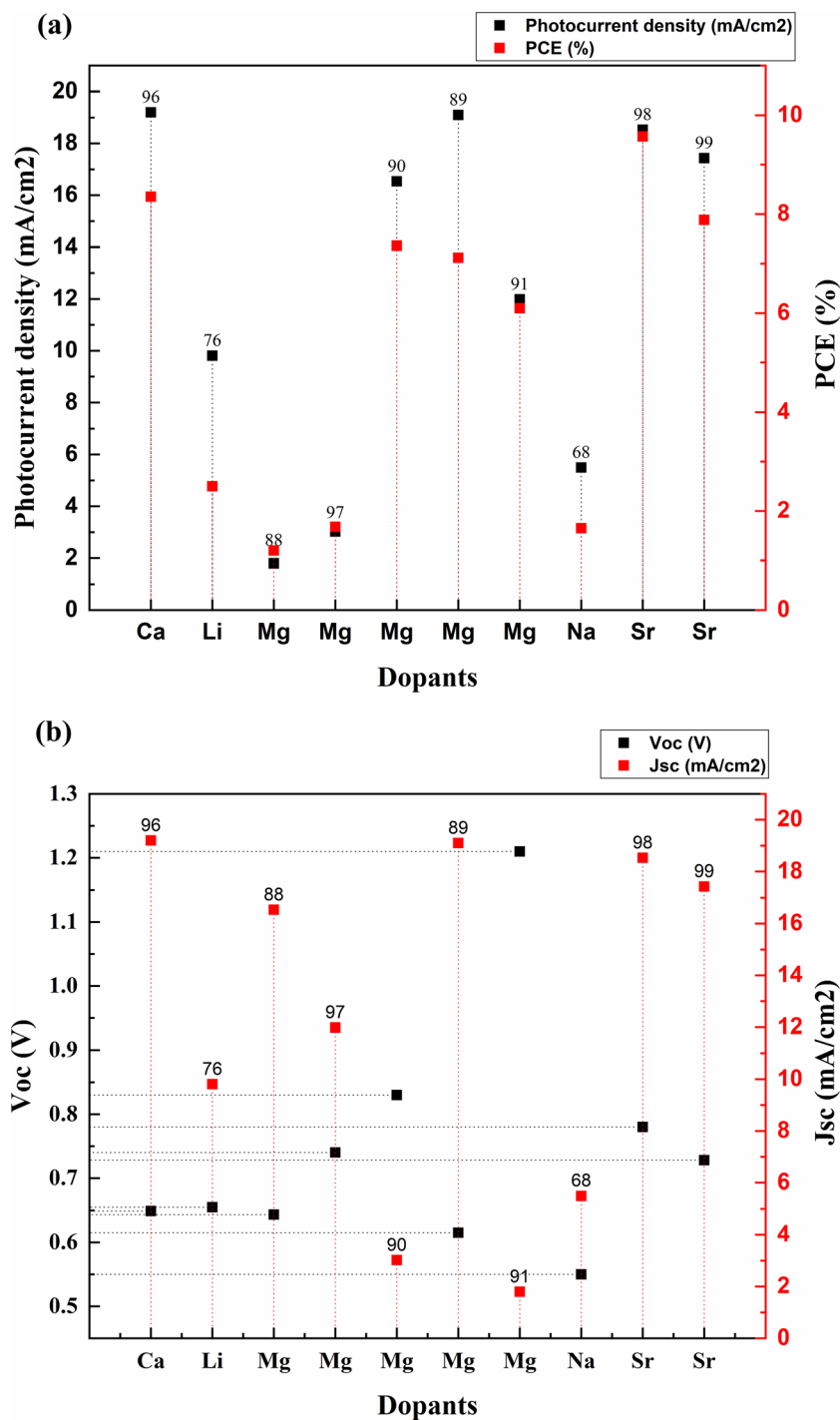
Fig. 7 (a) Performance of alkali & alkaline earth metal doped TiO_2 based DSSCs. (b) V_{oc} and J_{sc} values of alkali & alkaline earth metal doped TiO_2 based DSSCs. Data points are labelled with references.

absorption towards the visible region which is attributed to the lowering of the band gap due to the formation of another state between the O 2p VB and Ti 3d CB of the parent lattice. Mg doping increases the electron transport which improves the photocurrent density. Another work has reported a 65% increase in the efficiency of device performance on switching from single layer Mg doping to 7-layer Mg doping due to the increment in grain size and reduction in band gap.[90] Efforts must be made to

optimize the dopant concentration as higher concentrations can affect the crystal growth of the lattice and create defects which, in addition to increasing the charge recombination, also decreases the electron transport proficiency. Mg^{2+} significantly affects V_{oc}, increasing it by up to 1.2 volts.[91,92] There are works claiming that Mg doping causes a decrease in J_{sc} as well.[93]

Calcium (Ca). Doping of the TiO_2 lattice with Ca results in replacing quadrivalent Ti^{4+} with the divalent Ca^{2+} ions,
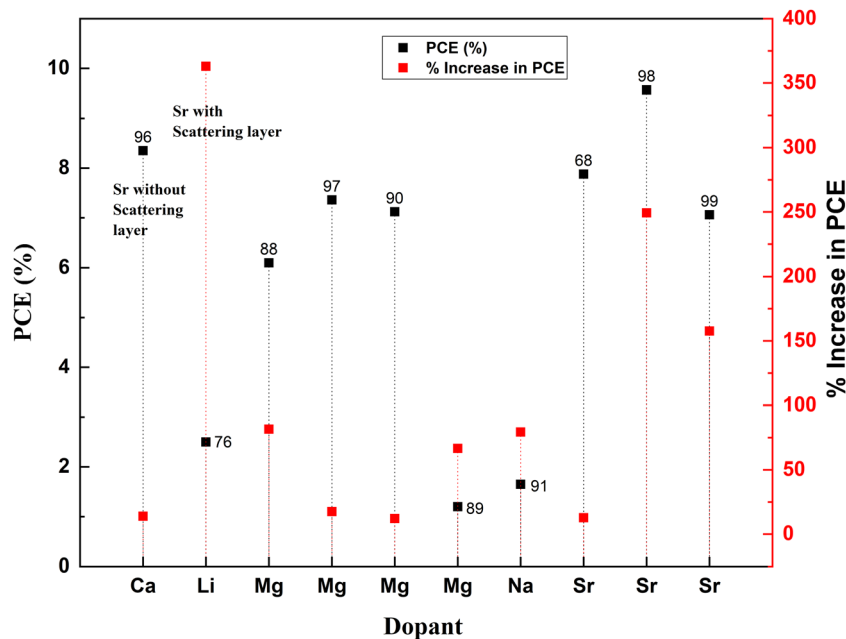
Fig. 8 Percentage increase in PCE due to alkaline and alkali metal doping. Data points are labelled with references.

resulting in oxygen deficiencies and donor levels. Ca doping is also observed to shift the flat band potential positively. These factors are responsible for enhanced electron density and electrical conductivity. Another notable impact of Ca doping is carrier relaxation. The rate of charge transport in the doped photoanode is faster than the relaxation of the excited state of the sensitizer dye. The recombination time is also higher, thereby increasing the photocurrent density. The reduction in band gap plays a significant role in shifting the absorption spectra to the visible region.[94–96]

Strontium (Sr). On increasing the concentration of Sr dopant, the crystallite size of TiO_2 is observed to reduce and cause TiO_2 lattice distortion. The local lattice distortion can be attributed to the mismatch of the sizes of the dopant Sr^{2+} ions (1.18 Å) and host Ti^{4+} ions (0.60 Å).[99] The higher ionic radius of Sr^{2+} than that of Ti^{4+} enhances the possibility of local lattice distortions due to the insertion of larger ions into the smaller lattice. Insertion of Sr in the TiO_2 lattice results in oxygen vacancy lattice defects that can trap photogenerated holes, thus prolonging the life of the photo-excited electrons and holes. This results in increased J_{sc}. The distortion of TiO_6 octahedra and the introduction of oxygen vacancies generate dipole moments. The internal polarization fields in the structure facilitate better charge separation efficiency of photogenerated electrons and holes and decrease the recombination probability. Due to the suppression of the recombination rate and the increment of the electron lifetime, the open circuit voltage of the device increases. Substitution of Ti^{4+} with Sr^{2+} has an effect on the electronic energy levels, which is supposedly near the conduction band edge, *i.e.*, Ti^{4+} 3d bands, as a result of which the band gap decreases and the absorption curve becomes red-shifted. Additionally, an optimum Sr concentration is also observed to increase the pore diameter, resulting in enhanced

dye adsorption. The narrowing of the band gap and enhanced dye adsorption facilitate better photoexcitation, thereby improving the electron density in the device.[99] Another work has reported an improved dielectric constant on adopting Sr doping. This is attributed to extrinsic and intrinsic effects like the development of Schottky barriers between semiconductor grains at insulating grain boundaries (interfacial/grain boundary effect) and the density of the samples. The work has also suggested the introduction of a light-scattering nanocrystalline TiO_2 layer due to the transparency of the $Ti_{1-x}Sr_xO_2$ film towards visible light. The $TiCl_4$ treatment can effectively prolong the charge carrier lifetime of the device, thus claiming its application for a long-term light conversion photovoltaic commercial device.[100]

3.3. Lanthanoids

Rare earth elements offer sharp and stable luminescence ideal for optoelectronic uses. Rare earth elements such as lanthanum (La),[101–103] neodymium (Nd),[80] samarium (Sm),[104,105] europium (Eu),[70] gadolinium (Gd),[106] terbium (Tb),[107] erbium (Er),[108,109] and ytterbium (Yb)[108–113] have been doped into TiO_2 to improve its optoelectronic properties.[77,80,104,107] Coupling of weakened ligands arising from 4f orbital shielding by 6s, 5p, and 5d orbitals and forbidden f–f transitions works in favor of stable and sharp luminescence for rare-earth ions. Due to their insolubility and thermal quenching, there were limitations in incorporating rare-earth ions into various semiconductors. However, combustion processing, sol–gel, hydrothermal, solvothermal and ball milling methods have made rare-earth doping possible.

Lanthanoids effectively alter the absorption range of semiconductors by enhancing visible photons' absorption. All but one lanthanide have significant chemistry associated with 4f orbital filling. 4f orbitals are effective in the adsorption of pollutants and increase photocatalysis. The 5d electronic

configuration of these ions contributes to high charge mobility and redox coupling. Lanthanoids are utilized to reduce the bandgap of TiO_2 and increase the surface area. There is an existing conflict regarding the position of lanthanum ions after doping. Some researchers claim that no rare earth elements can penetrate the TiO_2 lattice due to their larger ionic size. They tend to either be in the surface interstitial of TiO_2 or create Ti–O–La bonding on the surface. This bonding enhances the oxygen vacancies and surface area of TiO_2. Doping with rare earth elements improves the photovoltaic performance of TiO_2-based devices. However, there are also reports regarding La^{3+} located in the crystallite interstitials. This penetration can inhibit crystal growth as well.[114] The PCE performance of the Lanthanide group elements doped into TiO_2 is illustrated in Fig. 12(a) and (b). The statistics of doping and its effects are listed in Table 2.

Lanthanum (La). Doping lanthanum (La^{3+}) into TiO_2 does not change the binding energy of Ti2p peaks. This steady binding energy can be attributed to absorbed oxygen. Surface treatments with lanthanum promote its absorption into the surface of TiO_2. This absorbed oxygen counteracts oxygen vacancies and band bending effects with lanthanum co-doping. From DRS studies, it is evident that visible light photon absorption is reduced in La-doped TiO_2 in comparison with pure TiO_2. Doping La into TiO_2 distorts the O–Ti–O triad to induce oxygen vacancies. These distortion-generated oxygen vacancies act as deep and near-surface traps. These vacancies change the electron–hole interaction and thus avoid electron–hole recombination. As a result of doping, the absorption edges of the samples shifted to high-energy wavelengths and reduced visible light absorption. Oxygen vacancies generated from the doping, which act as trapping sites, increase the average free electron energy (Fermi energy) towards the conduction band edge minimum and increase the bandgap.[114–116]

Neodymium (Nd). Neodymium doping increases the surface area and reduces the pore diameter. Due to the increase in dye adsorption, a Nd-doped TiO_2 photoanode-based DSSC shows significant increases in the corresponding efficiency. Increasing the Nd-doping beyond a particular doping concentration reduces the efficiency due to the shielding of active sites. The high areal coverage by neodymium shields the TiO_2 and prohibits the absorption of photons. Additionally, excessive doping can introduce traps and defects into the TiO_2 lattice. Photogenerated electrons are trapped in defect centers, consequently inhibiting the electron transfer process, thus decreasing the photogenerated current. Nd-doped TiO_2 retained its superiority in all applications such as DSSCs, QDSSCs, and PECs. Nd doping affects the particle size and strain created in the TiO_2. The particle size decreases to a minimum and bounces back with an increase in doping both in QDSSCs (Fig. 10) and in DSSCs (Fig. 11). In this study, the change in the bandgap of TiO_2 according to the doping is portrayed perfectly (Fig. 9). Nd^{3+} doping provides additional energy states in the bandgap of TiO_2 by increasing the oxygen vacancy and enhancing the charge injection rate. This charge injection rate spike is a consequence of the higher dielectric constant exhibited by Nd doping. The 4f suborbitals of TiO_2 enabled by Nd atoms linked to the surface and reduction in oxygen vacancies.

Table 2 Current statistics of lanthanoid doping in TiO_2

| S. no.	Dopant	Structure	Synthesis method	V_{oc} (V)	Photocurrent density (mA cm^{-2})	FF	PCE (%)	Enhancement in PCE (%)	Bandgap (eV)	Application	Sensitizer/dye	Ref.
1	Europium (Eu)	Nanophosphors	Combustion and doctor blade	0.67	18.53	0.709	8.8	5.77	3.32	DSSC	N719	70
2	Europium (Eu)	Nanoparticles	Sol–gel, doctor blade	0.77	9.61	0.69	5.16	21.99		DSSC	N719	105
3	Gadolinium (Gd)	Spheres	Hydrothermal and spray pyrolysis	0.723	7.749	0.736	4.12	73.84		DSSC	N719	106
4	Gadolinium (Gd)	Mesoporous	Solvothermal	0.723	7.749	0.736	4.12	42.48		DSSC	N719	106
5	Neodymium (Nd)	Anatase	Hydrothermal	0.62	12.83	0.66	5.23	34.10	2.6	DSSC	N719	117
6	Neodymium (Nd)	Nanoparticles	Screen printing	0.78	11.5	0.683	6.15	13.89	3.2655	DSSC	N719	80
7	Samarium (Sm)	Nanoparticles	Hydrothermal	0.863	14	0.5032	6.08	72.72		DSSC	N719	104
8	Samarium (Sm)	Nanoparticles	Sol–gel, doctor blade	0.81	10.9	0.67	5.81	37.35		DSSC	N719	105
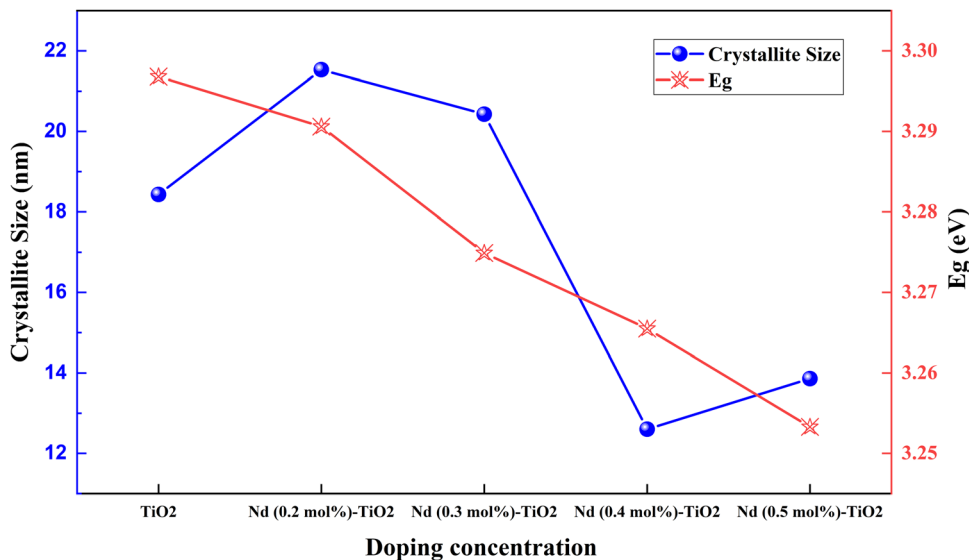
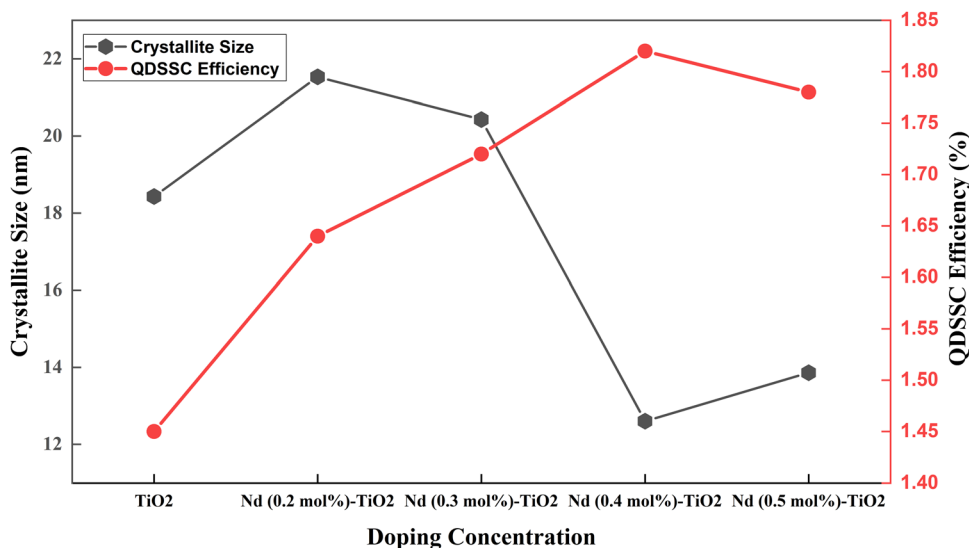**Fig. 9** Crystallite size and bandgap in Nd doped TiO_2.[117]

Fig. 10 Crystallite size and efficiency in a Nd doped TiO_2 based QDSSC.[117]

The oxygen vacancies prevent charge carrier recombination and consequently increase the charge transport.[117]

Samarium (Sm). Samarium (Sm^{3+}) doping into TiO_2 could transform the incident ultraviolet light into visible light with a down-conversion luminescence effect. The downconversion improves the utilization of sunlight and increases the ability of the dye to excite the electrons effectively. Samarium doping introduces traps into the TiO_2 photoanode. The trap density increases with the doping concentration, and some of the trapped electrons will reach the valence band and cause a nonradiative transition unfavorable to the efficiency of the cell. Samarium doping shifts the absorption edge towards a smaller wavelength. The increase in V_{oc} explains the observed increase in the band gap. Zala and coworkers claimed that a wide bandgap can make an effective energy barrier to suppress the recombination of electrons. Sm-doped photoanodes show enhanced absorption in the visible region compared with bare TiO_2 samples. Optimal doping significantly increases the efficiency and performance of doped photoanodes in the case of samarium. An increase in samarium doping concentration favors the efficiency until a particular point, and a further increase in doping decreases the efficiency.[104]

Europium (Eu). Nanophosphors synthesized through the solution combustion method with different concentrations of europium enhanced the efficiency of DSSCs. Eu^{3+} doping changed the morphology of TiO_2 from tightly packed spheres to a network of larger spheres. The porosity of the samples increased with the Eu doping concentration. These effects wear off when the doping percentage increases above a nominal range. The Eu doping decreases the defect emission in TiO_2
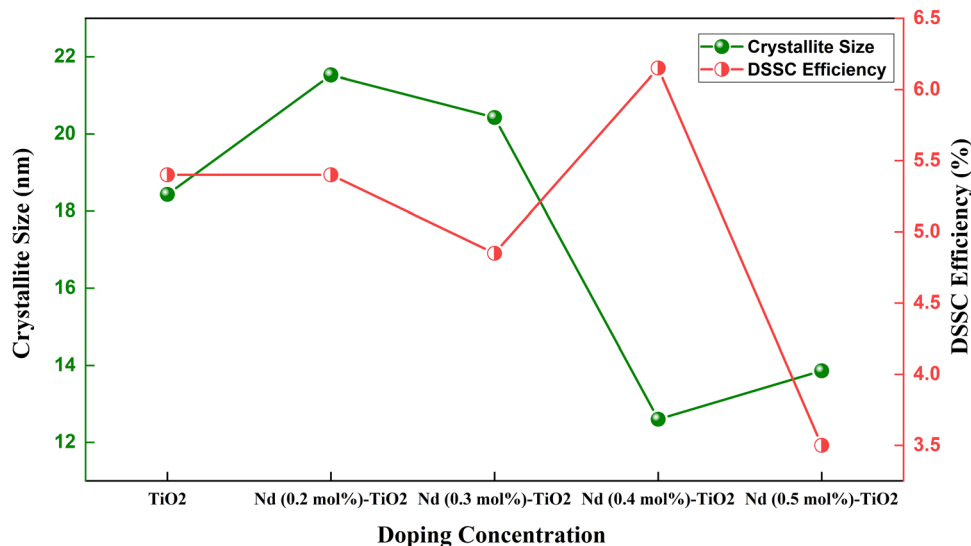
Fig. 11 Crystallite size and efficiency in a Nd doped TiO_2 based DSSC.[117]

samples. The Ti^{3+} defect level is below and the oxygen defect level is above the conduction band for TiO_2. Eu doping into TiO_2 reduces the defect emission due to their positions. Once UV radiation is absorbed, the energy is released to the defect states. Since the $^5D_0$ emitting state of Eu^{3+} ions is lower than TiO_2, the energy will be transferred to these crystal-field states of Eu^{3+}, and this energy transfer improves the PL intensity.[70,107]

Gadolinium (Gd). Gadolinium doping leads to a high surface area, interconnected nanostructures, better charge transport, and better light scattering that eventually lead to higher efficiencies in electrochemical cells, including DSSC and photo-related applications. Doping reduces the grain size of TiO_2 significantly and increases the specific surface area. Incorporating Gd in a small percentage into TiO_2 leads to elevated light absorption and shifting in absorption edge towards the red end. Gd has a half-filled 4f electronic configuration, which is stable. Compared to undoped TiO_2, Gd^{3+} doped samples exhibit higher photocatalytic degradation owing to the rearrangements in the 4f orbitals. When a Gd^{3+} ion traps an electron, this electron gets immediately transferred to an absorbed oxygen molecule to regain stability for Gd. In the case of DSSCs, this leads to the decomposition of methylene blue. Gd^{3+} ions at higher concentrations effectively become recombination centers due to the decomposition of methylene blue. However, at optimum doping concentrations, Gd^{3+} doping increases efficiency.[106]

Terbium (Tb). According to the literature, terbium isn't a particularly effective single dopant for TiO_2. Tb^{3+} doping drastically reduces the efficiency in a TiO_2 based DSSC. Tb^{3+} provides a p type doping effect by replacing Ti^{4+} with Tb^{3+} ions. This will cause an upward Fermi level shift. This shift contributes to the increment of open circuit voltage. So, whenever the Tb doping increases, the open circuit voltage increases by 6%. The Tb^{3+} doping endorses Ti^{4+} substitution, which produces excess charge and deep traps. This creates local recombination centers in the host material. These sink the electrons produced and reduce the current production. Even though there is a high

open circuit voltage production, the efficiency is reduced significantly owing to the low current efficiency. Nevertheless, co-doping TiO_2 with terbium with other rare earth elements shows excellent voltage and current output.[107]

3.4. Metalloids

Metalloids are also called semi-metals due to their mixed behavior of metals and non-metals. Boron,[118,119] antimony[120] and germanium[121] have been doped into TiO_2 for attaining better DSSC efficiencies. When doped with metalloids, it creates excess electrons in the system. Increased electron concentration will improve electron transport efficiency, enhancing photocurrent density.

Boron (B). Boron is doped into TiO_2 nanotubes to increase the efficiency of DSSCs. Doping is done *via* electrochemical anodization using a boric acid precursor. The introduction of boron into the lattice increases the electron lifetime and reduces the recombination rate. Undoubtfully, this is reflected in their high light-harvesting efficiency and short circuit photo-current density. Additionally, introduction of boron into the interstitial sites of TiO_2 contributes to the conduction band's shift.[122] The homogeneous and porous layer created by boron doping facilitates the absorption of significant amounts of dye, increasing J_{sc}.[123] Boron (B^{3+}) doping also favors the production of oxygen vacancies and conversion of Ti^{4+} into Ti^{3+}.[124,125] DFT calculations show that boron can exist either in the interstitial sites or substitutionally by replacing Ti^{4+} in the TiO_2 lattice.[119] The blue shift in the UV-vis absorption spectrum can identify boron interstitial doping.[126]

Antimony (Sb). When doped with Sb, Sb^{3+} ions are incorporated into the TiO_2 lattice. Unlike the theory, the donor density is significantly reduced when Sb is doped into TiO_2. However, IMPS measurements show that 1% Sb doped samples show faster electron transport, contributing to higher J_{sc} values. A positive shift in the flat band potential of TiO_2 increases the energy gap between the LUMO of dye and the conduction band
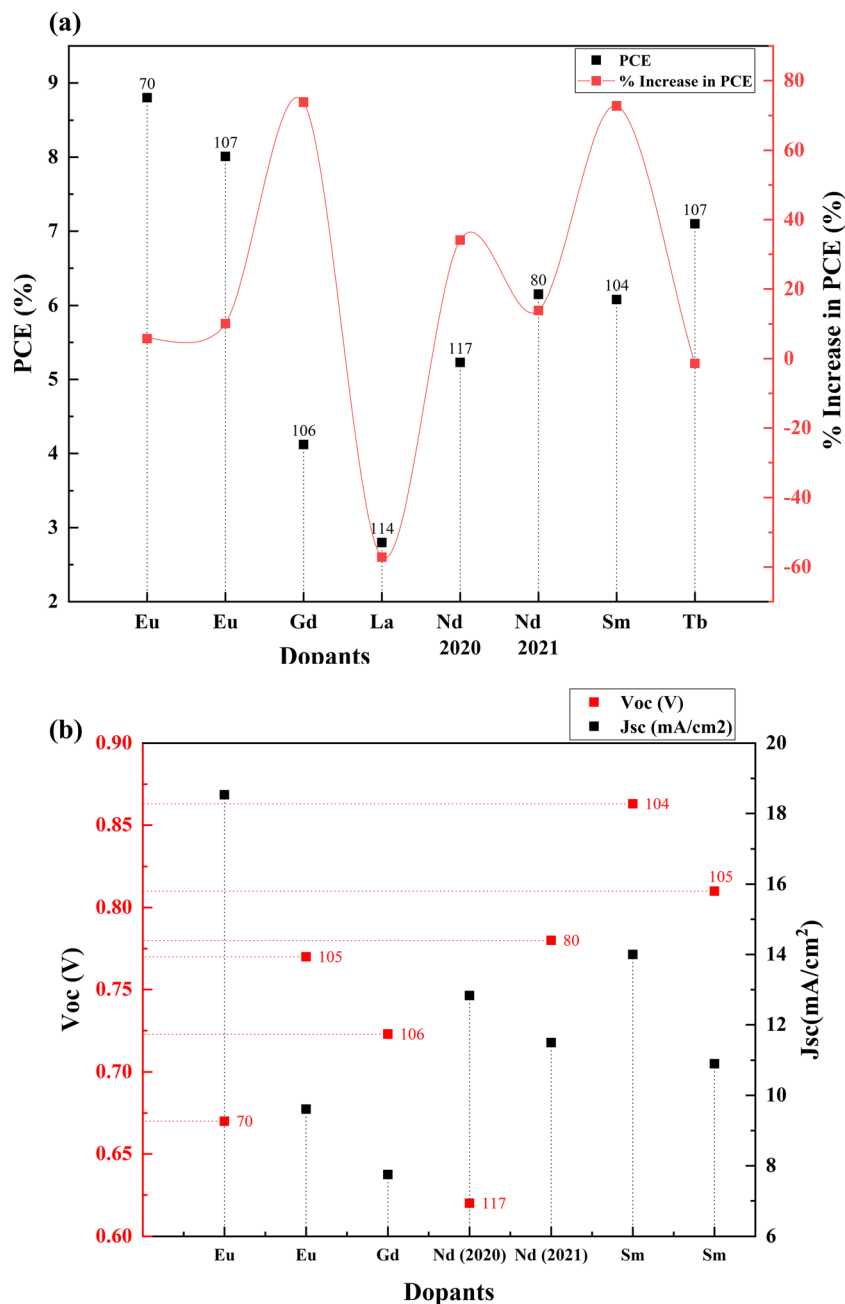
Fig. 12 (a) Percentage increase in PCE with lanthanide doping. (b) V_{oc} and J_{sc} values of lanthanoid doped TiO_2 based DSSCs. Data points are labelled with references.

of TiO_2. This increase in energy gap results in increased injection driving force and improves the electron injection from the LUMO of the dye to the conduction band of TiO_2. Sb doping also follows the trend like other doping methods under study that increase the efficiency to optimum doping and decrease. We can see the doping percentage–efficiency trend in Fig. 13.[120]

3.5. Transition metals

Transition metals are the largest set of cation providers in the periodic table. These elements have a partially filled d subshell or can provide cations with an incomplete d subshell. Transition

metals provide a large pool of complex ions with various oxidation states. Doping TiO_2 with transition metals creates additional energy levels in the CB due to the aforementioned partially filled d-orbits. This section discusses the effects of doping these elements into TiO_2 such as scandium,[127] vanadium,[128] chromium,[129,130] manganese,[131–133] iron,[134] cobalt,[135] nickel,[136] copper,[137–139] zinc,[140] yttrium,[141] zirconium,[78] niobium,[142] silver,[143] cadmium,[144] tantalum,[145] and tungsten.[146]

Scandium (Sc). On doping TiO_2 with Sc, the Ti^{4+} sites are found to be substituted by Sc^{3+}. This particular substitution positively affects atomic disorder (morphological alterations
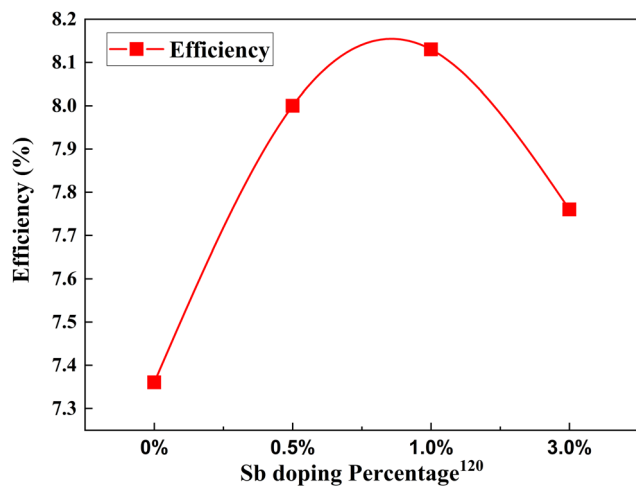
Materials Advances

View Article Online

Fig. 13   Change in PCE with Sb doping concentration.[120]

such as size and pore size distribution and deformation of the tetragonal lattice) and electronic disorder. The holes generated in the valence band counterbalance the donor levels evolving from the oxygen vacancies of anatase, resulting in a reduction of the energy difference between the conduction band and the LUMO level of the dye, in contrast to W doping. The reduction of the energy difference implies a reduction in the rate of electron injection. Sc doping does not have any positive impact on carrier density. The bandgap varies linearly with Sc concentration on TiO_2. The atomic disorder plays a vital role in governing the transport properties within the semiconductor layer. At an optimum concentration of 0.2 at% Sc, the photocurrent density increases due to the enhancement of electron lifetime. However, beyond this concentration, the transport rate suffers a detrimental impact, leading to a decrease in the photocurrent density. In summary, an increase in Sc concentration can have three effects – an increase in flat band energy and electron lifetime and a reduction in transport rate. In contrast to the expectation, the open circuit voltage decreases due to the voltage drop due to series resistance.[127]

The electron lifetime increases with the substitution of Ti^{4+} with trivalent ions such as Y^{3+} and Ga^{3+} but the transport rate decreases. In the VB group of the periodic table, as we move from top to down, the current increases (due to the increase in the concentration of carriers and reduction in film resistance), while the voltage decreases (due to the faster recombination of electrons and reduction of the energy difference between the flat band potential and the I^{3-}/I^- redox potential). Nb doping is more beneficial among the group VB elements. Group VB elements also improve the electron transport rate, improving the charge collection efficiency. The bandgap undergoes redshift, and there is also an increment in visible light absorption.

Vanadium (V). The advantage of using V is that it can extend the light absorption edge from the UV region to visible region of the TiO_2 semiconductor and increase the carrier lifetime. The increase in visible absorption and photogenerated e^-/h^+ is attributed to two facts: (1) the ionic radii of V are much close to Ti and (2) the tetragonal crystal structure of VO_2 is similar to

that of TiO_2. The positive shift of the flat band potential resulting from doping with V improves the driving force for injecting electrons from the LUMO of the dye to the conduction band of TiO_2 and the photocurrent. Charge transport was also seen to increase on doping with V. Since V has one electron more than Ti(IV), a donor level was created, which can increase the concentration of the carriers in the V doped TiO_2 material, which results in reduction in the film resistance.[145] In a different work, V is integrated into high surface area porous TiO_2. Lowering the cell's internal resistance increased the conductivity of TiO_2. Additionally, it offered higher chemical stability and improved electron transport compared to the undoped TiO_2.[147]

Chromium (Cr). The similar cationic radii of Cr^{3+} (0.755 Å) and Ti^{4+} (0.745 Å) have made Cr^{3+} a suitable dopant candidate, ensuring insertion of Cr^{3+} into the TiO_2 without damaging the structure, but causing a slight expansion. Cr doping reduces Ti^{4+} to Ti^{3+} by replacing Ti^{4+}.[148] Ti^{3+} states and oxygen vacancies have suppressed the recombination rate of electron–hole pairs. The oxygen vacancies are also referred to as hole-trapping defects. The generation of oxygen vacancies leads to the trapping of the positive carriers, thus making the carriers less mobile than usual. This results in electron mobility improvement and hence reduces charge recombination. This results in the improvement of the photocurrent efficiency of the device. Due to the different oxidation states, Cr can induce multiple mid-gap energy levels that modify the electronic properties of TiO_2. Cr doping decreases the bandgap energy owing to the formation of Ti^{3+} states and oxygen vacancies. Cr doping also enhances dye adsorption owing to the better binding of the dopant ions and dye molecules. Cr doping enhances the photocurrent density, which is attributed to the formation of mid-gap states. The mid-gap states reduce the movement of photoelectrons to the valence band, reduce the recombination with the oxidized state of dye and therefore strengthen the lifetime of electrons.[149,150]

Manganese (Mn). The ionic radius of Mn^{2+} (0.67 Å) almost equal to that of Ti^{4+} (0.605 Å) makes Mn a suitable dopant. Owing to the minimum difference between the ionic radii of Mn^{2+} and Ti^{4+}, Mn^{2+} doping is more prone to agglomeration. The doping mechanism can follow any of the following routes – exchange of parent ions with dopant ions, insertion of dopants into the interstitial sites of the parent lattice or surface doping of the parent lattice. Within a low level of Mn doping, the crystallinity of the parent lattice can be improved by increasing the amount of doping. Mn doping has been observed to follow the route of replacing Ti ions at the interstitial sites of the lattice. Contrary to the general perception of TiO_2 growth inhibition on doping, Mn doping increases the crystallite size. An increase in crystallite size can negatively impact efficiency due to the decrease in the surface area of the photoanode available for dye adsorption. Another suitable impact of Mn doping is the decrease in the bandgap for undoped TiO_2 crystals. Such a property can be attributed to the formation of impurity states between the conduction and valence bands of TiO_2. Additionally, the sp–d interaction between the band electrons of TiO_2 and localized dopant d cations is also responsible for the decrease in the band gap. The trap states induced by doping also influence the recombination process in

DSSCs, which can negatively impact efficiency. Therefore, an optimum doping concentration is required to determine the achievable PCE. It has been observed that the structural impact is more dominant than the recombination with high Mn doping on the device's efficiency.[151]

Iron (Fe). Fe doping increases the crystalite size of the TiO_2 lattice structure, resulting in decreased dye adsorption. Fe doping leads to the generation of Ti^{3+} trap states and induces band edge shift. The Ti^{3+} population is a result of the substitution of Ti^{4+} with Fe^{3+}. Creation of Ti^{3+} states and oxygen vacancies at deep levels increases electron density and causes a downshift in the quasi-Fermi level. The trap states act as photoactive sites facilitating electron transport *via* hopping and trapping/de-trapping events. Fe doping is observed to introduce lower defect concentration than Cu doping but higher defect concentration than Sn doping.[152] Fe doping also facilitates an increase in surface-hole concentration, a broad absorption peak and fast transient decay, thus resulting in poor current density at 430 nm compared to a Sn-doped, Cu-doped or undoped TiO_2 lattice. Compared to Cu and Sn, Fe doped TiO_2 photoanodes undergo faster recombination of injected electrons with surface holes, thereby leading to poor performance of the device. Fe doping induces an increase in oxygen vacancies and a reduction in the crystallite size of the TiO_2 lattice structure. The oxygen vacancies lead to defect concentrations of trapped holes. This results in trapped free electrons at sub-energy states (Fe^{2+}, Fe^{4+}, *etc.*) in the conduction band being quickly excited to the Ti^{4+} conduction band, causing higher absorbance. The oxygen vacancies also cause d–d transition within the distorted geometry of the transition metals, resulting in longer lives of excited states in Fe-doped TiO_2 photoanodes. The longer lifetime of excited states can prove detrimental to the device due to recombination. Fe doping has shown less photoelectric conversion efficiency relative to undoped TiO_2.[153,154] Fe-doped TiO_2 samples can be more beneficial for the near-visible photocatalytic reduction process due to their characteristic fast rate of decay of transient absorption kinetics at 430 nm.[154] This fast rate of decay is attributed to the increased concentration of holes in the doped sample. Recombination at the surface states of oxides plays a dominant role in deciding the cell performance with the Fe doped TiO_2 photoanode. Fe doping must be done with caution because excessive Fe^{3+} doping changes n type TiO_2 into p type TiO_2.[155]

Cobalt (Co). Co doping decreases TiO_2 lattice size attributed to the hindrance of the crystal growth of TiO_2 nanoparticles. The reduced size implies the availability of more surface area for dye adsorption. M. I. Khan reported the influence of using stacked Co doped TiO_2 multilayer thin films.[156] The exciting result of the work is the phase transformation of anatase TiO_2 to brookite TiO_2 on the introduction of multilayer thin films. Also, using a multilayer of Co doped TiO_2 films shifts the absorption spectra to the visible range due to the d–d electronic transition of Co^{2+} in octahedral coordination. Codoping also decreases the bandgap due to the formation of impurity states in the forbidden bandgap of TiO_2. Increasing layers also increases free carrier concentrations and decreases the

multilayer film's resistivity. However, an optimal number of layers must be decided to prevent internal resistance obtained from the increment in thickness.

Nickel (Ni). Ni doping increases the crystallite size of the parent TiO_2 lattice, which can be due to the insertion of Ni ions into the lattice. The increase in size is detrimental to the dye's adsorption capacity due to the reduced surface area. Counter to this effect, the decrease in bandgap induced by Ni doping in the TiO_2 structure results in little increase in the performance of cells.[140,157] Doping Ni into TiO_2 nanowires can enhance charge mobility. EIS studies of Ni-doped samples confirm lower charge transport resistance and reduced charge recombination. When Ni^{2+} replaces Ti^{4+}, the crystallinity is improved, and certain surface trap states are partially eliminated.[136,158]

Copper (Cu). The size similarity of the ionic radius of Cu^{2+} (0.73 Å) with that of Ti^{4+} (0.605 Å) has grasped attention among researchers to explore its suitability as a dopant. Cu doping is less likely to form agglomeration in the structure than other dopants like Mn.[151] With 1% and 2% Cu doping, there is a probability of the formation of CuO on the lattice. Cu doping can lead to an increase in the crystallite size.[151,159] Such a condition suggests the inclusion of Cu either at the interstitial site or on the surface of the anatase TiO_2 crystals. The formation of additional states between the conduction band and valence band of TiO_2 and the sp–d interaction between the band electrons of TiO_2 and localized dopant d cations decrease the bandgap and improve the optical response. The introduction of trap states impacts the bandgap in addition to the recombination process. Therefore, an optimum doping concentration is highly recommended to balance the positive and negative impacts of trap states. K. Sahu *et al.* reported an increment in V_{oc} from 714 to 781 mV with increased Cu doping. The Cu doping facilitates the space charge region owing to increased structural disorder. This increases the conduction band edge of TiO_2 and the upward shift of the Fermi level. Another significant impact of the shift of the Fermi level towards the conduction band edge is a decrease in electron injection efficiency from the dye into TiO_2 and thus a loss in current. Compared to Mn doped TiO_2 photoanodes, Cu doped TiO_2 photoanodes have lower electron lifetimes.[151] Another vital feature of Cu is its localized surface plasmon resonance (LSPR). The LSPR effect enhances the light absorption proficiency of dye molecules and boosts the separation of carriers by inducing a collective oscillation of metal free electrons at resonance. The LSPR effect induces a strong electromagnetic field around Cu nanoparticles, facilitating their interaction with dye molecules. This results in the effective resonant energy transfer between the excited state of the dye and surface plasmons.[151] Cu doping is responsible for increasing the light-harvesting efficiency of the dye sensitizer by enhancing the far-field scattering, inducing charge separation, or increasing near-field local surface plasmons. Another work[154] compared the concentration of defects introduced on TiO_2 and reported that it was in the order – Cu doped TiO_2 > Fe doped TiO_2 > Sn doped TiO_2 > pure TiO_2. The work also reported that the lower the oxidation number of the dopant, the more significant the broadening of the fundamental vibration modes
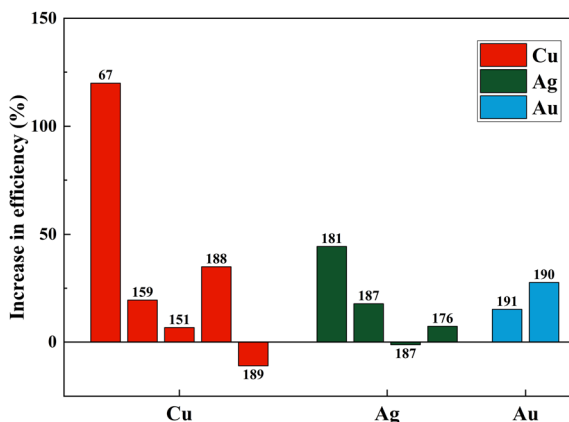
Fig. 14 Impact of the plasmonic behavior on percentage increase in efficiency (note: Au is used only as composites). Data points are labelled with references.

(Eg_1) in Raman peaks and the greater the generation of oxygen vacancies. Cu^{2+} leads to the generation of Ti^{3+} states due to the availability of more oxygen vacancies. At the oxygen deficient sites, trapped free electrons facilitate charge equilibrium, enhancing the electron density of states and increasing the light absorption. R. T. Ako *et al.* suggested that the significant factor for choosing a metal dopant for the photocatalytic or photovoltaic device should be governed by the elevation of surface free energy states of photoanodes rather than bulk defect generation. In view of this, their work concluded that the bulk defects in Cu doped TiO_2 can also lead to reduced electron density due to the electron–hole recombination. Along with Cu, the plasmonic behavior of Ag and Au also affects PCE, as illustrated in Fig. 14.

Zinc (Zn. The comparable ionic radii of Zn^{2+} (0.74 Å) and Ti^{+4} (0.75 Å) make Zn^{2+} the most effective choice among all the transition metals. Due to this, Zn^{2+} can easily substitute Ti^{4+} without altering the TiO_2 crystal structure.[160] Zn doping also decreases the bandgap due to the creation of energy bands between the bandgap of TiO_2. Zn doping also creates pores on the surface film. The porous structure aids dye adsorption and provides a high volume ratio for incrementing charge collection and transportation efficiency on the surfaces of $Zn–TiO_2$ thin films.[161–164] $Zn–TiO_2$ exhibits suitable photocatalytic properties owing to its porous surface and introduction of conductive channels. The increment in short circuit current density can be attributed to the improvement in the incident light harvesting, enhancement in conductivity due to the generation of more electron–hole pairs, reduction in internal resistance, and reduction of electron traps.[74]

Yttrium (Y). Y(III) contains one 4d occupied orbital and can quickly produce several electron configurations.[165] The larger ionic radius of Y^{3+} (0.90 Å) relative to the Ti^{4+} radius (0.61 Å) prevents the easy penetration of Y into the TiO_2 lattice. The effect of Y doping on the crystallite size is reported differently by different research groups. For easy penetration into a porous film, X. Qu *et al.* reported the fusing yttrium nitrate solution and observed that Y_2O_3 covered the surface of TiO_2 or, if

annealed, formed the sub-grains among grain boundaries.[166] A. K. Chandiran *et al.* reported the shrinkage of crystallite size along [001] on Y doping and suggested the accommodation of Y^{3+} at the interstitial site of TiO_2.[141] B. Zhao *et al.* reported the expansion of the TiO_2 lattice by incorporating Y^{3+}.[165] Such an increment in specific surface area and pore volume helps more extensive dye loading. Such structures can enhance light harvesting capability by increasing the number of excited electrons. When dopant levels of Y-doped anatase TiO_2 are created near the conduction band, the f electrons from Y^{3+} are transferred to the conduction or valence band of TiO_2. This results in a lowering of optical bandgap energy compared to pristine TiO_2. The increased conductivity of the TiO_2 lattice on Y doping can be attributed to the introduction of a point defect. Low electrical resistance is another side effect of moderate trivalent dopant concentration, which prolongs the effects of in-Y doping on the short-circuit current and fill factor while barely affecting the photovoltage. It has also been reported that Y substitution has a negligible impact on the energy distribution and density of the trap states available below the conduction band.[141] The formation of the Ti–O–Y complex can lead to the generation of charge imbalance of the lattice. To compensate for the charge imbalance, more recombination of –OH with –COOH radicals can occur when more –OH radicals are absorbed. This results in the improvement of dye loading capacity.

Zirconium (Zr). Similar to titanium, Zr is a quadrivalent element with a slightly larger cation radius. This suggests that Zr doping can either replace Ti^{4+} or locate in the interstitial sites. Introducing Zr in TiO_2 reduces the crystallite size and increases the porosity of Zr-doped TiO_2 electrodes, enhancing the dye adsorption capacity. The decrease in crystallite size on Zr doping is attributed to the segregation of Zr^{4+} in the grain boundaries of anatase titania grains, implying the location of Zr^{4+} at interstitial locations. The negative impact of a highly porous structure on Zr doping can deteriorate the cell performance. Large porous structures can act as electron traps and can be associated with the depth of traps that participate in the electron motion, affecting the diffusion coefficient value. Thus, an optimum porosity is highly required, implying an optimum doping concentration of Zr.

Another exciting feature of Zr doping is that this transition metal accelerates the anatase to rutile transformation.[167] Doping of anatase with elements have valency smaller than 4^+ provides a charge compensation by forming vacancies, amplifying the ionic transport in anatase, thereby increasing the anatase to rutile transformation. However, ions with a valence higher than 4^+ form Ti^{3+} cations and hinder the change. This high rutile content for Zr-doped TiO_2 also leads to a slighter difference between the Fermi level and the redox potential of the electrolyte. A recent research study reported that Zr-doped TiO_2 exhibits the lowest bandgap relative to Fe-doped, Ni-doped, and undoped TiO_2. It also suggests that Zr gets doped into TiO_2 on the surface and inside the lattice.[72] Zr transition metal doping can improve photocatalytic performance at higher rates. The decrease in bandgap implies that it enhances the light absorption capacity of the electrode. A decreasing trend in the V_{oc} can also be

observed at a higher level of Zr concentration, suggesting an increase in recombination processes.

Niobium (Nb). The most extensively researched dopant for TiO$_2$ is niobium, which is incredibly promising for DSSCs. Because of its superior optical and electrical properties, it is an ideal dopant for TiO$_2$ in photovoltaic applications.[56,168–170] XPS analysis reveals the shift of the Fermi level away from the conduction band minimum (CBM) for low Nb content attributed to the passivation of oxygen vacancies at the surfaces of the TiO$_2$ nanoparticles but towards the CBM for high Nb content. T. Nikolay *et al.* reported that the inclusion of Nb inhibits the formation of rutile phase TiO$_2$ while supporting the growth of the anatase phase of TiO$_2$.[171] Low Nb doping leads to a slight shift of Fermi energy and a decrease in the concentration of oxygen vacancies on the TiO$_2$ surface. The passivation of oxygen vacancies by Nb available at the surface site of the lattice occurs because of the attraction between oxygen and Nb. The dangling bonds of the attracted oxygen neutralize the donor defects of Nb. This results in the suppression of recombination at the sturdy junction of the TiO$_2$/electrolyte interface due to the widening of the space charge region. This also plays a vital role in enhancing the open circuit voltage for low Nb doping levels. Nb doping has been seen to lower the CBM relative to the undoped sample which can impact the electron injection from the dye to the conduction band of TiO$_2$.

The optimum amount of Nb dopant results in the substitution of Ti^{4+} with Nb^{5+} so that the Ti^{3+} 3d^1 and Nb^{5+} 4d^0 levels exist in the nanostructure, resulting in the formation of intraband states in the structure. This improves the charge transport and driving force for electron injection from the dye to the TiO$_2$ conduction band.[171,172] Also, the Ti 3d orbital has one excess electron for each Nb^{5+} substitution, thus implying that an increase in electron concentration improves electron conductivity. Such improvements in electron conductivity and increment of electron injection induced by the positive shift of the CBM enhance J_{sc} in addition to incident photon-to-current conversion efficiency, and the suppression of surface recombination at the TiO$_2$/electrolyte interface along with a shift in Fermi energy results in the influence of V_{oc}. Doping TiO$_2$ with Nb also results in the decrease in bandgap. H. Su *et al.* demonstrated the long-term stability of Nb doped photovoltaic devices by a 1200 h-aging test.[142] The group showed a 10–20% improvement in efficiency and J_{sc} of Nb doped cells relative to undoped cells. Fig. 15 illustrates the influence of Nb doping on the average size of TiO$_2$ nanoparticles. Similarly, Fig. 16 shows the variation of V_{oc}, J_{sc}, FF, and efficiency with time of the Nb-doped TiO$_2$-based DSSCs.

Nb loading influences the parent structure's morphology, pore volume, and porosity. Parameters like J_{sc}, V_{oc}, and FF determine the photoelectron conversion efficiency. To achieve higher efficiency, the primary requirements are higher J_{sc} and larger V_{oc}. J_{sc} can be determined by factors listed below:

(1) Sunlight harvesting efficiency – it is directly related to the surface area of photoanode structures that determines light scattering and dye adsorption abilities. Low Nb doping was found to be suitable for utilizing solar light effectively. However, the absorbance property was reduced, implying a reduction in
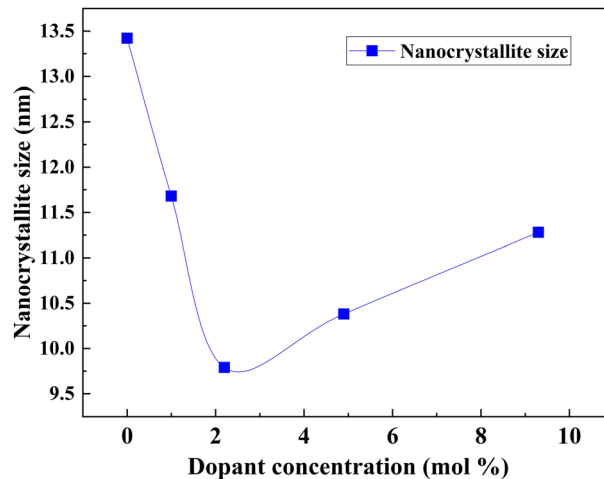

Fig. 15 Influence of Nb doping on the average size of TiO$_2$ nanoparticles.[173]
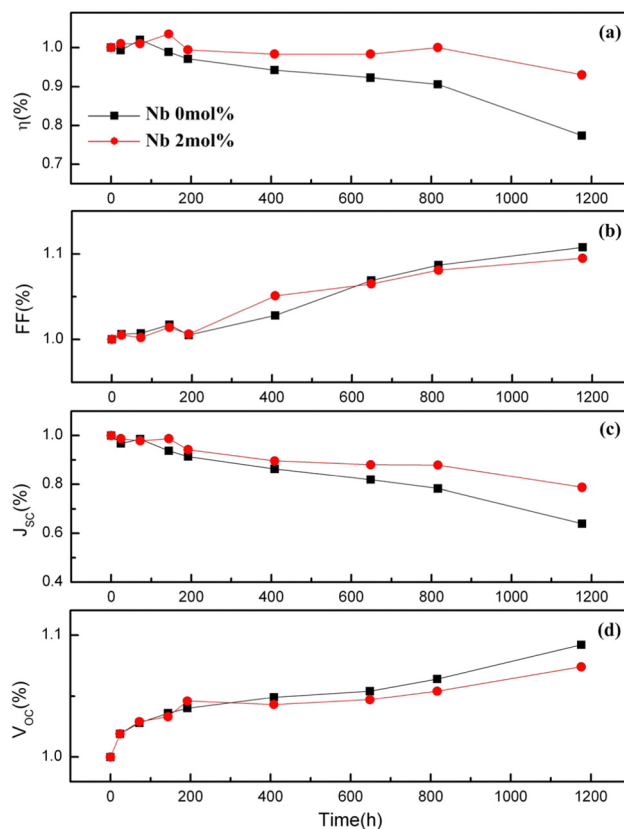

Fig. 16 Variation of V_{oc}, J_{sc}, FF and efficiency with time for Nb doped DSSCs. Reproduced from ref. 142 with permission from Elsevier.[142]

surface area. With high doping, in addition to the reduction in light scattering, the structure also suffered from the reduction of dye adsorption. Thus, it has been concluded[138] that the enhanced conversion efficiency should not be determined by morphological modification of Nb-doped TiO$_2$ composite structures.

(2) Photoelectron injection efficiency – with the increase in Nb dopant, the flat band potential (V_{fb}) exhibited a positive
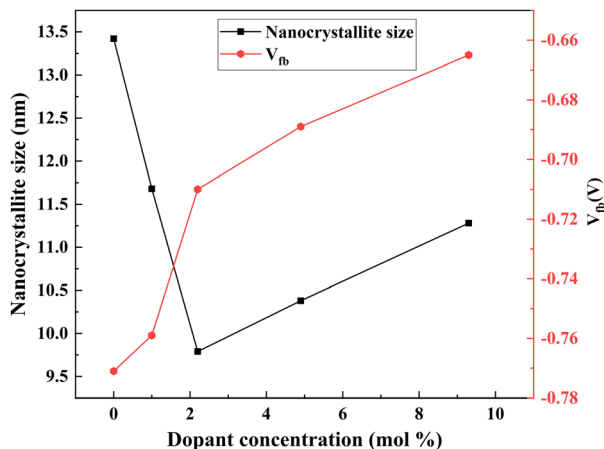
Fig. 17 Nb dopant crystallite size and V_{fb}.[138]

shift, implying an increase in photoelectron injection (Fig. 17). The active and easy electron injection resulted in an improvement in photocurrent density. The shape and defect of the structure influence the V_{fb}. A smaller size might induce a positive shift of V_{fb}, thus increasing the photoelectron injection efficiency.

(3) Electron collection efficiency – it is determined by the electron transport ability, electron transfer resistance, and electron recombination resistance. Thorough experiments are required to determine optimal doping to attain maximum electron collection efficiency (Fig. 18).

Another work reported the use of a blocking layer along with a Nb-doped TiO$_2$ photoanode structure.[174] DSSCs with a blocking layer exhibited pronounced increments in V_{oc} and J_{sc}, which is attributed to the suppression of the electron recombination process. The advantage of using a blocking layer is that it

prevents backward electron transfer at the FTO/electrolyte interface. An alternative study focusing on annealing revealed an increase in efficiency when annealing was followed by H$_2$O$_2$ treatment.[175] Fig. 19 shows how the PCE of DSSCs using Ti–Nb photoanodes with and without H$_2$O$_2$ treatment after annealing under different conditions and the corresponding improvement in efficiency percentage of Ti–Nb compared to Ti photoanodes.[175]

Silver (Ag). Plasmonic photoanodes have significant benefits, including easy fabrication, minimal use of photoanode materials, and high potential for incredibly high light absorption through the localized surface plasmon resonance (LSPR) effect, making them potential candidates for investigation.[176] The added advantage of the electron sink effect or photocharging effect in metallic nanoparticles improves the electron lifetime, lowers the recombination rate, and enhances electron transfer. A study showed that Ag doping increased the size of TiO$_2$, indicating the facilitation of interstitial substitution in the tetragonal lattice.[177] Another work reported that despite the decrease in the surface area with the introduction of Ag, the doped photoanode did not negatively impact the dye-loading capacity.[176] In contrast to the usual trend, the unexpected impact is attributed to the modification of trap states. The Ag atom being a donor atom contributes to the shifting of Fermi energy toward the conduction band. As compared to a single layer and an undoped layer of TiO$_2$, thicker layers of TiO$_2$ with Ag doping at the bottom layer exhibit a smaller bandgap. An optimum film thickness is highly recommended to facilitate high interfacial surface area, a low recombination rate, and easy mass transfer. With the dopant being a good conductor, it can be ensured that the conductivity of the doped material is enhanced manifold by improving the electron transfer rate. Additionally, the multiple layers acting as blocking layers between the electrolyte and conducting substrates cease the
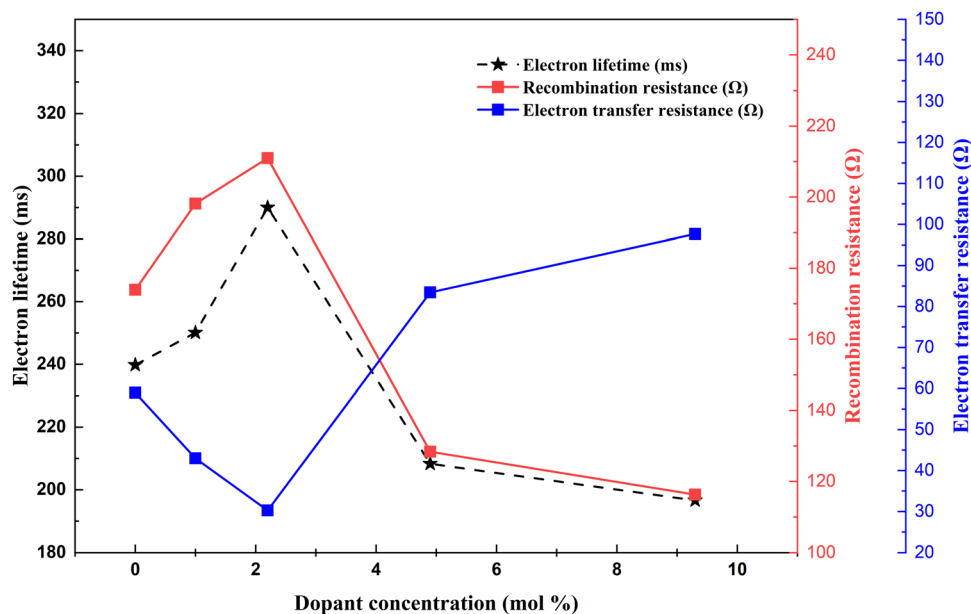

Fig. 18 Nd dopant electron lifetime, recombination resistance and electron transfer resistance correlation.[138]
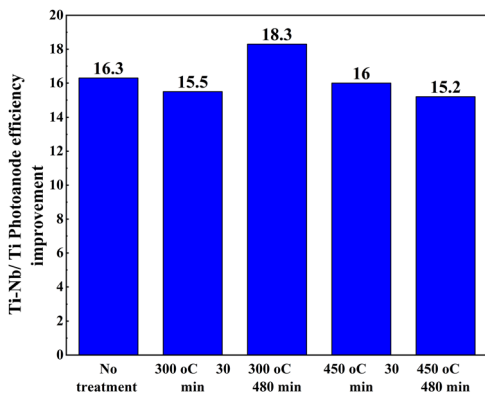
Fig. 19 The conversion efficiency of DSSCs using Ti–Nb photoanodes with and without H_2O_2 treatment after annealing at (a) 300 °C and (b) 450 °C for 30 and 480 min and (c) the improvement in efficiency percentage of Ti–Nb compared to Ti photoanodes.[175]

recombination of holes and electrons, thereby facilitating increased conductivity. The dye and plasmonic nanoparticles show a synergistic impact through an improvement in absorption. P. Nbelayim *et al.* showed in their work that the absorption enhancement effect is indeed complementary; *i.e.*, plasmonic nanoparticles aid in achieving a broadband optical absorption effect with a significant enhancement effect in the regions where the dye exhibits weak absorbance (Fig. 20).[176]

An optimal concentration of Ag aids in enhancing the short circuit current density and reducing in V_{oc}, which is attributed to the optimal lowering of the Fermi level of the photoanode and efficient electron injection. Optimal doping concentration is necessary to balance the positive and negative effects of plasmonic doping. The advantages are improved charge transport and lower recombination owing to the electron-sink effect. The disadvantage is poor charge injection efficiency due to increasing Fermi levels.

Cadmium (Cd). Compared to undoped TiO_2 samples, cadmium (Cd) doped TiO_2 exhibits a small improvement in UV and visible light absorption. M. Motlak *et al.* reported that Cd doping does not have any impact on the bandgap. Cd doping, when it leads to the formation of CdO in the lattice structure, significantly reduces the electron–hole recombination rate.

Thus, it can be concluded that Cd doping could not strongly influence the electrode's optical properties.[144]

Tantalum (Ta). Ta has a 5^+ valence, and it has one more electron than Ti. Therefore, introducing Ta increases the electron concentration and the conductivity of undoped TiO_2.[178] The doping of TiO_2 with Ta results in the following effects: (1) a positive shift of the flat band potential, (2) an increase in electron density (from $(TiO_2) = 8.43 \times 10^{18}$ cm^{-3} to ND $(TaTiO_2) = 1.89 \times 10^{19}$ cm^{-3}), (3) a decrease in open circuit voltage, (4) improvement of the driving force of injected electrons from the LUMO of the dye to the conduction band of TiO_2, (5) acceleration of the transfer rate of the electrons and (6) improvement of the fill factor of the solar cell and reduction of the bandgap. Due to the d–d transitions and various gap states, the Ta dopant induces redshift and increment in the absorption of the visible spectral regime. Another work showed inverse opal Ta–TiO_2 electrode structures that could support infiltration of the hole-transport material in films due to large, interconnected cavities/pores and achieved a 23% increment in photoconversion efficiency.[179] These structures also had the added advantage of trapping light due to their sizeable inner scattering. The doping concentration was optimized to 3.4 atom% to avoid the decrease in electron mobility at high defect concentration and to avoid increased charge recombination by the defects and increased electron recombination. With vertically aligned nanostructured films of tantalum-doped TiO_2 nanoparticles, the DSSC achieved a 65% increase in photocurrent and around 39% improvement in overall cell efficiency compared to undoped TiO_2. Doping TiO_2 with Ta does not impact the percentage of dye adsorption.

Tungsten (W). The radius of W(VI) (0.06 nm) is comparable to the radius of Ti^{4+} (0.0605 nm), thereby making the doping of W into TiO_2 feasible. The high ionic conductivity of W^{4+} suggests it to be a favorable dopant to form titanium dioxide-based photoanodes. Increasing W doping at a low level positively shifts the conduction band of TiO_2 on the one hand and acts as a trapping site for retardation of charge recombination on the other hand. The positive shift of the CB is expected as WO_3 has a lower CB edge relative to TiO_2. W doping suppresses the charge recombination, which, in addition to the downward movement of the conduction band, increases the driving force for electron injection and thus results in the remarkable improvement of the short

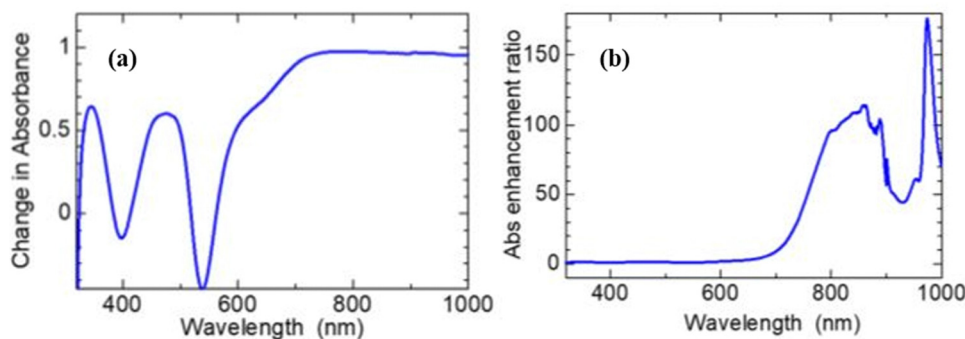**Fig. 20** Optical absorption spectra showing enhanced broadband light absorbance of the N719 dye: (a) absorbance of [0.12 mg ml^{-1} dye] − absorbance of [dye-only]. (b) The absorbance of [0.12 mg ml^{-1} dye] ÷absorbance of [dye-only].[176]

circuit photocurrent and charge collection efficiency. Therefore, it is preferable to switch to W doping when the dye used for the cell has an insufficiently high LUMO compared to the CB in comparison to the undoped TiO$_2$. W dopant also significantly improves the electron lifetime. The positive conduction band shift and electron lifetime increment result in almost constant V_{oc} for a shallow doping level. Nevertheless, for higher doping levels, the V_{oc} decreases.

Fig. 21(a)–(c) and Table 3 summarize the performance of dopants which increased the efficiency by more than ten percent. However, dopants that increased the PCE by less than 10% are also included in Table 1. As seen in Fig. 21, copper, zinc, and zirconium increased the efficiency drastically when doped.[67,74,180] However, Ag, Cr, Nb, Ta, W, and Y showed an increase in PCE (locked below 50%).[146,166,181–184] At the same time, in a different study, the highest-performing zirconium and copper showed a decrease in PCE.[154,185,186] Other than these, Ag, Fe, Ni, Mn, and Co also reduced the efficiency of DSSCs compared to the control DSSC when doped into a TiO$_2$ photoanode.[72,135,187]

Even though doping research is thriving, associated bandgap data are relatively less noted. Fig. 22 shows the variation of bandgap and the corresponding effect on PCE with doping. When the bandgap is reduced, there is an increase in PCE and *vice versa*. Nevertheless, TiO$_2$ nanofiber does not follow this order. When the bandgap is higher, the PCE increases.

3.6. Post-transition metals

Post-transition metals are poor metals with lower reactivity. They are also brittle and generally have low boiling points than transition metals. These include aluminum, gallium, indium, tin, thallium, lead, and bismuth. Except for thallium and lead, all other post-transition metals were doped into TiO$_2$ to increase conductivity, change the absorption to the visible region for better charge-hole separation, decrease the recombination, and tailor the surface defects for better charge transfer by changing dimensionality.[81,197–201]

Aluminum (Al). Aluminum doping introduces oxygen vacancies into the TiO$_2$ lattice, increasing the carrier generation and improving the internal conductivity.[202–204] In addition to the increase in conductivity, Al doping introduces electron traps into TiO$_2$.

These traps effectively reduce the photocurrent through charge recombination. However, aluminum doping has a positive effect on DSSCs despite the drop in the photocurrent.[202] Not just in DSSCs, Al^{3+} doped TiO$_2$ has a positive influence on PCE when used as an electrode material in QDSSCs. But the study by R. Li *et al.* published in 2016 showed that doping aluminium into the mesoporous TiO$_2$ followed by 500 °C sintering increased the PCE significantly over the other two studies in 2011[202] and 2017.[71] Aluminum doping into the mesoporous layer increased the PCE by around 67 percent. The incorporation of Al ions into the TiO$_2$ causes a change in the concentration of defect states. The flat band potential plays a vital role by increasing the electron injection rate and charge collection efficiency. Altogether, they contributed to the efficiency in the

DSSC. Even though the efficiency is much lower in the study by R. Li *et al.*, the effect of aluminum doping stands out.

Bismuth (Bi). Metal–nanocomposites can enhance the efficiency of DSSCs through electron transfer kinetics at the crystal surface, reducing the probability of electron–hole recombination. Bismuth doping through crystallization produced Bi-doped TiO$_2$ nanocubes. Doping and crystallization increased the efficiency of a doped TiO$_2$-based DSSC compared to the undoped TiO$_2$-based DSSC. In 2016, M. C. Wu *et al.* doped bismuth into TiO$_2$ nanofibers and used them as a scattering layer.[66] This study by M. C. Wu *et al.* has better efficiency than M. N. An'amt *et al.* study. Also the effect of doping is comparative in both studies.[201] Bi^{3+} replaces Ti^{4+}. The ionic size difference between Ti^{4+} (0.061 nm) and Bi^{3+} (0.103 nm) causes a slight shift in the crystalline peak of the Bi-doped sample's XRD pattern. Doping with bismuth almost increases the PCE by 70 percent compared to the undoped TiO$_2$. Bismuth doping extends the absorption spectra of TiO$_2$ from the UV to visible region. Nanofibers scatter the light more than the bare TiO$_2$ scattering layer, contributing to the increase in PCE. It is clear from Fig. 23(a), (b) and Table 4 that all other post-transition metals have a minimal doping impact on increasing the PCE when compared to aluminium and bismuth.

Gallium (Ga). Gallium's ability to increase the photocatalytic effect on doping into TiO$_2$ attracted the attention of J. Chae and his group in 2011. According to J. Chae *et al.*, while doping, Ga^{3+} is inserted into the Ti^{4+} sites and also between the lattices. This insertion helps in donating electrons to the neighboring oxygen ions. AFM of doped samples agrees with this observation. The free ions generated due to the charge balance will improve the electron flow more easily to the conduction electrode and FTO glass. The improved electron flow leads to better electron movement compared to the pure TiO$_2$ electrode, resulting in an increase in the PCE of DSSCs.[209] Immediately after this article, in 2011, gallium was again considered for doping. Trivalent elements in the TiO$_2$ lattice can create intermediate acceptor levels and improve the charge collection efficiency. This can enhance the PCE without compromising the V_{oc}.

Indium (In). Significant recombination occurs in contacts such as TCO and TiO$_2$ interfaces, which leads to the introduction of indium into TiO$_2$. Indium is also well known for its low toxicity and better transparency. Doping TiO$_2$ with indium leads to better electronic properties and decreases the DSSC's internal resistance when used as an electrode material. B. Baptayev *et al.* surface doped TiO$_2$ with indium (In^{3+}) using a simple immersion technique. An optimum surface doping in TiO$_2$ positively affects the V_{oc} and FF, thus the PCE. At the same time, higher surface doping leads to faster recombination through an increased number of surface trap states. Nevertheless, on comparing these two works, it was found that doping indium into TiO$_2$ and applying above FTO resulted in a slightly high percentage increase in PCE than doping indium into the mesoporous layer of DSSCs. However, indium surface-doped DSSCs have somewhat lower efficiency than bulk doping.[199] Recent research on indium doped TiO$_2$ showed a remarkable increase in TiO$_2$ electronic properties. Indium's ability to be transparent and low toxicity became an added quality to consider it for doping into TiO$_2$.
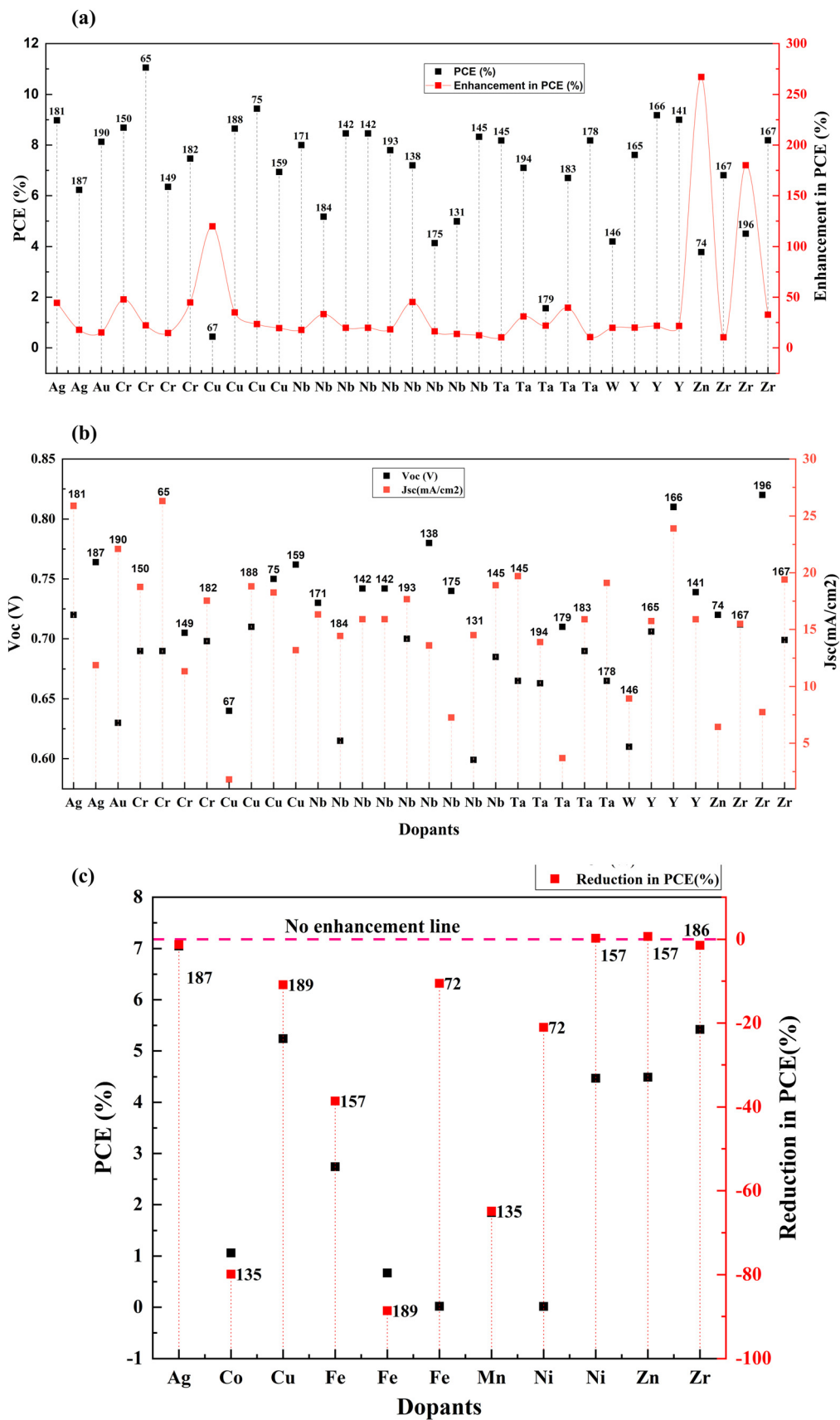
Fig. 21 (a) Performance of transition metals when doped into TiO_2 for DSSC fabrication. (b) J_{sc} and V_{oc} of transition metals when doped into TiO_2 for DSSC fabrication. (c) Reduction in PCE when transition elements are doped into TiO_2 for DSSC fabrication. Data points are labelled with references.

Table 3 Current statistics of transition metal doping in TiO$_2$

S. no.	Dopant	Treatment/coating	Structure	Synthesis method	V_{oc} (V)	Photocurrent density (mA cm^{-2})	FF	PCE (%)	Enhancement in PCE (%)	Bandgap (eV)	Application	Sensitizer/dye	Ref.
1	Chromium (Cr)		Nanoparticles	Hydrothermal and doctor blade	0.705	11.34	0.69	6.35	14.62		DSSC	N719	149
2	Chromium (Cr)		Bilayers, NPs, nanotubes	Microwave assisted hydrothermal	0.69	18.75	0.66	8.69	47.79		DSSC	N719	150
3	Chromium (Cr)		Nanoparticles, nanotubes	Microwave assisted hydrothermal	0.69	26.29	0.6	11.05	22.10		DSSC	N719	65
4	Chromium (Cr)		Nanoparticles, nanotubes	Sol–gel, spin coating	6.98	17.54	0.609	7.47	44.77		DSSC	N719	182
5	Cobalt (Co)		Nanoparticles	Hydrothermal, doctor blade	0.6	3.12	0.571	1.06	−79.89		DSSC	N719	135
6	Cobalt (Co)		Nanoparticles	Microwave assisted hydrothermal	1.201	6.87	0.59	4.85	8.74		DSSC	N719	157
7	Cobalt (Co)		Brookite	Spray pyrolysis	0.87	11.04	0.59	5.66		3.3	DSSC	N719	156
8	Copper (Cu)		Core–shell nanostructures, nanowires	Doctor blade	0.75	18.26	0.68	9.44	23.40		DSSC	N719	75
9	Copper (Cu)		Nanowalls	Liquid phase deposition	0.64	1.8	0.0038	0.44	120.00	3.32	DSSC	N719	67
10	Copper (Cu)		Nanoparticles	Microwave assisted hydrothermal	0.762	13.2	0.689	6.94	19.45	2.96	DSSC	N719	159
11	Copper (Cu)		Nanoparticles	Microwave assisted hydrothermal	1.073	7.34	0.65	5.09	6.71		DSSC	N719	151
12	Copper (Cu)		Nanoparticles	Sol–gel	0.71	18.8	0.642	8.65	34.95	2.7	DSSC	N719	188
13	Copper (Cu)		Nanoparticles	Sol–gel, hydrothermal	0.76	10.68	0.585	5.24	−10.88	3.23	DSSC	N719	189
14	Gold (Au)		Thin shell, hollow sub-microspheres	Hydrothermal	0.63	22.1	0.64	8.13	15.16		DSSC	N719	190
15	Gold (Au)		Nanoparticles		0.7	0.7	0.5611	6.51			DSSC	N719	191
16	Iron (Fe)		Nanoparticles	Microwave assisted hydrothermal	0.939	8.37	0.35	2.74	−38.57		DSSC	N719	157
17	Iron (Fe)		Nanoparticles	Sol–gel	0.29	0.22	0.0027	0.017	−10.53	3.13	DSSC	N719	72
18	Iron (Fe)		Nanoparticles	Sol–gel, hydrothermal	0.71	1.14	0.731	0.67	−88.61	3.24	DSSC	N719	189
19	Manganese (Mn)		Nanoparticles	Hydrothermal, doctor blade	0.656	4.241	0.667	1.85	−64.90		DSSC	N719	135
20	Manganese (Mn)		Nanoparticles	Microwave assisted hydrothermal	1.181	7.52	0.55	4.87	2.10		DSSC	N719	151
21	Nickel (Ni)		Nanoparticles	Microwave assisted hydrothermal	1.126	7.75	0.51	4.47	0.22		DSSC	N719	157
22	Nickel (Ni)		Nanoparticles	Sol–gel	0.31	0.17	0.0029	0.015	−21.05	3.15	DSSC	N719	72
23	Niobium (Nb)		Nanorods	Electrochemical anodization	0.615	14.43	0.583	5.17	33.25		DSSC	N719	184
24	Niobium (Nb)		Nanoparticles	Horizontal ultrasonic spray pyrolysis deposition (HUSPD)	0.74	16.9	0.6026	7.5	4.75	2.8	DSSC	N719	192
25	Niobium (Nb)		Nanoparticles	Hydrothermal	0.7	17.67	0.63	7.8	18.18		DSSC	N719	193
26	Niobium (Nb)		Nanoparticles	Hydrothermal	0.742	15.907	0.717	8.459	19.78		DSSC	N719	142
27	Niobium (Nb)		Nanoparticles	Hydrothermal	0.685	18.9	0.64	8.33	12.26		DSSC	N3	145
28	Niobium (Nb)		Porous microspheres	Hydrothermal method followed by heat treatment	0.599	14.5	0.575	4.99	13.67		DSSC	N719	131
29	Niobium (Nb)		Nanoparticles	Hydrothermal synthesis and screen printing	0.742	15.907	0.717	8.459	19.78		DSSC	N719	142
30	Niobium (Nb)		Nanoparticles	Screen printing	0.74	7.26	0.76	4.14	16.29		DSSC	N719	175
31	Niobium (Nb)		Nanoparticles	Sol–gel, co-hydrolysis, hydro-thermal treatment	0.73	16.32	0.68	8	17.65	3.12	DSSC	N719	171
32	Niobium (Nb)		Nanoarrays, nanoparticles	Two-step hydrothermal, spin-coating approach	0.78	13.6	0.68	7.2	45.16		DSSC	N719	138
33	Scandium (Sc)		Mesoporous beads/nanoparticles	Controlled hydrolysis	0.752	19.1	0.675	9.6	6.67		DSSC	N719	127
34	Silver (Ag)		3D flower like microstructures	Hydrothermal, photoreduction	0.72	25.88	0.49	8.98	44.37		DSSC	N719	181
35	Silver (Ag)		Nanoparticles	Polyol, electrospinning	0.764	11.88	0.685	6.23	17.77		DSSC	N719	187
36	Silver (Ag)		Nanoparticles, nanofibres	Polyol, electrospinning	0.752	13.68	0.685	7.05	−1.26		DSSC	N719	187
37	Silver (Ag)		Nanoparticles	Sol process	0.744	8.93	0.591	5	7.30		DSSC	N719	176
38	Silver (Ag)	Ag coating	Nanoparticles		0.71	4.24	0.62				DSSC	N719	177

Table 3 (continued)

S. no.	Dopant	Treatment/coating	Structure	Synthesis method	V_{oc} (V)	Photocurrent density (mA cm^{-2})	FF	PCE (%)	Enhancement in PCE (%)	Bandgap (eV)	Application	Sensitizer/dye	Ref.
39	Tantalum (Ta)		Nanoparticles	Atomic layer deposition	0.71	3.69	0.6	1.56	21.88		DSSC	N719	179
40	Tantalum (Ta)		Nanoparticles	Hydrothermal	0.665	19.7	0.65	8.18	10.24		DSSC	N3	145
41	Tantalum (Ta)		Nanoparticles	Hydrothermal	0.665	19.1	0.65	8.18	10.54		DSSC	N3	178
42	Tantalum (Ta)		Nanoparticles	Laser ablation	0.69	15.9	0.61	6.7	39.58		DSSC	N719	183
43	Tantalum (Ta)		Nano spheres	Screen printing method	0.663	13.89	0.77	7.1	31.00		DSSC	N719	194
44	Tungsten (W)		Nanoparticles	Modified sol–gel	0.61	8.94	0.77	4.2	19.76		DSSC	A new coumarin dye	146
45	Vanadium (V)		Nanoparticles	Hydrothermal	0.687	17.6	0.65	7.8	5.12		DSSC	N3	145
46	Yttrium (Y)		Nanoparticles	Gel–sol	0.706	15.74	0.6846	7.61	19.97		DSSC	N719	165
47	Yttrium (Y)		Nanoparticles	Hydrothermal	0.739	15.9	0.77	9	21.62		DSSC, QDSSC	C101 Ru(+II)	141
48	Yttrium (Y)		Nanoparticles	Hydrothermal	0.81	23.9	0.4724	9.18	21.79		DSSC	N719	166
49	Zinc (Zn)		Nanowalls	Liquid phase deposition	0.66	10.68	0.28	1.98			DSSC	N719	195
50	Zinc (Zn)		Nanoparticles	Microwave assisted hydrothermal	1.097	7.85	0.52	4.49	0.67		DSSC	N719	157
51	Zinc (Zn), cobalt (Co)			Sol–gel	0.72	6.44	0.82	3.78	266.99	2.9	DSSC	N719	74
52	Zirconium (Zr)			Ball milling, dissolving, impregnation, mixing, screen printing	0.7067	10.527	0.75	5.42	−1.45		DSSC	N719	186
53	Zirconium (Zr)		Nanoparticles	Sol–gel	0.712	15.5	0.626	6.81	10.37	3.1	DSSC	N719	167
54	Zirconium (Zr)	CNT coating	Nanoparticles	Sol–gel	0.699	19.4	0.602	8.19	32.74		DSSC	N719	167
55	Zirconium (Zr)		Nanoparticles	Sol–gel	0.45	0.13	0.0034	0.02	5.26	3.09	DSSC	N719	72
56	Zirconium (Zr)		Nanofibers	Sol–gel, electrospinning	0.82	7.74	0.71	4.51	180.12	3.22	DSSC	N719	196

Sol–gel produced TiO_2 photoanodes showed a 17.4% increase in PCE. This increase is due to the decrease in recombination and internal resistance. An elaborate recombination study was done by Baptayev *et al.*, guiding us through the indium doping and the cell's internal resistances. By setting the dark conditions and voltage to a bare minimum of 0.4 V, they analyzed the voltage decay of doped samples one by one to eliminate the effect of recombination through back contact. The study showed that doping has a positive impact on reducing recombination. According to Baptayev *et al.*, there are three mechanisms for charge recombination:

(1) Direct transfer from the conduction band to electrolyte.

(2) Indirect transfer from monoenergetic deep surface states.

(3) Indirect transfer from the distribution of bandgap surface states.

In the indium doping case, the surface trap states are dominant trap states and lead to decreased recombination centers, eventually benefiting the PCE.[199]

Tin (Sn). Tin is the most explored element among post-transition metals doped into TiO_2.[208,210,211] From 2012 to 2016, a series of TiO_2–Tin doping studies were conducted. When Sn increases in the TiO_2 lattice, the oxygen vacancies increase. Subsequently, the oxygen vacancies favor photocatalytic reactions.[81] When Sn^{4+} is doped into the TiO_2 lattice, the potential of the flat band (E_{fb}) shifts depending on the doping concentration. A negative shift in E_{fb} means a shift in redox potential. However, efficiency increases when the redox potential varies with increasing open-circuit voltage.[208] The source of tin doping has a significant effect on efficiency. Y. Duan *et al.* strongly suggested choosing an appropriate source when doping TiO_2 in DSSCs.[69] R. T. Ako *et al.* also agreed with the increase in defect concentration while doping Sn into TiO_2. This lower defect concentration resulted in slower transient states and consequently less recombination. d–d transitions of untrapped electrons also had a longer excitation lifetime.[189] Y. Akhila *et al.* doped tin into TiO_2 nanorods and prepared nanorods with various Sn concentrations. However, in their study, 1% Sn doping was found to increase oxygen vacancies in TiO_2, favoring photocurrent conversion.[81]

Analyzing PCE to understand doping is deceiving because it does not give any information about what it does to efficiency. Meanwhile, an increase in PCE provides vital information regarding the effect of doping. From the graph, it is clear that indium and tin have higher PCEs owing to their preparation methods. Aluminum, bismuth, and gallium when doped into TiO_2 have significantly changed the DSSC's efficiency.

3.7. Halogens

Among halogens, fluorine and iodine showed effective narrowing of the bandgap attributed to their higher ability to absorb visible light. This observation is supported by DFT calculations of n-type iodine-TiO_2 doping and p-type nitrogen-TiO_2 doping. Comparatively, iodine doping improved the conductivity and increased the visible light absorption of anatase TiO_2. From 2011 on, iodine and fluorine alternatively have become the best dopants for TiO_2 from the halogen group. The statistical
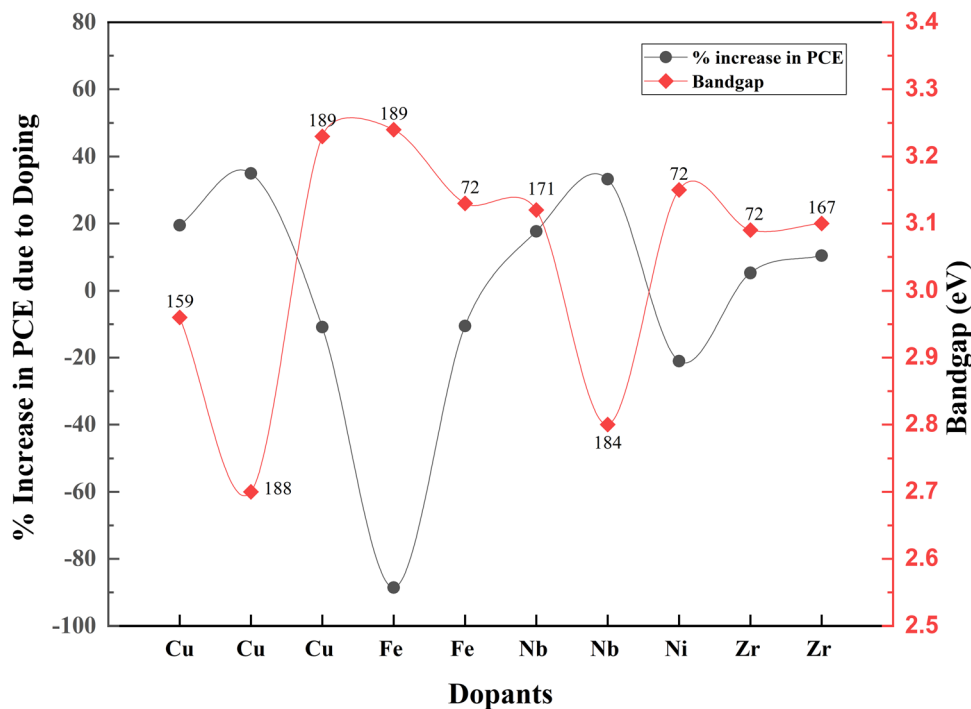
Fig. 22 Bandgap and increase in PCE with doping in transition elements. Data points are labelled with references.

information about halogen doped TiO_2 based DSSCs is summarized in Table 5.

Iodine (I). In 2011, Hou and coworkers reported a higher photon conversion efficiency of 10 percent by doping TiO_2 nanocrystals with iodine (I-TNC). In the iodine doped samples, recombination of electron–hole pairs may be inhibited due to the ability of iodine to act as a trapping site for photogenerated electrons. Even though the article strongly suggests iodine as a futuristic dopant, it requires focused research to understand the energy conversion mechanism.[212] Iodine exhibits multiple valencies of I^-, I^{5+}, and I^{7+}. Nevertheless, XPS results indicated that I^{5+} (0.062 nm) doped into the titania matrix and substituted Ti^{4+} (0.064 nm). Compared to the bare TiO_2 samples, the iodine doped samples exhibited an extended response in visible light absorption. By reducing the recombination and improving the conductivity, I^{5+} doping increased the J_{sc} of DSSCs.[213,214]

Fluorine (F). Song and coworkers created a multifunctional electrode with F-doped TiO_2 hollow nanoparticles to reduce charge recombination and contact resistance. However, the lack of details on undoped DSSCs makes it unable to distinguish whether the method stands out. It can be seen that there is no significant difference in surface area in F-doped hollow TiO_2 spheres and undoped samples. This F doping is an example of retaining the morphology and structure of TiO_2 even after doping; thus, there will not be a dramatic change in the dye loading or light scattering. However, there is a 13% increase in the efficiency of a DSSC with F-doped TiO_2.[215]

The idea of high-quality blocking layers that are non-metallic leads to the use of fluorine as a dopant for TiO_2. Noh and coworkers introduced a new concept of dense layers into DSSCs for creating a non-ohmic layer between the nanoporous TiO_2

layer and FTO glass. High interfacial resistance has hindered the efforts to develop adequate blocking layers. For example, Nb doping on the TiO_2 dense layer increased the conductivity of the $SrTiO_3$ substrate, but the thermal instability and production cost were high. Compared to the undoped samples, this work shows that the doping effect on DSSCs is substantially less.

Nevertheless, considering that this is one of the first works in fluorine-doped TiO_2, this study used a low-cost method and materials for doping and successfully introduced a fluorine-doped dense layer. This layer prevented back electron transfer, a breakthrough in DSSC research.[216] Fluorine (F^-) is a superior anionic dopant due to its high electronegativity. It disrupts the CB and inhibits electron recombination by its strong electronegativity. Fluorine ions can penetrate the lattice and induce Ti^{3+} species generation, which helps in charge collection efficiency. Fig. 24 shows that the fluorine content increases in the TiO_2 electrode and the bandgap increases. Consequently, the efficiency of the DSSC increases. On the optimal doping we discuss throughout this paper, at 6% doping, the F-doped TiO_2-based DSSC reaches maximum efficiency. Beyond this doping point, fluorine doping adversely affects the DSSC's efficiency. F-doped TiO_2 nanocubes with a nanovoid/pore morphology play a crucial role in confining light and favoring electron transfer. Nanocubes increase the surface area, thus enhancing dye loading and light trapping. These naturally result in the percentage improvement in the efficiency of the F-doped TiO_2 based DSSC compared to the bare TiO_2-based DSSC. The presence of nanovoids at the surface of TiO_2 influences the grain boundary resistance by increasing the electron concentration. Consequently, this leads to an increase in charge transportation rate. However, the F-doping concentration increases with space
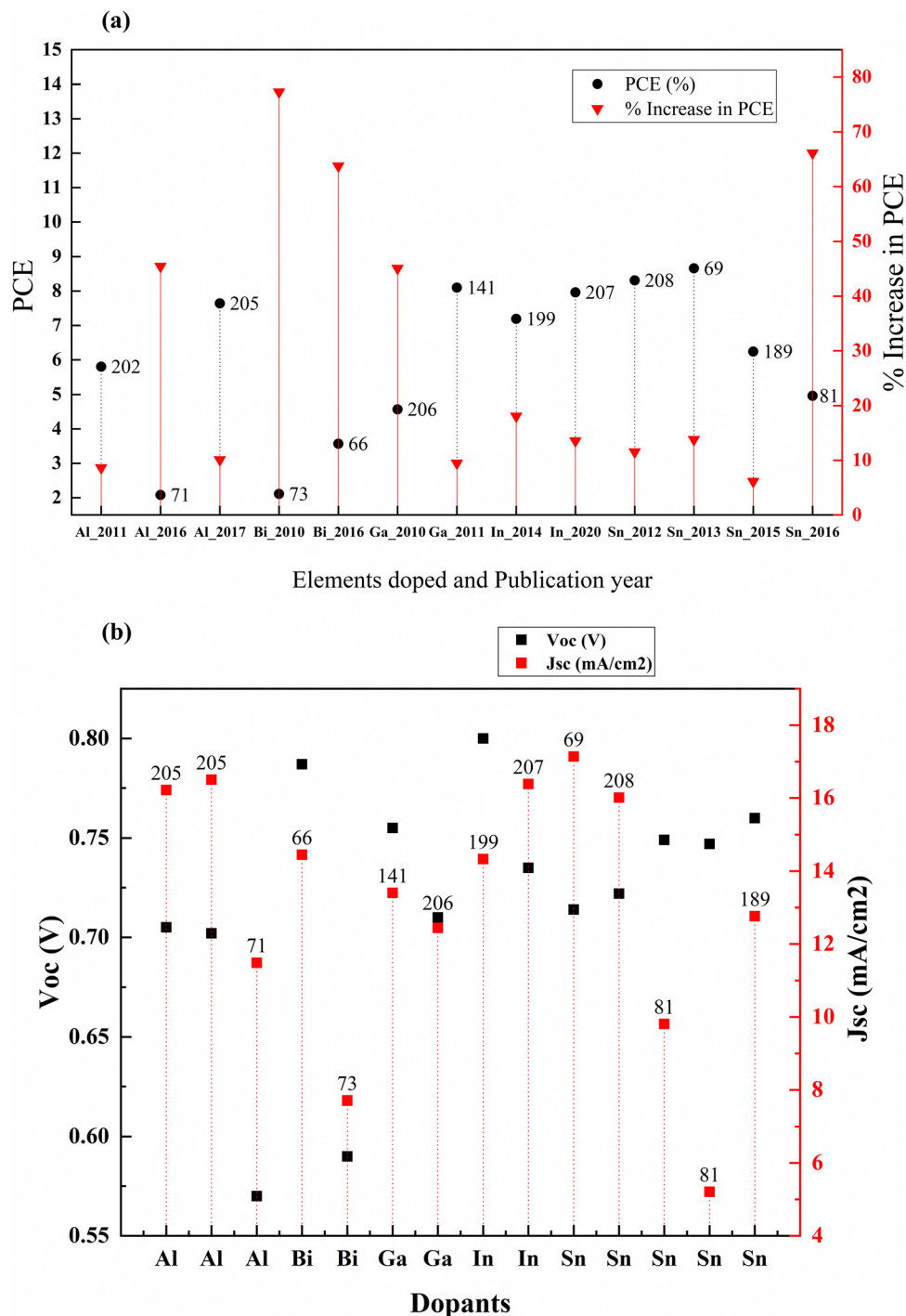
Fig. 23 (a) Percentage increase in PCE in post-transition metals with doping. (b) J_{sc} and V_{oc} of post-transition metals when doped into TiO$_2$ for DSSC fabrication. Data points are labelled with references.

charge polarization effects due to intensive charge carriers, resulting in more recombination.[217]

Defects generated by mesoporous TiO$_2$ result in numerous electronic sub-bandgap trap states.[221] Peng Xiang *et al.* doped TiO$_2$ with iodine and applied it in a quasi-solid state DSSC. From Fig. 25(a), it is clear that iodine doping is vital in improving the cell performance by 34 percent, owing to the distributed pores, which increase the surface area. Nevertheless, compared to

fluorine, the percentage efficiency improvement achieved is insignificant in this study.[222] Fig. 25(b) provides the comparison of V_{oc} and J_{sc} data of halogen doped TiO$_2$ based DSSCs. Recently, microwave-assisted solvothermal doping of fluorine into TiO$_2$ was explored. This preparation method is very competitive with all other fluorine doping techniques. Compared to other methods, this method is non-toxic and non-corrosive as well. In this study, F-doped TiO$_2$ forms a quasi-cubic morphology due to the

Table 4 Current statistics of transition metal doping in TiO$_2$

S. no.	Dopant	Treatment/coating	Structure	Synthesis method	V_{oc} (V)	Photocurrent density (mA cm^{-2})	FF	PCE (%)	Enhancement in PCE (%)	Bandgap (eV)	Application	Sensitizer/dye	Ref.
37	Aluminium (Al)		Mesoporous	Chemical bath deposition	0.705	16.22	0.6677	7.64	10.09		DSSC	N719	205
38	Aluminium (Al)		Nanoparticles	Doctor blade	0.702	16.5	65.75	7.66	9.12		DSSC	N719	205
39	Aluminium (Al)		Nanoparticles	Screen printing	0.57	11.49	0.318	2.08	45.45		QDSSC	CdS/ZnS	71
40	Bismuth (Bi)		Nanofibres	Hydrothermal	0.787	14.45	78.2	3.57	63.76		DSSC	N719	66
41	Bismuth (Bi)		Nanocubes	Sol–gel hydrothermal	0.59	7.71	0.46	2.11	77.31		DSSC	N3	73
42	Gallium (Ga)		Nanoparticles	Hydrothermal	0.755	13.4	0.79	8.1	9.46		DSSC, QDSSC	C101 Ru(+ii)	141
43	Gallium (Ga)		Nanoparticles	Hydrothermal	0.71	12.44	0.51	4.57	45.08		DSSC	N3	206
44	Indium (In)		Nanoparticles	Simple surface doping technique by immersing TiO$_2$ films with In^{3+} acidic solution at different soaking times at 70 °C followed by sintering at 450 °C	0.8	14.33	0.63	7.19	18.06		DSSC	C264 triphenylamine dye	199
45	Indium (In)		Nanoparticles	Sol–gel, spin coating	0.735	16.384	0.661	7.96	13.55		DSSC	N719	207
46	Tin (Sn)		Nanoparticles	Hydrothermal	0.714	17.14	0.71	8.66	13.80		DSSC	N3	69
47	Tin (Sn)			Hydrothermal	0.722	16.01	0.707	8.31	11.54		DSSC	N3	208
48	Tin (Sn)	Post-treated with Zr and HNO$_3$	Nanorods	Sol–gel, hydrothermal	0.749	9.81	0.674	4.96		2.99	DSSC	N719	81
49	Tin (Sn)	Post-treated with Zr and HNO$_4$	Nanorods	Sol–gel, hydrothermal	0.747	5.21	0.534	2.09		2.99	DSSC	Leaves of Camellia sinensis	81
50	Tin (Sn)		Nanoparticles	Sol–gel, hydrothermal	0.76	12.76	0.577	6.24		3.27	DSSC	N719	189

Table 5 Information about halogen doping in TiO$_2$

| S. no.	Dopant	Treatment/coating	Structure	Synthesis method	V_{oc} (V)	Photocurrent density (mA cm^{-2})	FF	PCE (%)	Enhancement in PCE (%)	Bandgap (eV)	Application	Sensitizer/dye	Ref.
1	Fluorine (F)		Nanoparticles	Hydrolysis	0.67	13.89	0.57	5.24	10.08		DSSC	N719	218
2	Fluorine (F)		Nanocuboids	Hydrothermal	0.603	17.621	0.6984	7.463	62.45	3.1	DSSC	N719	84
3	Fluorine (F)		Hollowspheres	Hydrothermal	0.754	11	0.761	6.31			DSSC	N719	215
4	Fluorine (F)		Quasi-cubic structures	Microwave assisted solvothermal	0.745	18.74	0.59	8.2	63.35		DSSC	N719	219
5	Iodine (I)		Nanocrystals	Hydrolysis, hydrothermal	0.715	14.1	0.67	7	42.86	2.4	DSSC	N3	212
6	Iodine (I)		Spheres	Hydrothermal, screen printing	0.616	13.81	0.75	6.38	34.03		Quasi-solid state DSSC	N719	220
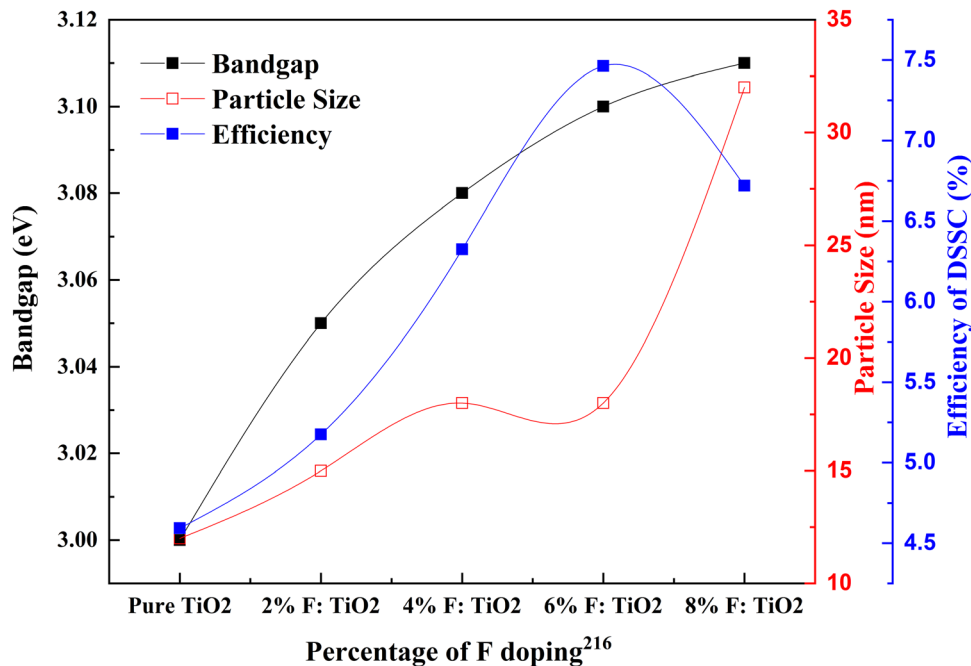
Fig. 24 Correlation of the percentage of F doping with bandgap, particle size and efficiency.

fluorine iron doping. F doping introduces mesoporous structures. The ability of fluorine to separate charges is crucial in DSSC efficiency. Fluorine doping also induces facets that have high surface energy and lead to the formation of heterojunctions. This improves the photogenerated carrier density. The high adsorption capacity of fluorine creates Ti–F and Ti–F–Ti bonding by replacing oxygen. This action favors charge separation.[83]

Since 2011, halogen group elements have been used as prospective candidates for improving the conductivity of photo-anodes for DSSCs. Researchers successfully doped TiO_2 into blocking layers into various TiO_2 structures such as hollow spheres, nanocuboids, and mesoporous structures. Since the introduction of hierarchical TiO_2 layers and quasi-solid-state DSSCs, fluorine doping increases the conductivity, improves dye absorption, and quickens electron transport. Around 2020, researchers looked into the possibilities of non-corrosive, non-toxic, green synthesis routes and green precursor materials like polyvinylidene fluoride (PVDF).

3.8. Other nonmetals

Non-metal ions are thermally stable and suitable candidates for engineering the bandgaps by shifting the band edges compared with metal ionic dopants. Nitrogen is the most attractive non-metal for doping into TiO_2 due to its comparable atomic size with oxygen. In 2009, Soon Hyung Kang and co-authors tried to enhance the DSSC photocurrent using a nitrogen-doped TiO_2 anode. They incorporated urea into the sol–gel technique to obtain nitrogen-doped TiO_2 for photovoltaic applications. Compared to the bare TiO_2 samples, these samples were smaller in crystallite size. DSSCs fabricated with optimally doped samples exhibited an efficiency of 4.86%. Even though nitrogen is a frequent dopant, sulphur doped TiO_2 was also

used to prepare DSSCs for achieving better efficiencies.[223,224] An increase in PCE of DSSCs when TiO_2 is doped with all other non-metal elements is depicted in Fig. 26. Statistics of other nonmetal doped TiO_2 based DSSCs are provided in Table 6.

Nitrogen (N). Recently, there has been interest in nano-crystalline materials such as nanoparticles, nanotubes, nanofibers, and mesoscopic spheres. TiO_2 nanoparticles have roughly 50 nm radii and behave like single atoms but are generally bulk materials called mesoscopic spheres. When doped TiO_2 took the form of mesoscopic spheres, the DSSC efficiency shot up to 10.7%. These nitrogen-doped mesoscopic spheres broadened the absorption from the UV region into the visible region. Applying this technology to QDSSCs achieved a two percent increase in efficiency through fast electron transport in the nitrogen-doped TiO_2 film. This remarkable achievement improved electron transport, charge collection efficiency, and photocurrent density.[224] The direct conduction path for electrons and high surface area for dye absorption made nanotubes and nanorods desirable for DSSC applications. M. Motlak and his group developed nitrogen-doped pristine TiO_2 nanofibers as a photoanode material. They argued that nitrogen doping created a high Schottky barrier that facilitated electron capture. Nitrogen added intermediate electronic levels between the conduction and valence bands of the metal oxide.[225] Nitrogen-doped nanofibers increased the efficiency by 3 percent compared to the normal TiO_2. V_{oc} and I_{sc} increased with nitrogen doping, but the increase in current was relatively higher.

Wang and his group incorporated 1D structures and nano-particles and increased the efficiency percentage by 0.27 times that of a bare TiO_2-based DSSC. Depositing nanoparticles in the walls of nanotubes is effective for increasing efficiency. These aligned nanotubes and dispersed nanoparticles provide a higher surface area. This anode material can be further modified using
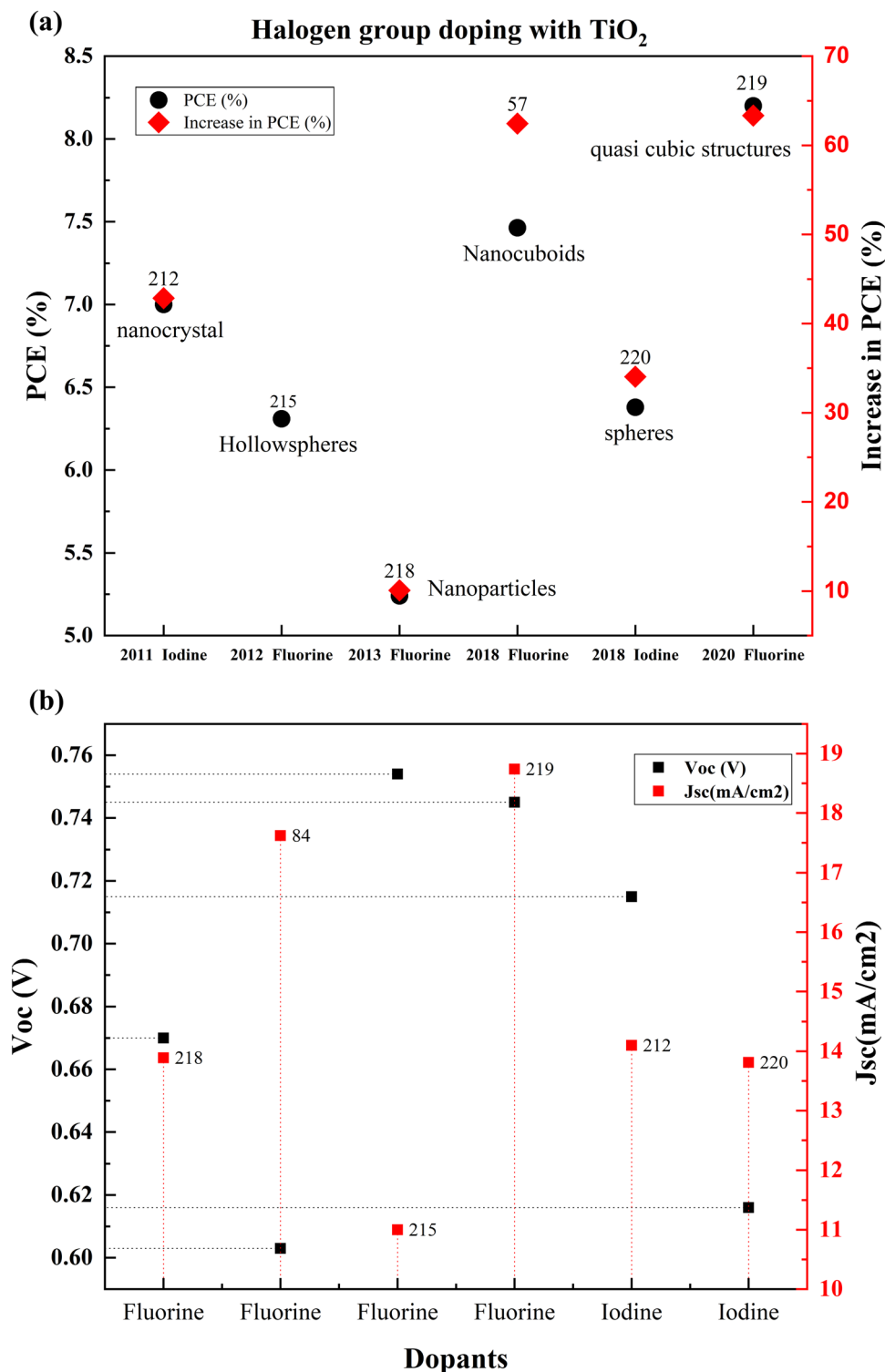
(a)

(b)

Fig. 25 (a) Comparison of the PCEs of different halogen doped TiO$_2$ based DSSCs from 2011. (b) J_{sc} and V_{oc} of halogen doped TiO$_2$ based DSSCs. Data points are labelled with references.

nitrogen doping. By limiting electron and hole recombination, elements doped into TiO$_2$ can increase efficiency. Nitrogen-doped nanoparticles decorated with TiO$_2$ were obtained by the solvothermal method. Small nanocrystals along the wall were confirmed with SEM and HRTEM. This modified structure was

treated with Ti(OH)$_3$, which was found to have a more significant influence on the morphology and photoelectric–chemical properties. The photoanode made with doped-nanoparticle-modified films showed improved light-harvesting efficiency. These nanoparticles that stuck on the nanotubes acted as light scattering
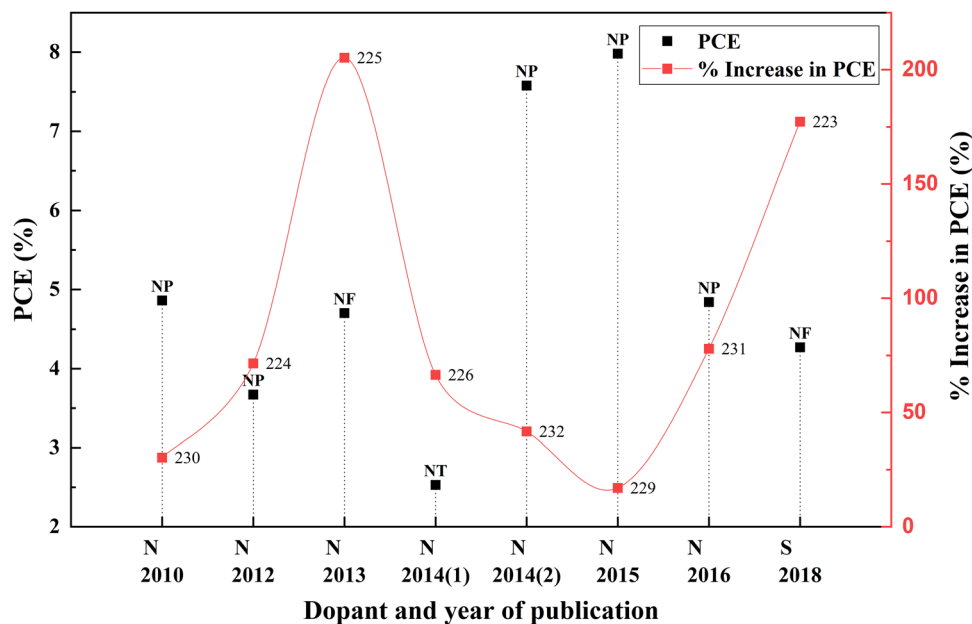
Fig. 26 Increase in PCE with other nonmetal category dopants. Data points are labelled with references.

centers, which reflected in the higher reflectivity. This Ti–O–N bonding, with nanotubes acting as vertical transport channels for photoinduced electrons and adsorbed nanoparticles together, increased the efficiency of DSSCs by 1.68 times the original efficiency.[226] While the exact position of N remains debatable, Ti–O–N linkages point to the presence of N-ions in the TiO$_2$ lattice by replacing the oxygen atom.

When the scattering layer came under the spotlight and became an essential part of DSSCs, doping and modifying the scattering layer attracted more comprehensive attention. Mixing nitrogen-doped aggregated sub-micron size particles into commercial TiO$_2$, and using this as a scattering layer, increases the scattering percentage without any drawback in electrical properties. The IV characteristics of DSSCs with these mixed-phase scattering layers seem to be improved, and the efficiency is increased by 0.14 times that of the commercial scattering layer. Adding a scattering layer introduced the concept of multilayers to DSSC researchers. So, doping and introducing these multilayers into DSSCs has become the next challenge. Multilayers were introduced to increase the J_{sc} by adding the TiO$_2$ layer (scattering, P25, Doped P25) into the FTO substrate. Using a compact layer, a P25 layer, and a N-doped TiO$_2$ layer doubled the J_{sc} when compared with using an undoped TiO$_2$ layer in the DSSC. However, this reduced the fill factor slightly and increased the efficiency. The charge transfer resistance of the TiO$_2$/electrolyte interface is significantly less when a DSSC is prepared with N-doped samples. The resistance–efficiency relationship in these DSSC samples is commendably complex. When the TiO$_2$ layers use P25, the charge transfer resistance is meager. When undoped TiO$_2$ is replaced with P25 particles, nearly half of the original charge transfer resistance is increased. Even though doped multilayers considerably improved the solar performance of DSSCs, when N-doped layers are used in place of undoped

TiO$_2$, the charge transfer resistance, ion diffusion resistance, and shunt resistance simultaneously decreased.[229]

In general, nitrogen induces a redshift in the absorption band edge due to the positive shift in flat band potential of TiO$_2$.[233–239] Incorporation of N^{3-} into the TiO$_2$ lattice can cause replacement of Ti^{4+} and fill up interstitial sites. Even when there is a higher J_{sc} due to increased dye absorption and improved electron injection, charge transport can be affected by lattice distortion.[239,240] However, most studies agree with increased charge transport rates and reduced carrier recombination.[226,241–244]

Sulfur (S). Considering the fact that nitrogen has been researched thoroughly and is a very successful dopant for TiO$_2$, sulfur is also exploited to enhance the photoactivity of TiO$_2$. The presence of 3p orbitals in sulfur, together with TiO$_2$, has a significant role in narrowing the bandgap and increasing the valence bandwidth.[230] Mahmoud *et al.* doped sulfur into hydrothermally prepared TiO$_2$ nanofibers and prepared DSSCs. IV-characteristics show a drastic increase in FF, J_{sc}, V_{oc}, and efficiency. Nevertheless, this study requires more data to confirm the effects of sulfur on DSSCs. To understand this doping effect in detail, it is essential to understand the dependency of IV characteristics on sulfur concentration.[223] Even though sulfur has different oxidation states from S^{6+} to S^{2-}, there is no evidence of S^{2-} (1.7 Å) replacing O^{2-} (1.22 Å) atoms; instead, S^{6+} (0.29 Å) replaces Ti^{4+} (0.64 Å). There is also a chance for random replacement of Ti^{4+} and O^{2-} by ions with polyoxidation states simultaneously, causing severe lattice distortions.[245,246] Over the past few years since 2009, we have seen a systematic approach to doping and using doped materials for implementing DSSCs. First, it was doping into a single TiO$_2$ layer, and later researchers started doping into tubes, structures, dense layers, and mesoporous particles.[247]

Table 6 Information about doping other non-metals into TiO_2

S. no.	Dopant	Treatment/coating	Structure	Synthesis method	V_{oc} (V)	Photocurrent density (mA cm^{-2})	FF	PCE (%)	Enhancement in PCE (%)	Bandgap (eV)	Application	Sensitizer/dye	Ref.
1	Carbonate		Microspheres	Solvothermal	0.76	16.6	0.625	7.65	48.26		DSSC	N719	227
2	Graphidyne (GD)		Nanoparticles	Homocoupling reaction, ball milling	0.8	13.73	0.7434	8.03	20.92	2.89	DSSC	N719	228
3	Nitrogen (N)		Nanoparticles	Doctor blade	0.73	18.76	0.58	7.98	17.01		DSSC	N719	229
4	Nitrogen (N)		Nanofibres	Electrospinning process, hydrothermal treatment	0.75	11.16	0.56	4.7	205.19		DSSC	N719	225
5	Nitrogen (N)		Nano spheres	Hydrothermal and doctor blade	0.474	12.03	0.64	3.67	71.50		QDSSC	CdSe	224
6	Nitrogen (N)		Nanoparticles	Sol-gel	0.726	10.52	0.636	4.86	30.29		DSSC	N719	230
7	Nitrogen (N)		Nanotubes	Solvothermal	0.67	8.82	0.4266	2.53	66.45		DSSC	N719	226
8	Nitrogen (N)		Nanoparticles	Wet chemical	0.7426	9.52	0.6854	4.84	77.94	3.13	DSSC	N719	231
9	Nitrogen (N)			Wet method, screen printing	0.83	12.4	0.7362	7.58	41.68	3.15	DSSC	N719	232
10	Sulphur (S)		Nanofibers	Sol-gel, hydrothermal, electrospinning	0.683	10.66	0.59	4.27	177.27		DSSC	N719	223

4. Co-doping

The light absorption, charge transport, and charge transfer characteristics of an anode determine the efficiency of an electrochemical cell. Successful doping of suitable elements into TiO_2 improves these fundamental properties. However, single elemental doping is inadequate to satisfy the requirements of TiO_2 as an anode material. These monodoped atoms act as recombination centers due to their partially occupied impurity-generated energy bands. Even though contradictory arguments and theoretical calculations exist against passivation theory, many researchers are still on board with passivation theory.[248] Investigations by Dhonde *et al.* show that co-doping with more than one foreign atom can passivate or cause doping asymmetry to these impurity bands. In addition, co-doping effectively modulates the charge equilibrium.[79] Consequently, co-doping increases the surface area and shifts the band edge in TiO_2.[82]

Alkaline earth metals, transition metals, post-transition metals, metalloids, and other non-metals investigated for codoping are marked in Fig. 27. Depending on the type of dopant, there are three types of strategies: metal–metal codoping, metal–nonmetal codoping, and nonmetal–nonmetal codoping.

4.1. Metal–metal codoping

Mono-metal dopants in TiO_2 create serious recombination centers and deteriorate carrier transport. Metal atom doping of TiO_2 causes the inhomogeneous distribution of dopants and requires high-temperature sintering, leading to particle agglomeration.[249] Metal doping also causes rapid recombination of immobilized charge species and thermal instability of TiO_2. However, it improves band structure and shifts absorption towards a longer wavelength. Codoping focuses on increasing V_{oc} and J_{sc} simultaneously through the synergetic effect of dopants. The metal dopant combinations are Al–La, Ca–La, Eu–Tb, Mg–La, Ni–Zn, Nb–Fe, Sr–V, Sr–Cr, Zn–Mg, and Zn–Ga. Fig. 28 shows the effects of these metal codoped TiO_2 based DSSC efficiency enhancements.

Amid metal dopants, Zn–Ga combinational doping into TiO_2 exhibits the highest efficiency in DSSCs. Changes in the electronic structure of TiO_2 facilitate oxygen ion movement in the lattice, superior crystallization, and lattice expansion. During doping, Zn^{2+} and Ga^{3+} move into the lattice, facilitating the breaking and formation of new bonds. Zinc, an n-type dopant, causes a shift in Fermi level towards the conduction band, leading to an increase in the redox potential of electrolyte and a consequent increase in open-circuit voltage. Furthermore, the trap state distribution in TiO_2 has been reduced through zinc doping and has abetted the increase in short circuit current.[200]

A high concentration of trap sites reduced electron transport and formed an impurity-grazed bandgap in Al–La-doped TiO_2. Furthermore, insertion of Al^{3+} ions into the TiO_2 lattice increased the recombination rate and resulted in inefficiency. In Mg–La, Mg–Ca, and Mg–Al doping, the ionic radius plays a vital role in solar cell efficiency. Titanium has smaller ionic radii than La^{3+}, Mg^{2+}, and Ca^{2+}. While doping, these atoms cannot penetrate the lattice. However, Al^{3+} quickly enters the
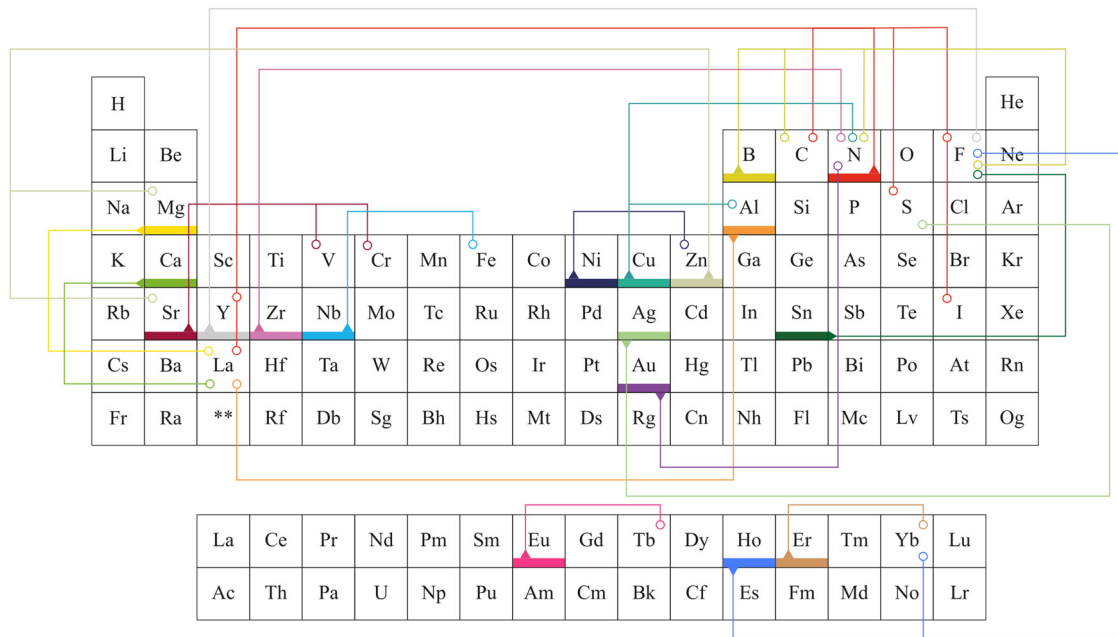
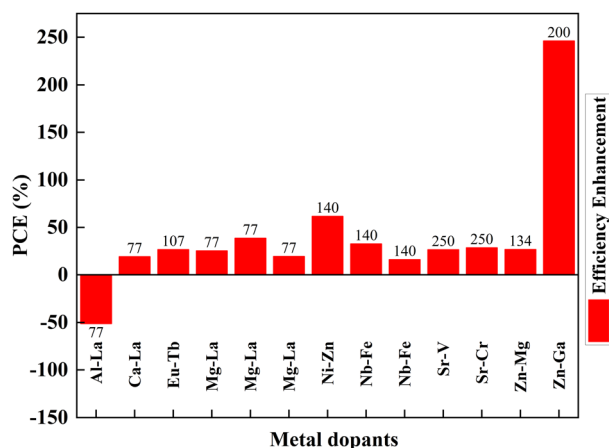**Fig. 27** Elements explored for codoping into TiO_2 for DSSC applications.

Fig. 28 Effects of metal-doped TiO_2 in the efficiency profile of DSSCs. Data points are labelled with references.

lattice without further problems. Prominent ions, Ca^{2+} and La^{3+}, cannot penetrate the TiO_2 lattice after doping.[77]

Consequently, these bigger atoms remain on the surface, facilitating better charge transfer. Relative to these systems, an Al–La codoped system has inefficient charge transfer resulting in low cell efficiency. Mg^{2+} ions are slightly larger than Ti^{4+} ions. During doping, Mg^{2+} enters the lattice and causes slight distortions in the parent material lattice. Moreover, while larger atoms induce surface charge trapping, Mg^{2+} doping provides deep charge trapping in the materials. However, Mg^{2+} ion substitution substitutes Ti^{4+}, resulting in band edge shift.[77]

Ni–Zn doping into TiO_2 achieves more than a 50 percent increase in efficiency than the undoped material. This achievement requires tricky bandgap engineering. Ni produces a

negative shift, and Zn causes a positive shift in flat band potential. Consequently, Ni increases the open-circuit voltage and reduces the short-circuit current. It is *vice versa* for Zn. Ni–Zn doping mainly shifts the fundamental absorption edge and reduces the band energy. However, finding the optimum point for the maximum V_{oc} and J_{sc} is challenging. Nb–Fe doping shifts the conduction band edge. Subsequently, the absorption changes from UV to visible light. Fe and Nb dopants serve as trap states and increase the electron lifetime *via* trapping and de-trapping events over trapping sites of Ti^{3+}, Nb^{5+} and Fe^{3+}. Another research study on the same dopants suggests that Fe and Nb at ultralow concentrations generate Ti^{3+} donor trap states. These trap sites facilitate efficient charge diffusion and collection in titania nanobelts.[140]

Sr,V codoped TiO_2 shows lower electron transit time, higher electron diffusion, and lower resistance, aiding efficiency. The increased charge separation and electron transformation demonstrated through EIS analysis confirm the doped sample's improved efficiency. The synergistic effect of Sr and Cr doping is vital for increasing efficiency. Cr incorporation into the TiO_2 lattice produces isolated energy levels adjacent to the conduction band, narrowing the band gap. Cr^{3+} has excess valence electrons, leading to the generation of holes near the valence band, further contributing to the reduction in the bandgap.[250]

When the crystallite size decreases, the efficiency increases in metal codoped TiO_2. Except for the Zn–Ga sample, this observation concludes that large crystallites have an adverse effect on efficiency. Analysing the specific Zn–Ga doping instance, data shows that the DSSC generated with the sample having a crystallite size of around 19 nm has the highest efficiency, in line with the most recent studies. A detailed investigation shows that when the crystallite size increases more than 20 nm, a DSSC exhibits a
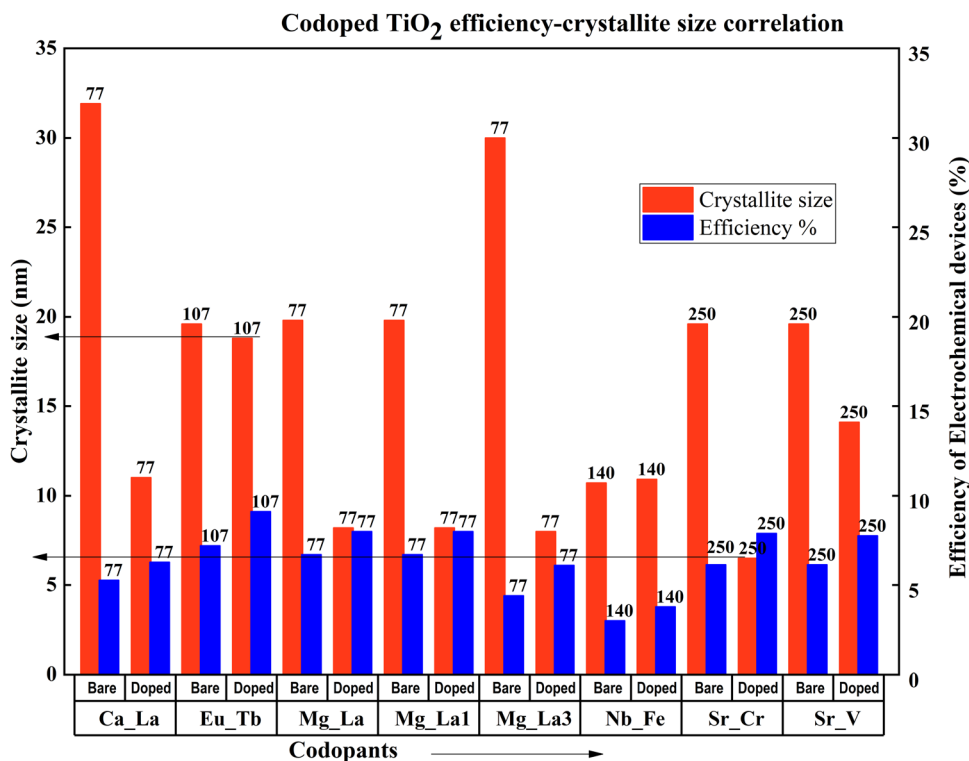
Fig. 29 Codoped TiO$_2$ efficiency−crystallite size correlation. Data points are labelled with references.

drastic decrease in DSSC efficiency (Fig. 29). Optimum crystallite size plays a significant role even in the doping-related efficiency profile. The notable point is that doping affects crystallite size in general. An optimum doping amount exists for each dopant, which decreases the crystallite size to an optimum size. Further doping from this point consequently reduces the efficiency and increases agglomeration.

All the doped TiO$_2$ samples except for Zn–Ga and Nb–Fe doped samples have nanoparticle structures. Nb–Fe doped samples are in the form of nanobelts synthesized *via* a hydrothermal method. Zn–Ga has a thin-film structure prepared and fabricated by sol–gel and dip coating. These structural differences might have contributed to the efficiency increase in the Zn–Ga doped TiO$_2$ sample. Compared with other sample preparation methods, the sol–gel technique is extensively used to prepare metal-codoped TiO$_2$ samples. Doctor blade coating, screen printing, and dip coating are the fabrication methods used to prepare TiO$_2$ anode materials for DSSCs.[134]

4.2. Metal–nonmetal codoping

The thermal instabilities of metal-doped TiO$_2$ instigated the search for non-metal dopants for TiO$_2$. Nitrogen, fluorine, sulfur, and boron are successful non-metal dopants. Doping with these non-metals alone brings changes in photocatalytic activity. However, the latest research indicates that codoping can further improve photocatalytic activity and promote the transportation of photogenerated electrons through the hybridization orbitals. Non-metal codoping is still a feeble area in doping TiO$_2$. Yuanyuan and co-authors illustrated how doping

increases the formation of the pure anatase phase rather than the rutile phase. A set of experiments with different concentrations of mesoporous N, S doped TiO$_2$ and P25 particles has been conducted to understand the effect of doping into TiO$_2$. Excess doping always worsens the DSSC's properties among purely doped TiO$_2$ and undoped TiO$_2$. This efficiency reduction is due to the larger particle size and lower surface area of the doped TiO$_2$ sample. While mixing the doped TiO$_2$ with undoped TiO$_2$, the cell efficiency increases from 5% to 20%, reaches a peak, and decreases. The 10% N, S doped TiO$_2$ sample mixed with 90% Degussa P25 shows a 35.6 percent increase in efficiency yield. This work claims that unique mesoporous nanoparticles and hierarchical structures increase dye absorption and facilitate electrolyte diffusion. Su Pei Lim and co-authors obtained similar results when TiO$_2$ was doped with nitrogen and sulphur. Both the samples achieved a more than 30 percent enhancement in efficiency.[251,252] Fig. 30 compares the increase in PCE with non-metal codoping, which is discussed in this section.

Conductivity is a critical property of TiO$_2$. Each doping attempt is towards achieving this goal. Fu Lv *et al.* doped anatase TiO$_2$ with nitrogen, fluorine, and iodine to induce carriers in the lattice. This process eventually improves conductivity. N–I codoping shows the best blocking effect compared to undoped and single non-metal doped samples. The magnitude of internal charge recombination resistance (R_{rec}) decides the scale of the blocking effect. Usually, the charge recombination is dominated by the interfacial mesoporous TiO$_2$, but the compact underlayer also has an influence on charge recombination. The aforementioned blocking effect
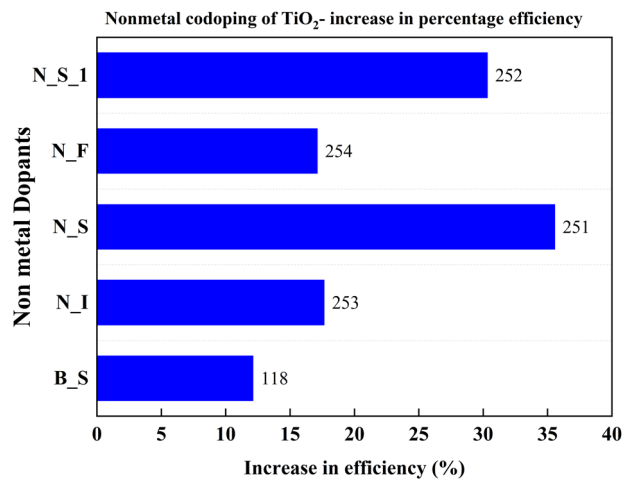
Fig. 30 Increase in PCE of nonmetal codoped TiO$_2$. Data points are labelled with references.

Fig. 31 Increase in PCE with metal–nonmetal codoped TiO$_2$. Data points are labelled with references.

empties the impurity band and improves the conductivity of TiO$_2$ with N–I doping. So, the N–I doping inhibits electron recombination, leading to higher current density and efficiency. The N–I codoping increases electron injection between porous TiO$_2$ and the compact layer by tuning the conduction band. The synergetic effects of the dopants result in a 17.67% increase in efficiency.[253]

Trap states in the conduction band of nanostructured TiO$_2$ play a vital role in its photochemical properties. The current–time profiles of N–F doped samples are greatly influenced by the applied potential. They depend on the trap state density's current decaying behavior. At low trap density, the trap filling is fast; at high trap density, the trap filling is slower. Calculations show that the N–F doping significantly reduces the trap density due to the ability of nitrogen and fluorine to bind at the under-coordinated surface sites of TiO$_2$.[254]

Doping improves the performance of DSSCs and has similar effects in other electrochemical systems. B–S doping in QDSSCs is an excellent example of codoping and consequent efficiency increase. Doping TiO$_2$ with B–S results in bandgap narrowing and redshift in electronic absorption, leading to the increase in photocurrent response. The doping-induced efficiency is 12 percent greater compared to the bare TiO$_2$–based QDSSC.[118]

4.3. Metal–nonmetal codoping

Metal–nonmetal codoping is constantly highlighted as a solution to the difficulties generated by single metal and single non-metal doping. The synergetic effect of both metal and non-metal provides higher thermal stability, lower bandgap values, and enhanced surface area. Furthermore, it reduces the carrier recombination and enhances the short circuit current.[255] Doping Cu/S into the TiO$_2$ lattice minimizes the particle size and scattering effect. In the study by Gupta *et al.*, the concentration of sulfur remains fixed, while the copper concentration is changed from 0 to 0.5 percent.[256] Fig. 31 demonstrates the increase in PCE with metal–nonmetal codoped TiO$_2$.

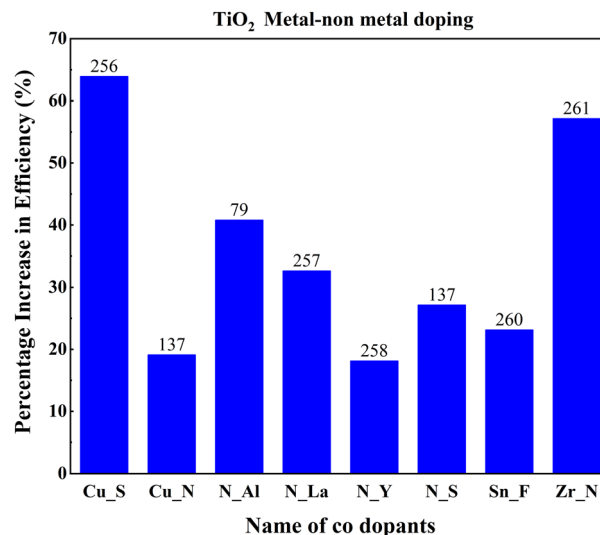The synergetic effect of hybridized Cu-3d and S species with Ti-3d orbitals significantly reduced the band gap of TiO$_2$.

Consequently, this dip improved the redshift in favor of efficiency. Fig. 32 shows the varying crystallite size with 0.05 percent sulfur and copper concentration. Optimal doping plays a significant role in the Cu/S doping technique. When the doping level increased, crystals with smaller sizes started to agglomerate, clogged the microspores, and caused a severe drop in efficiency. The probability of an improved efficiency point between 0.2 and 0.3 percent doping is shown in Fig. 32. A more detailed and precise study requires finding the optimum point for maximum efficiency in Cu–S doped TiO$_2$ anode-based cells.

Copper and nitrogen codoping was also investigated in the same way as copper and sulfur codoping. A DSSC made with doped TiO$_2$ particles (crystallites) shows different efficiencies at the doping concentration of copper. Fig. 33 shows an optimum
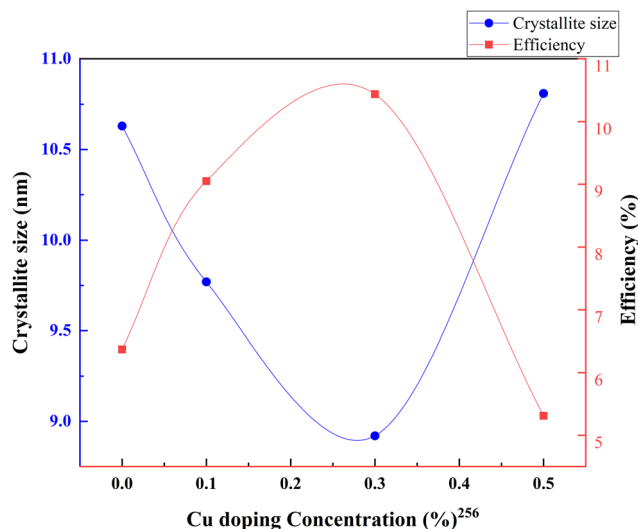
Fig. 32 Variation of crystallite size and efficiency with copper doping concentration. Data points are labelled with references.
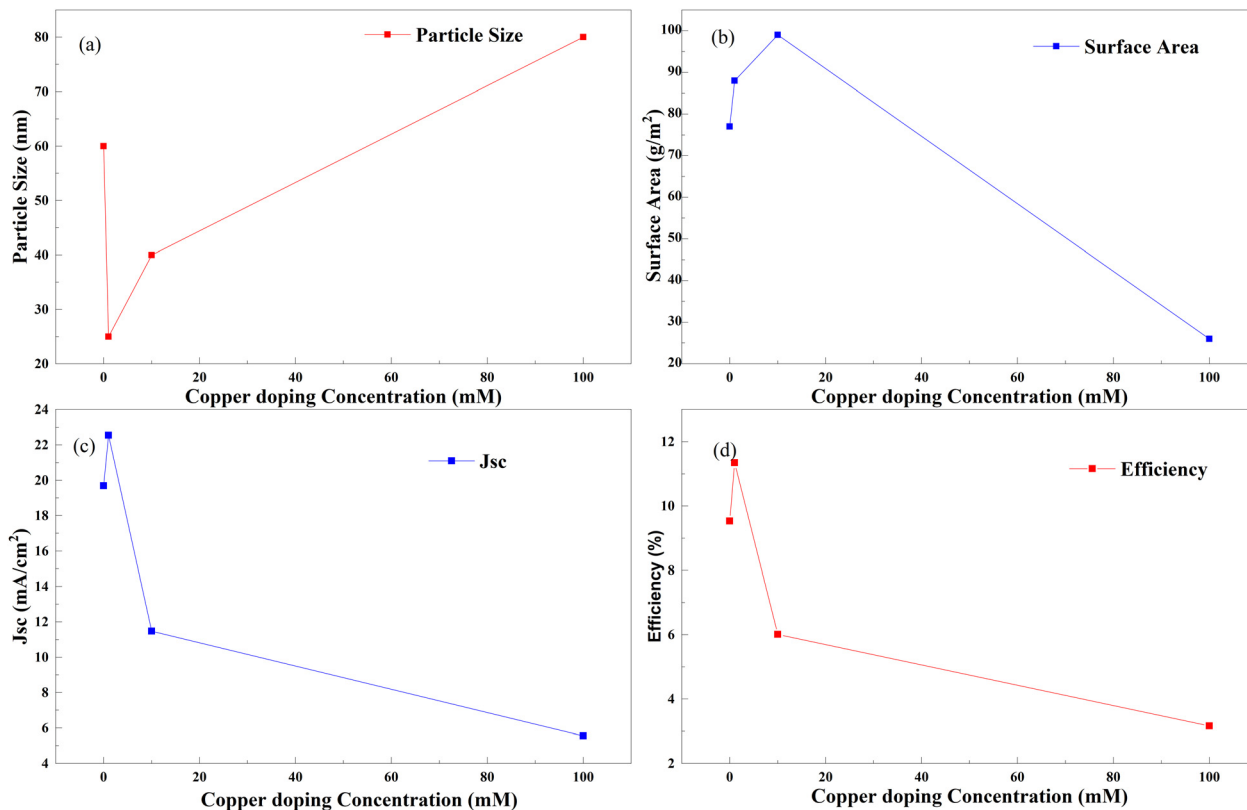
Fig. 33 Copper doping concentration with (a) particle size, (b) surface area, (c) J_{sc} and (d) efficiency.[137]

doping point in Cu–N doping, as discussed in all other examples. In this case, a maximum efficiency is attained when TiO$_2$ is doped with copper by adding 0 to 20 mM copper nitrate into the paste, keeping the doping amount of nitrogen constant for all experiments. This tendency trails in the current generation through reduced crystallite size and increased surface area. When linking copper doping with nitrogen and sulfur, copper–nitrogen doping exhibits only a 19 percent increase in efficiency due to doping. The absence of data between 1 mM and 20 mM copper–nitrogen doping is probably the reason. According to the observations, a better optimal point for doping exists further to increase the efficiency of anodes.[137]

The same trend is observed in nitrogen–aluminum doping as well. However, as the doping increases and aluminum enters the TiO$_2$ lattice, a gradual fall in the peak intensities of the TiO$_2$ anatase phase is observed. This fall is an indication of anatase crystal growth obstruction. An appropriate combination of aluminum and nitrogen could effectively contribute to the efficiency. Higher doping causes severe agglomeration of the nanoparticles, leading to sluggish charge transfer and enhanced charge recombination. In this case, the codoping of aluminum and nitrogen leads to a gradual decrease in bandgap energies and an electron–hole lifetime.[79]

Nitrogen and lanthanum codoping leads to a decrease in charge transport resistance, which effectively increases the dye absorption of the photoanode. Besides, the formation of new bonds with N, O, and lanthanum causes an increase in the

disorder of the lattice structure of TiO$_2$ and the generation of trap states. Consequently, J_{sc} increases, which reflects in efficiency.[257]

Yttrium–nitrogen doping into TiO$_2$ shows a significant observation with an XPS scan. The TiO$_2$ anode shows a discrepancy in the amount of dopant added through precursors and dopant in the nanoparticles synthesized. When the nominal molar ratio of added precursors TiO$_2$–N–Y for synthesis is 100–100–0.5, the XPS observed concentrations of nitrogen and yttrium are 0.30% and 0.48%, which are different from the one we have prepared. Most studies with added precursors for doped products may have this discrepancy if the dopant ratio is not determined through the characterization technique. Nitrogen–yttrium doping also follows the same trend as other dopants in doping concentration and efficiency. The maximum efficiency is attained for a 100–300–0.5 nominal molar ratio combination sample. This is 18 percent higher compared to pure TiO$_2$ electrodes.[258]

Instead of producing an efficient DSSC, silver–sulfur codoped TiO$_2$ offered an environmentally conscious preparation approach. Even though 0.50% Ag was added for the codoping, XPS analysis showed that the anode had 0.75% silver in the atomic composition. Similar to our previous observations, when the anode had a doping concentration of 0.75% silver and 0.70% sulfur, it had the highest synergy and high-efficiency output.[259]

Zirconium doping with titanium increases the electron density and uplifts the Fermi level of TiO$_2$.[78] Tin is a

homovalent atom to zirconium. Similar to zirconium, tin also offers lower transport resistance.[81] The electron transport resistance decreases after tin doping and increases with fluorine doping. Impedance analysis shows that the dual doping increases interfacial charge recombination resistance. This resistance effectively decreases the recombination. A shorter transport time, measured with IMPS, implies a faster electron transport rate. The faster electron transport rate is favorable for charge collection and photocurrent density. The bonding may play a significant role in increasing efficiency as well. F atoms are bonded with the surface fivefold that of Ti, and the binding energy is 1 eV, showing strong chemisorption. Detailed density functional theory implementation gives more robust validation to existing arguments. Stronger bonding with Ti–F than Ti–O lowers the energy of the electrons of the valence band and leads to shifting the Fermi level towards the valence band and extending the bandgap. Both lead to the production of charge-trapping sites on the surface and subdue the charge recombination at the interface by holding trapped electrons, thus ending up in a longer electron lifetime. The longer electron lifetime is confirmed with IMVS measurements.[260]

Zirconium and nitrogen doping in TiO_2 results in high surface area, enhanced charge transfer, and reduced charge recombination in electrochemical devices. When P25 TiO_2 particles showed an efficiency of 8.32%, codoping with 0.01 zirconium and nitrogen increased the efficiency to 12.62%. While increasing the doping percentage of Zr/N in the anode, the efficiency of the cell decreased drastically. While the nitrogen doping shifts the absorption of TiO_2 into the visible light region, adding zirconium

amplifies the short-circuit current. The dip in the efficiency is not discussed in detail in the paper but is ambiguously correlated with the dye absorption. We conclude that an optimum efficiency point exists where various properties such as charge transfer resistance, less electron–hole recombination, and bandgap tuning increase the maximum attainable efficiency. Above this point, the doping could negatively affect the efficiency and properties of the TiO_2 anode.[261]

4.4. Bandgap tuning and codoping

Doping is considered to be the best option to tune the bandgap of any material.[77] When we introduce foreign materials into the TiO_2 lattice, they can alter the properties in both ways. The Burstein–Moss effect explains the increases in the bandgap when TiO_2 is doped with Cu, Ni, and Cr.[262] Here, doping populates the conduction band and pushes the absorption edge to higher energies, resulting in an increased bandgap. At lower doping concentrations, doping can decrease the band gap. Doping with different elements can introduce additional energy levels within the bandgap of the TiO_2. Subsequently, these levels will allow electrons with lower photon energy to reach the conduction band. Fig. 34 shows the quantitative relationship between the doped TiO_2 bandgap and the corresponding increase in efficiency. The V_{oc}, J_{sc}, PCE, and bandgap values of codoped TiO_2 are provided in Table 7. A more detailed dataset is provided in the ESI.† While the bandgap changes between 2.5 and 4 electron volts, the PCE increases to 6 percent, an enormous difference. Whenever the TiO_2 bandgap increases above 3, the efficiency tends to decrease. Finding the exact
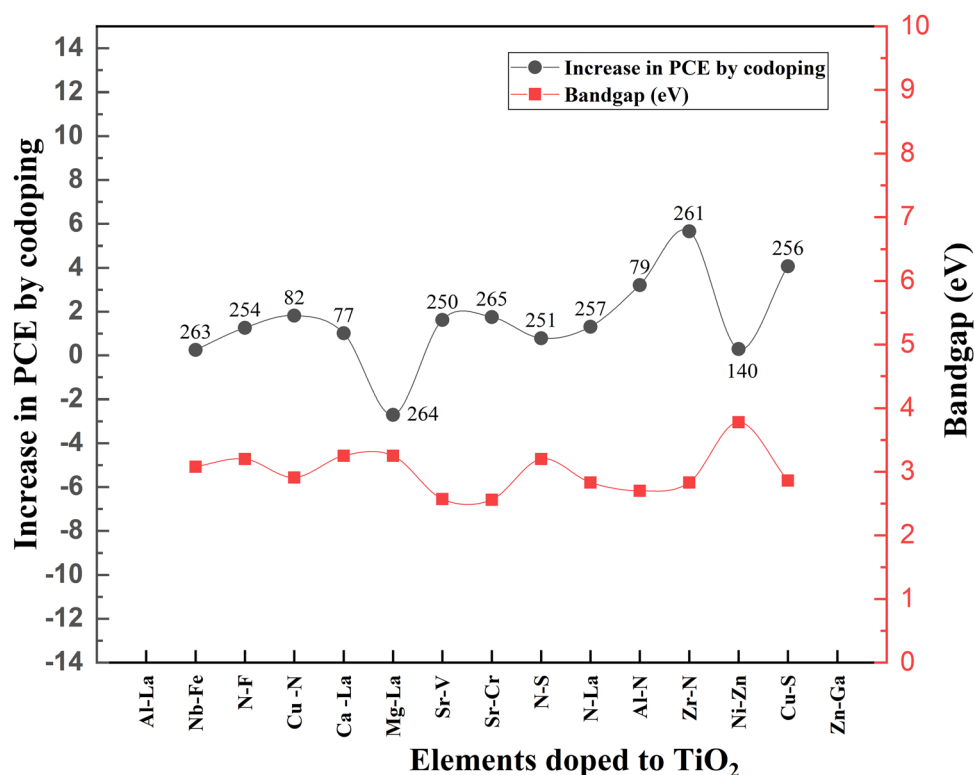

Fig. 34 The quantitative relationship between the bandgap and increase in PCE. Data points are labelled with references.

Table 7 Quantitative relationship between the bandgap and increase in PCE in numbers

S. no.	Elements doped into TiO$_2$	Bandgap (eV)	Increase in PCE through doping (%)	Ref.
1	Al–La	3.25	1.33	77
2	Nb–Fe	3.08	0.25	263
3	N–F	3.2	1.26	254
4	Cu–N	2.91	1.82	82
5	Ca–La	3.25	1.01	77
6	Mg–La	3.25	−2.7	264
7	Sr–V	2.57	1.62	250
8	Sr–Cr	2.56	1.75	265
9	N–S	3.2	0.78	251
10	N–La	2.83	1.31	257
11	Al–N	2.7	3.21	79
12	Zr–N	2.83	5.65	261
13	Ni–Zn	3.78	0.29	140
14	Cu–S	2.86	4.07	256
15	Zn–Ga	3.2	3.1	200

bandgap–efficiency relationship in electrochemical devices required extensive and pointed research in doping of TiO$_2$. Doping with zirconium and nitrogen tunes the bandgap to 2.83 eV, and the increase in the PCE is 5.65%. Doping TiO$_2$ with N–La, Al–N, Zr–N, and Cu–S tunes the bandgap around 2.7 to 2.86 eV. In this range, the efficiency is maximum for TiO$_2$ based devices.[79,256,257,261]

TiO$_2$ conduction band edges with doping Mg^{2+} ions are well studied, but La doping is not profound. The Mg–La doping increases the bandgap by 0.05 eV with doping. Contradictory to this, Ca–La and Al–La codoping results in the decrease of the bandgap. Lower V_{oc} values associated with Ca–La codoping in TiO$_2$ are found to reduce the bandgap. Nevertheless, all these band gap observations are made using Tauc plots, which could affect the accuracy of these measurements. A dopant with a smaller ionic radius than Ti^{4+} can enter the titanium lattice. When this dopant goes in, it can create more impurity levels and increase the recombination rate. Consequently, these impurity levels are due to the bandgap changes in the case of Al^{3+} and Mg^{2+}. Moreover, Ca^{2+} ions have larger ionic radii than Ti^{4+} ions and cannot enter the lattice and get blocked outside. Doping with Ca–La causes a decrease in bandgap and has a positive impact on charge transfer.[77,114]

In copper and sulfur codoping into TiO$_2$, the copper doping concentration changes while keeping the sulfur doping concentration at 0.05%. Their doping ratios are validated with EDAX. When the copper doping increases, the band gap of the doped sample is reduced due to the synergic effect of both dopants.

Table 8 Distribution of dopants in TiO$_2$ – summary with references

| Name of the element	Ionic state	Ionic radius (pm)	Lattice interaction	Ref.
Lithium	Li$^+$	76	Going into interstitial sites	86
Boron	B^{3+}	11	Going into interstitial sites	126
Nitrogen	N^{3-}	146	Substituting O^{2-}	239
Fluorine	F$^-$	133	Substituting O^{2-} and inducing Ti^{3+} formation	217
Magnesium	Mg^{2+}	83	Substituting Ti^{4+}	88
Aluminium	Al^{3+}	53.5	Substituting Ti^{4+}	77
Sulfur	S^{6+}	12	Complex behavior	245–247
Calcium	Ca^{2+}	100	Substituting Ti^{4+} and distorting the lattice	77
Scandium	Sc^{3+}	74.5	Substituting Ti^{4+}	127
Vanadium	V^{5+}	58	Substituting Ti^{4+}	147
Manganese	Mn^{2+}	83	Substituting Ti^{4+}	151
Chromium	Cr^{3+}	61	Substituting Ti^{4+} and producing Ti^{3+}	250
Iron	Fe^{3+}	64.5	Substituting Ti^{4+} and producing Ti^{3+}	153–155
Cobalt	Co^{2+}	74.5	Substituting Ti^{4+}	156
Nickel	Ni^{2+}	69	Substituting Ti^{4+}	136,158
Copper	Cu^{2+}	73	Substituting Ti^{4+} and producing Ti^{3+}	151,154,159
Zinc	Zn^{2+}	74	Substituting Ti^{4+}	200
Gallium	Ga^{3+}	62	Substituting Ti^{4+}	209
Strontium	Sr^{2+}	118	Substituting Ti^{4+}	99
Yttrium	Y^{3+}	90	Substituting Ti^{4+}	141,165,166
Zirconium	Zr^{4+}	72	Substituting Ti^{4+}	72,167
Niobium	Nb^{5+}	64	Substituting Ti^{4+}	171,172
Cadmium	Cd^{2+}	95	Substituting Ti^{4+}	144
Indium	In^{3+}	80	Substituting Ti^{4+}	199
Tin	Sn^{4+}	69	Substituting Ti^{4+}	203
Iodine	I^{5+}	95	Substituting Ti^{4+}	213,214
Tantalum	Ta^{5+}	64	Substituting Ti^{4+}	178
Tungsten	W^{4+}	66	Substituting Ti^{4+}	146
Bismuth	Bi^{3+}	103	Substituting Ti^{4+}	66,201
Lanthanum	La^{3+}	103	Surface interstitials	114–116
Neodymium	Nd^{3+}	98	Surface interstitials	117
Samarium	Sm^{3+}	95	Surface interstitials	104
Europium	Eu^{3+}	94.7	Surface interstitials	70,107
Gadolinium	Gd^{3+}	100	Surface interstitials	106
Terbium	Tb^{3+}	92	Surface interstitials	106
Erbium	Er^{3+}	89	Surface interstitials	108,109
Ytterbium	Yb^{3+}	86	Surface interstitials	107
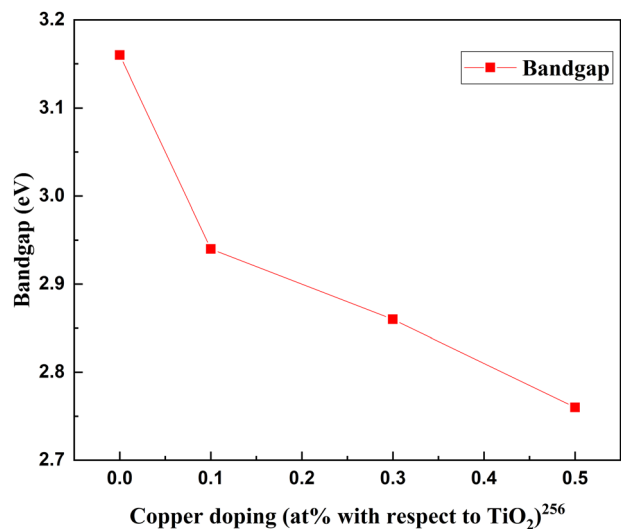
Fig. 35 Decrease in bandgap with Cu/S codoping.

The 3d and s species of copper hybridize with Ti-3d orbitals and produce localized defect levels above the maximum of the valence band. These defect levels effectively shift the valence band towards a longer wavelength. Impurity levels and oxygen doping can widen or narrow the bandgap.[256] Fig. 35 exemplifies the decrease in bandgap with Cu/S codoping.

Impedance measurements by intensity-modulated photocurrent spectroscopy (IMPS) and intensity-modulated voltage spectroscopy (IMVS) are standard techniques for understanding charge carrier kinetics in oxides. The time constant can be calculated from the impedance semicircle of the Nyquist plot. IMPS and IMVS analysis can provide electron lifetime and transport time details. IMPS spectra consist of two semicircles, one representing the trap limited transport time and the trap free transport time. The effect of doping can be determined from the trap mediated transport time and electron lifetime.

Doping TiO$_2$ with Fe has a shorter trap limited transport time and a longer electron lifetime than bare TiO$_2$. Nb–Fe codoped TiO$_2$ samples take longer trap limited transport times and longer electron lifetimes than the other samples. This observation leads to the guesstimation that during Fe doping of TiO$_2$, there is the formation of Ti^{3+} donors and Fe traps. Shallow Ti^{3+} donors cause shorter transport times, while Fe has multiple trapping and de-trapping events, causing a longer lifetime. Fe and Nb codoping introduces Nb^{5+} into the TiO$_2$ lattice, creating further shallow Ti^{3+} donors and Nb^{5+} traps. These shallow donors extend the electron lifetime through electron excitation and trapping transport, allowing more diffusion under illumination. Oxygen vacancies generated during doping can act in favor of or against the charge collection during transport. However, open circuit photo-potential transient analysis shows that the Nb addition to Fe-doped TiO$_2$ facilitates charge relaxation through the passivation of deep oxygen vacancies generated by Fe doping. So, considering the OCP analysis, deep oxygen vacancies in the shallow levels may favor electron capture and de-trapping during photoexcitation.[134]

Doping TiO$_2$ with Fe does not contribute much to bandgap engineering. Nevertheless, doping with Fe and Nb together significantly tunes the valence band position. The Nb doping reduces the bandgap by 0.01 eV, and the valence band position shifts to 0.11 eV. There are also similar effects on the conduction band edge. Even though the final bandgap of TiO$_2$ does not seem affected, there is an influential band re-tuning with the codoping. Only doping, donor generation, and trap state generation can account for this bandgap tuning.

Nitrogen and sulfur codoping also shows a reduction in the bandgap. Nitrogen is responsible for bandgap reduction, and sulfur facilitates the electron transfer process. Considering strontium and vanadium codoping, V doping into TiO$_2$ ends up in the stoichiometric reduction of Ti^{4+}. Vanadium is also responsible for the formation of isolated energy levels near the conduction and valence bands, contributing to the PCE. The reduction facilitated by V leads to increased carrier density and improvement in photoresponse. At the same time, introducing strontium, a relatively high ionic radius ion (Sr^{2+}), causes distortions in the TiO$_2$ lattice. These distortions accumulate oxygen vacancies across the lattice and extend the life of photoexcited electrons and holes. Chromium doping introduces isolated energy levels near conduction and valence bands like V. The reason for these isolated energy levels is excess holes. These holes are responsible for the acceptor band near the TiO$_2$ valence band.[250–252,265]

Similar to copper–sulfur doping, zirconium–nitrogen codoping causes an increase and decrease in the bandgap.[261] Fig. 36 shows the Zr/N doping concentration in TiO$_2$ and the corresponding change in the bandgap.

This study argues that the change in bandgap is connected with particle size variation (Fig. 37). When the particle size increases, the bandgap decreases. Simultaneously the reduction in bandgap results in increased cell efficiency. On the other hand, aluminum–nitrogen doping shows a similar bandgap trend to Zr/N.[79] There is a limitation to concluding the doping
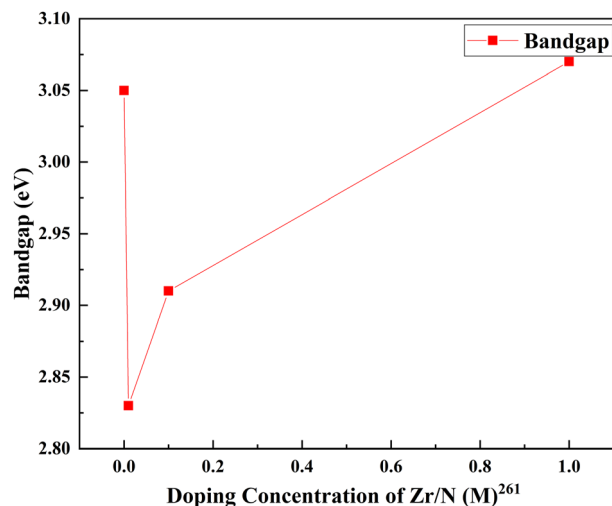

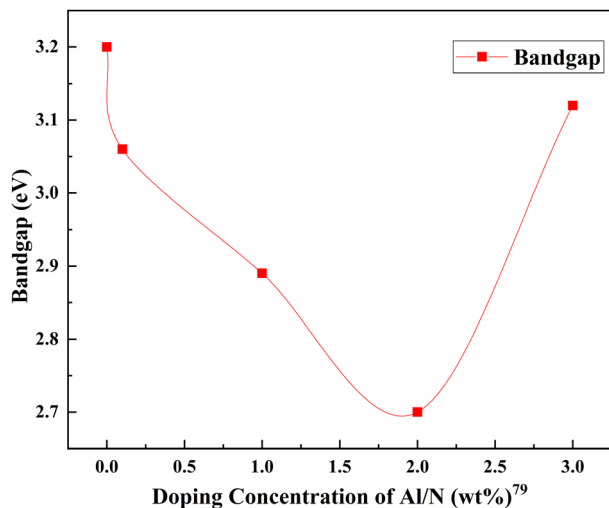**Fig. 36** Zr/N doping concentration in TiO$_2$ and the corresponding change in bandgap.

Fig. 37 Doping concentration *vs.* bandgap.

concentration and bandgap relationship due to the non-uniformity of reported doping concentration units. Fig. 36 roughly describes the connection between the bandgap and doping concentration. More or less, each dopant pair shows a decrease in the bandgap when materials are added in small amounts. However, adding materials beyond an optimum point decreases the doping effect and increases the bandgap.

5. Composite doping

Composite materials are macroscopic combinations of two or more distinct materials having a finite interface. They have been introduced into several industries in diverse forms. Doping and adding composites into TiO_2 have attracted considerable attention since they have significantly increased the PCE of DSSCs. Adding various composite nanostructures into TiO_2, including nanoparticles, nanobelts, and nanofibers, through different synthesis methods has advantages in tailoring its properties. Creating TiO_2-elemental composites plays a significant role in the flexibility and performance of the resulting material. In some studies a significantly low amount of material is added into TiO_2 for better performance. This is called composite doping. This composite impurity added to the TiO_2 can alter the photoanode performances and increase the efficiency. Composite dopants include metal composites, MW CNT composites, semiconductor composites, polymer carbon nitride composites, carbonate composites, and amine composites.[266–269]

Functional nanocomposites involving metals improve the photocatalytic electron transfer process. Semiconductor–metal composites can sustain charge separation to a great extent. When Pt creates an ohmic type contact with ZnO, Au–ZnO creates a Schottky type contact.[270,271] Introducing Au into bulk TiO_2 and producing a metal nanoparticle composite reduces charge recombination, increases thermal and chemical stability, and inhibits non-radiative quenching.[272] In this case, the Au–TiO_2 composite has higher absorption due to the surface plasmon effect provided by Au. In another study, 0 to 0.6 wt% of

Ag nanowires coated with SiO_2 were applied to TiO_2. The strength of the material, photon capture ability, and J_{sc} were significantly increased.[273] F. Zheng and Z. Zhu showed that Au nanoparticles in TiO_2 nanofibers exhibited broad surface plasmonic absorption. The Au concentration in the anode conversely affected the DSSC performance beyond the optimum loading.[274] Considering the available metal composite data, a N,S codoped silver nanoparticles decorated photoanode showed an exceptional increase in PCE. When the control sample (bare TiO_2 based) had 2.57 percentage efficiency, a codoped composite sample-based DSSC exhibited 8.22 percentage efficiency. The concentration of Ag NPs plays a dynamic role in the efficiency of the DSSC. When N,S doping reduced the bandgap, shifted the optical absorption towards the visible region, and suppressed the charge recombination, Ag nanoparticles harvested more light owing to the surface plasmon effect. The synergetic effect of codoping and Ag silver nanoparticles amplified the photocurrent generation, and consequently the efficiency of the DSSC.[252] Fig. 38 compares the effect of metal composite doping on the percentage increase in PCE.

TiO_2, dyes, and electrolyte interfaces have been studied since the beginning of the DSSC invention. Significant research is on the electron injection from dyes into the conduction band of TiO_2 since it is a crucial mechanism in determining efficiency. Various semiconductors were developed and deposited over TiO_2 to modulate the interfacial properties. Some include metal oxide semiconductors with wide bandgaps such as NiO, Bi_2S_3:Eu^{3+}, Cu_2O, NiO, NiO:Eu+Tb, and ZnO nanobelts. ZnO and TiO_2 exhibit identical physical properties and bandgap values. The electron mobility and crystallization ability of ZnO are better than those of TiO_2. But ZnO-based photoanodes have comparatively lower PCEs than TiO_2 based DSSCs. This is primarily due to the poor dye-ZnO electron injection kinetics. The synergy of ZnO nanobelts and TiO_2 contributes to PCE by improving charge transfer efficiency and large surface area. ZnO nanobelt@TiO_2 also shows an increased carrier lifetime and fast electron transfer.[269]

Similarly, Bi_2S_3:Eu^{3+} can act as the down-conversion luminescent composite anode material. Bi_2S_3 transfers electrons to TiO_2, and the Eu^{3+} metal ion improves photocatalytic performance. P-type NiO is a wide bandgap semiconductor that is thermally and chemically stable. A photoanode, a combination of NiO and TiO_2, enhances the charge separation and increases the PCE.[275] These samples—Bi_2S_3:Eu, NiO, NiO: Eu, and Tb—display excellent efficiency and only a slight increase in PCE due to composite doping. On the other hand, Cu_2O shows a tremendous increase in PCE. Cu_2O studies have been conducted by fabricating QDSSC, CdS, and ZnS layers. Cu_2O is one of the most potential p-type semiconductors for photovoltaic applications. It has high charge mobility and high minority carrier diffusion length. When the control QDDSC shows mere 1.17% efficiency, a Cu_2O incorporated QDDSC offers 3.01% efficiency. Contrary to the PCE, the effect of adding Cu_2O is much higher.[276] Fig. 39 shows the increase in PCE with each semiconductor composite dopant we have discussed.

Carbon nitrides, carbonate groups, amines, and carbon nanotubes have also been used for creating composites. A graphene–C_3N_4–TiO_2 composite exhibits a 29.3% improvement in PCE when used as a photoanode in a QDSSC. It has a suitable band structure
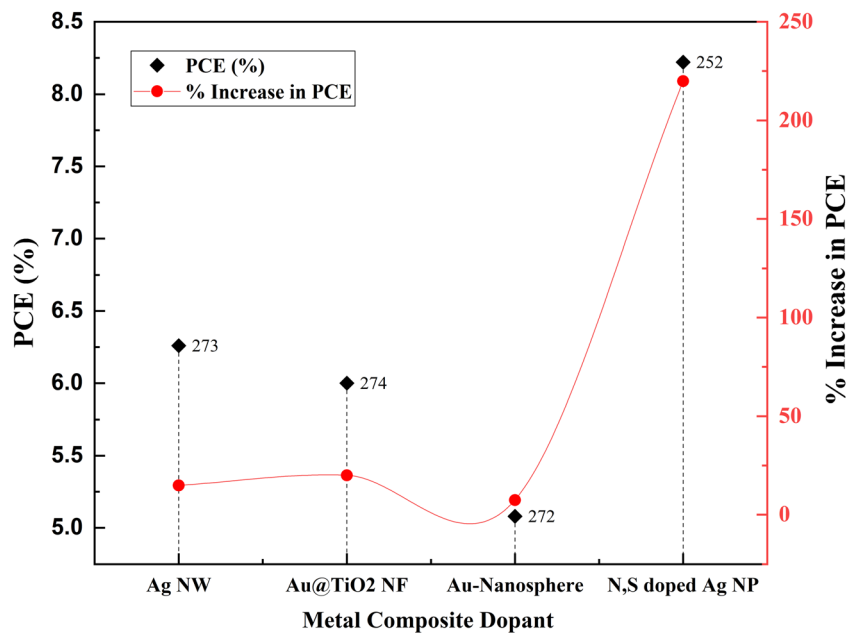
Fig. 38 Metal composites and percentage increases in PCE. Data points are labelled with references.
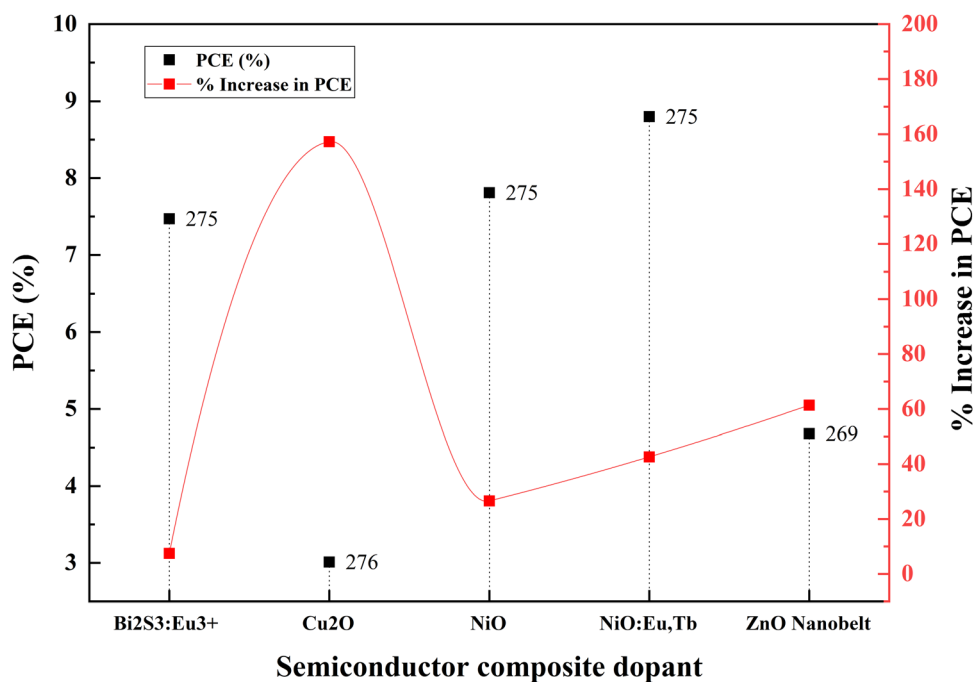

Fig. 39 Increase in PCE with different semiconductor composite dopants. Data points are labelled with references.

and chemical-thermal stability for use as a photoanode. This material increases the roughness and makes the loading of CdS QDs easier.[268]

When comparing the efficiencies of other composite dopants, the efficiency of g-C$_3$N$_4$@TiO$_2$ seems to be less. There are two studies on carbonate doped TiO$_2$: one in 2016 and the other in 2018.[227,277] Carbonate doping results in a structure called a carbonate doped mesoporous microstructure (doped MS). A carbonate-doped mesosphere structure-based DSSC has higher PCE than carbonate doped MS nanospheres. Nevertheless, the increase in PCE is more in DSSCs based on carbonate based MS nanospheres.[227] Carbonate doping produces a band tail state which effectively reduces the bandgap. Carbonates increase porosity and decrease electron recombination, and enhance the redox coupling. In the case of a carbonate-MS-NS@TiO$_2$-based photoanode, the carbonate reduced the internal cell resistance and improved the electron lifetime. The reduced internal cell resistance led to high light absorption and fast electron transport
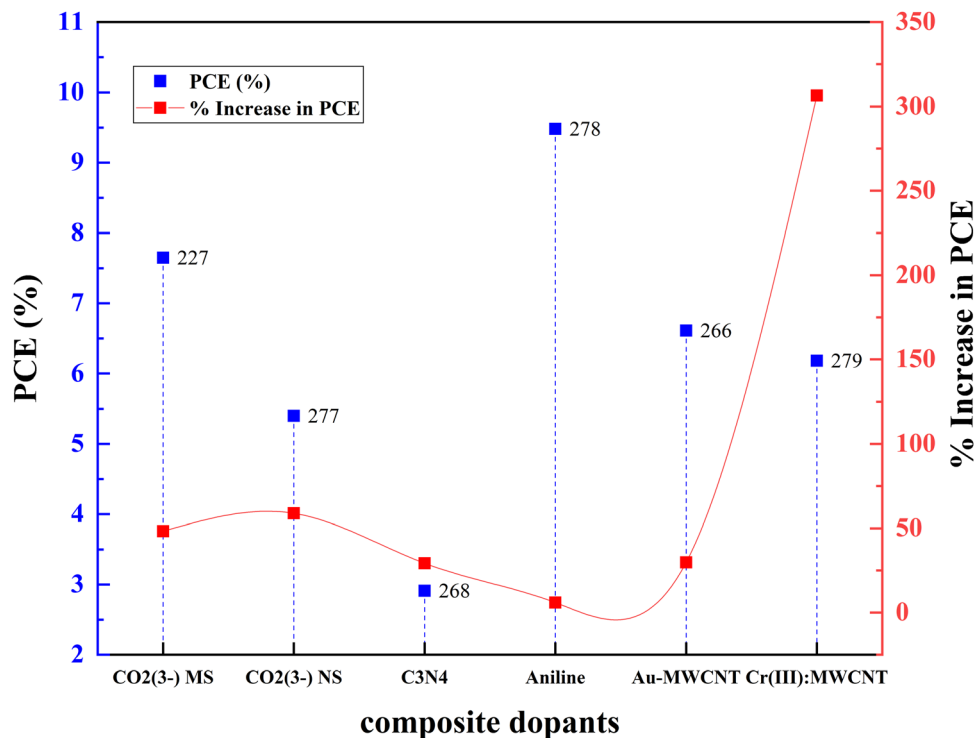
Fig. 40 Increase in PCE with different composite dopants. Data points are labelled with references.

in carbonate based DSSCs.[277] Fig. 40 shows the increase in PCE with different composite dopants such as carbonates, amines, and carbon nanotubes.

Aniline, an amine, has recently been doped into TiO_2 to achieve better photocurrent generation. Reduction of TiO_2 nanocrystal size using long-chain monoamines decreases the transmission. Amine capping improves efficiency and increases light scattering to a great extent. Amine groups such as aniline and o-phenylenediamine have active sites that can enhance PCE. The ability of nonmetal dopant's N2p and O2p orbitals to modify TiO_2 and reduce the deposition in interstitial sites has drawn attention towards non-metal doping. The operational strategy behind amine group doping is to improve photocurrent generation, increase electron transfer dynamics and reduce recombination in the scattering layer. It has long been known that amines affect morphology (by controlling TiO_2 size and providing an increased surface area) as well as reflectivity and PCE.[278] In this study, aromatic amine passivated TiO_2 is prepared through a hydrothermal method. After amine capping, there is a reduction in crystallinity, and broadening in the XRD peak. Due to the formation of coordination bonds, there is a shift observed in the XRD peak. From reflectance studies, it is evident that amines increase the absorbance. By using FTIR, it is clear that the broadened N–H stretching reveals the fermi resonance of N–H and O–H peaks. The overlapping of N–H and Ti–OH bonds confirms the presence of aromatic amines in the TiO_2 lattice. The increase in reflectivity is due to the amines attached to the crystal surface. These amines reduce light penetration into the TiO_2 surface and the pi electrons in aromatic rings absorb light. This effectively reduces the

scattering and increases the absorption.[267] However, the control cell efficiency and amine-doped photoanode-based cell efficiency are high. The effect of amine capping is insignificant compared to other composite dopants.[267]

Cr(III) doping into TiO_2/MWCNTs results in an incredible increase in PCE. Impurities in the TiO_2 lattice act as charge trapping sites and improve the rate of charge transport in DSSCs. MWCNT@TiO_2 alone increases the efficiency by 4.6 percent. The percentage increase in PCE is around 300%. When Cr(III) is added to the matrix, the percentage increases from 6.18% to 7.69%. The overall increase in efficiency becomes 6.17 percent, which is around a 400 percent increase.[279] Au nanoparticles and MWCNT composites also enhance the PCE by 30 percent. Compared with Cr(III), this is less. However, the control DSSC cell efficiency is higher here (5.09%) than the Cr(III)@MWCNT composite (1.52%). An Au@MWCNT composite-based DSSC has comparable efficiency (6.61%). This improvement in efficiency is attributed to the synergetic effect of Au and MWCNTs through improved charge generation and enhanced light absorption.[266]

6. Dopant distribution in the TiO_2 lattice – summary

Numerous studies have examined how dopants are distributed and where they are located within the TiO_2 lattice. This positioning information is collected from XPS, FTIR and XRD observations. The TiO_2 lattice can integrate a dopant to:

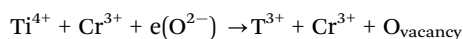(a) Substitute Ti^{4+},
(b) Substitute Ti^{4+} and produce Ti^{3+},

(c) Substitute O^{2-},

(d) Substitute O^{2-} and induce Ti^{3+} formation,

(e) Go into interstitial sites and

(f) Go into surface interstitials.

The ionic radius of the dopant is a critical factor influencing the nature of doping. Dopants with a comparable atomic size of Ti^{4+} substitute it and causes slight rearrangements and distortions in the lattice. In rare cases, these substitutions lead to the surge of Ti^{3+} in the lattice. The ionic radius depends on factors such as coordination number, spin state, crystal radius, and electron configuration. Even in detailed ionic radius studies, if there is an uncertainty in coordination number or a deviation from the radius *vs.* valence plots then the obtained ionic radius values may not be that reliable.[280] Keeping that aside, a significant number of dopants replace Ti^{4+} such as Mg^{2+}, Ca^{2+}, Sr^{2+}, Sc^{3+}, Y^{3+}, Zr^{4+}, V^{5+}, Nb^{5+}, Ta^{5+}, W^{4+}, Cr^{3+}, Mn^{2+}, Fe^{3+}, Co^{2+}, Ni^{2+}, Cu^{2+}, Zn^{2+}, Cd^{2+}, In^{3+}, Sn^{4+}, Bi^{3+}, and Al^{3+}. Among these, bigger ionic radius atoms such as Sr^{2+}, Bi^{3+}, and Ca^{2+} cause lattice distortions and changes in crystalline information.

It has been suggested that replacing Ti^{4+} ions may result in Ti–O–Cr structures and oxygen vacancies. This Ti^{4+} withdraws electrons from superficial hydroxyl groups and reduces to Ti^{3+}:

$$Ti^{4+} + Cr^{3+} + e(O^{2-}) \rightarrow T^{3+} + Cr^{3+} + O_{vacancy}$$

Iron (Fe^{2+}) and copper (Cu^{2+}) also result in the creation of Ti^{3+} trap states, just like chromium (Cr^{3+}) does. In a way analogous to this, fluorine (F^-) substitutes oxygen and produces Ti^{3+} ions, improving the effectiveness of charge collection. Due to its great electronegativity, it interferes with the CB of TiO_2 and prevents electron recombination. Since oxygen (O^{2-}) and nitrogen (N^{3-}) have similar ionic sizes, nitrogen

can easily replace oxygen. There are some conflicts regarding the oxidation state and position of nitrogen dopant in the TiO_2 lattice. The presence of Ti–O–N bonding indicates the presence of N^- ions.[55,224,229–231,281] FTIR, XPS, and XRD studies show that lithium (Li^+) and boron (B^{3+}) are introduced into the interstitial sites.

Some researchers claim that no rare earth elements can pass through the TiO_2 lattice due to the larger ionic size. They either form Ti–O–La bonding on the surface or are in the surface interstitials of TiO_2. This bonding increases the surface area and oxygen vacancies of TiO_2. When doped with rare earth elements, photovoltaic devices that use TiO_2 perform better. When doped, La^{3+}, Nd^{3+}, Sm^{3+}, Eu^{3+}, Gd^{3+}, Tb^{3+}, Er^{3+}, and Yb^{3+} remain in the surface interstitials.

Sulfur shows a peculiar behavior when doped into TiO_2. It is challenging to establish the oxidation state of sulfur when doped.[223] Although sulphur has oxidation states ranging from S^{6+} to S^{2-}, there is no evidence that S^{2-} (1.7 Å) would replace O^{2-} (1.22 Å) atoms; instead, S^{6+} (0.29 Å) would replace Ti^{4+} (0.64 Å). In addition, O^{2-} and Ti^{4+} ions with various oxidation states might get randomly substituted, significantly disturbing the lattice.[245,246] The entire discussion is summarized in Fig. 41, which illustrates the distribution of dopants in the TiO_2 lattice.

7. Conclusion

This review developed a framework to analyze the doping of TiO_2 based on the PCE of sensitized solar cells. This review helps researchers to identify, analyze and plan doping in TiO_2 electrode-based power sources. Beyond this review, this framework can be used for all electrochemical systems, including hydrogen generation, supercapacitors, and batteries. We

Fig. 41 Distribution of dopants in TiO_2 (references provided in Table 8).

identified and summarized significant elements in the periodic table doped into TiO_2 and their effect on the material's PCE, J_{sc}, V_{oc}, FF, and morphology.

We compiled information on TiO_2 dopants, such as the treatment/coating used, sub-type of doping, structure, synthesis and fabrication method, V_{oc} (V), photocurrent density (mA cm^{-2}), FF, PCE (%), percentage increase in efficiency due to doping, bandgap (eV), application, sensitizer/dye, and periodic classification of element types (which are included in each section). We have 106 observations where single-element doped TiO_2 is used for developing DSSCs, 34 data points where codoped TiO_2 is used when making DSSCs, and 15 data points where composite doped TiO_2 is employed to fabricate DSSCs. According to our knowledge, this is the largest, complete information data set available until now.

Doping is not merely creating a change in electronic band structure; rather, it is altering the morphology and distribution of atoms throughout the lattice, and how these factors affect PCE. Throughout the review, we discussed how doping impacts the TiO_2 crystal structure, alters the bandgap, and affects PCE. According to electron transfer dynamics studies, the morphology of the crystal surface influences the inhomogeneous distribution of the conduction band.[27,29] Fig. 42 features how doping increases and decreases PCE. In general, all the post-transition element dopants, nitrogen, Al–La, Zr–N, and Ca–La (codopants)

show high charge transfer resistance compared to other dopants. It is also found that bigger atoms that are not able to penetrate the lattice facilitate the charge transfer process.

Three main factors which affect the PCE have been identified as the concentration of dopant, the size of doped TiO_2 particles, and the band gap of the doped TiO_2 electrode. The concentration of dopant is critical in the doping procedure. The concentration of dopant affects the size of dopant, recombination rate, transport rate, film resistance, diffusion coefficient, and oxygen vacancies. These effects are discussed with examples of Sr, Gd, Sc, V, Zr, and Nb doping.[99,106,127,145,170,184,228] The efficiency decreases when the dopant concentration is below or above an optimum amount. The challenge involved in doping is finding the optimum point of peak performance. Having a control sample is necessary to understand the research progress in global standards. Many research papers lack data on the bare TiO_2-based control cell to compare the doping effect and understand the role of doping in PCE. V_{oc}, J_{sc}, or FF alone is not enough to comprehend the effect of doping. We need to determine the increase in PCE from that of the control-based DSSC sample. However, to summarize, V_{oc} is increased using Mg, Cu, Nb, W, Ga, In, N, and S-doped TiO_2, whereas Zr, Ag, and Ca–La doped TiO_2 reduce V_{oc}. The short circuit current increases in Sr, B, Sb, Nb, I, N, S, N–L, Ag, and Au-doped TiO_2, but the J_{sc} decreases in Mg-doped TiO_2.
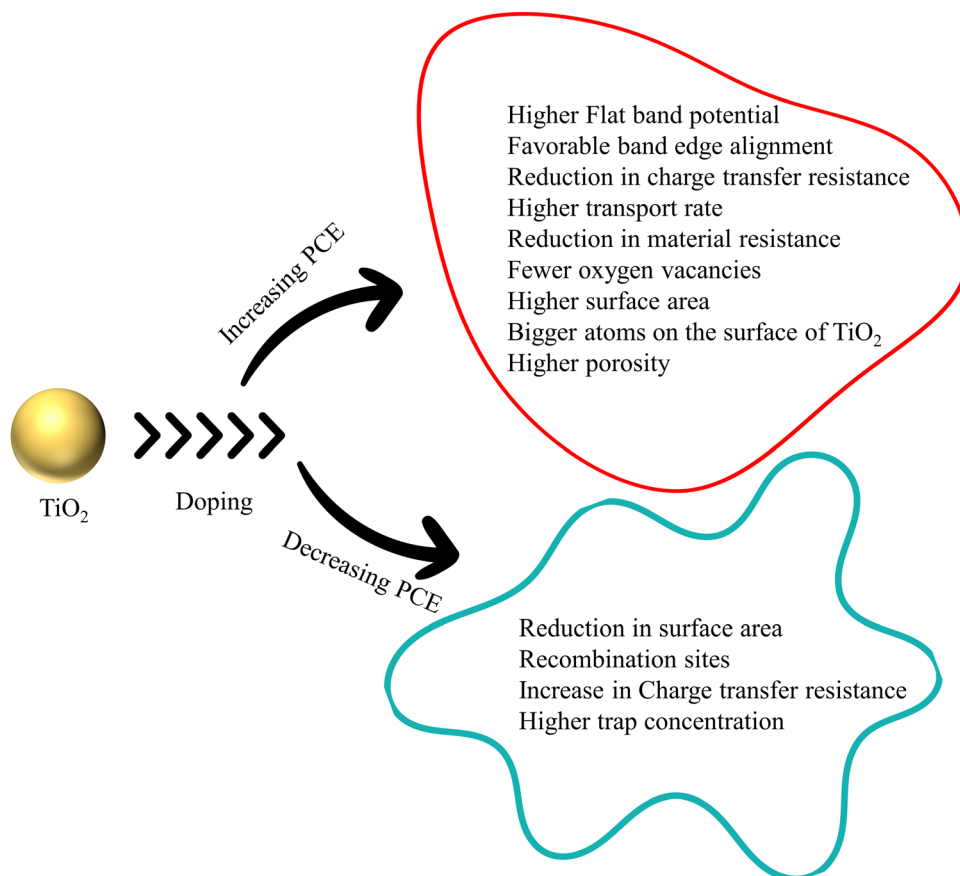

Fig. 42 Summary of TiO_2 doping.

The size and morphology of the doped samples are altered by doping. As a result of doping, nanoparticles, nanowalls, nanotubes, nanowires, and nanoflower structures have been created. The doped material has optimum dimensions that provide the highest PCE, similar to the concentration's influence on PCE. When the dimensions increase above this optimum point, the PCE is drastically reduced. The particle/crystallite size and doping concentration impact PCE. A material's bandgap has an impact on its electrical and optical characteristics. The PCE increases as the bandgap narrows. Some scientists contend that the bandgap influences PCE as a result of the bandgap influencing crystallite size.

Among all of the doping methods, codoping might be referred to as sensible doping. Codoping correlates the synergistic effect of two or more dopants, contributes to both V_{oc} and J_{sc} simultaneously, and improves PCE. Single dopants contribute to either V_{oc} or J_{sc}. Their synergetic effect also contributes to thermal stability, reduction in the bandgap, and enhanced surface area. One element enhances the short-circuit current, boosts electron transfer, and minimizes carrier recombination. The other element contributes to V_{oc}, provides isolated energy levels close to the conduction band, lowers the bandgap, and participates in codoping. Codoping significantly boosts carrier density and enhances photoresponse.

Regarding green energy technology, doping has a bright future in research and applications. A negligible amount of resources can alter the properties of non-toxic, abundant semiconductors so they serve as excellent light-harvesting energy materials. This review has the highest PCE data to the authors' best knowledge. It gives a holistic view of doping of TiO_2 based on PCE in sensitized solar cells. This review will help future researchers understand the role of TiO_2 dopants in PCE.

Author contributions

Prasanth Ravindran – supervision and writing (review & editing). Aparna Markose and Debanita Das – conceptualization, data curation, investigation, methodology, writing, and data analysis – (original draft). Aparna Markose – visualization and graphics.

Conflicts of interest

The authors declare no conflict of interest.

Acknowledgements

References

1 C. C. Raj and R. Prasanth, Review—Advent of TiO_2 Nanotubes as Supercapacitor Electrode, *J. Electrochem. Soc.*, 2018, **165**(9), E345–E358.

2 C. C. Raj, R. Sundheep and R. Prasanth, Enhancement of Electrochemical Capacitance by Tailoring the Geometry of TiO_2 Nanotube Electrodes, *Electrochim. Acta*, 2015, **176**, 1214–1220.

3 M. Grätzel, Photoelectrochemical Cells, *Nature*, 2001, **414**, 338–344.

4 M. Grätzel, Solar Energy Conversion by Dye-Sensitized Photovoltaic Cells, *Inorg. Chem.*, 2005, **44**(20), 6841–6851.

5 A. G. Vega Poot, D. Reyes Coronado and G. Oskam, Application of Three TiO_2 Polymorphs in Photoelectrochemical Solar Cells, *ECS Meet. Abstr.*, 2006, **MA2006-02**(38), 1737.

6 M. Zhang, T. Chen and Y. Wang, Insights into TiO_2 Polymorphs: Highly Selective Synthesis, Phase Transition, and Their Polymorph-Dependent Properties, *RSC Adv.*, 2017, **7**(83), 52755–52761.

7 T. Zhu and S. P. Gao, The Stability, Electronic Structure, and Optical Property of TiO_2 Polymorphs, *J. Phys. Chem. C*, 2014, **118**(21), 11385–11396.

8 A. J. Frank, N. Kopidakis and J. V. D. Lagemaat, Electrons in Nanostructured TiO_2 Solar Cells: Transport, Recombination and Photovoltaic Properties, *Coord. Chem. Rev.*, 2004, **248**(13–14), 1165–1179.

9 B. O'Regan and M. Graetzel, A Low-Cost, High-Efficiency Solar Cell Based on Dye-Sensitized Colloidal TiO_2 Films, *Nature*, 1991, **354**, 737–740.

10 H. Tributsch and M. Calvin, Electrochemistry of Excited Molecules: Photo-Electrochemical Reactions of Chlorophylls, *Photochem. Photobiol.*, 1971, **14**(2), 95–112.

11 B. N. Dimarco, R. N. Sampaio, E. M. James, T. J. Barr, M. T. Bennett and G. J. Meyer, Efficiency Considerations for SnO_2-Based Dye-Sensitized Solar Cells, *ACS Appl. Mater. Interfaces*, 2020, **12**(21), 23923–23930.

12 A. Le Viet, R. Jose, M. V. Reddy, B. V. R. Chowdari and S. Ramakrishna, Nb_2O_5 Photoelectrodes for Dye-Sensitized Solar Cells: Choice of the Polymorph, *J. Phys. Chem. C*, 2010, **114**(49), 21795–21800.

13 D. Devadiga, M. Selvakumar, P. Shetty and M. S. Santosh, Dye-Sensitized Solar Cell for Indoor Applications: A Mini-Review, *J. Electron. Mater.*, 2021, **50**(6), 3187–3206.

14 U. Mehmood, Z. Malaibari, F. A. Rabani, A. U. Rehman, S. H. A. Ahmad, M. A. Atieh and M. S. Kamal, Photovoltaic Improvement and Charge Recombination Reduction by Aluminum Oxide Impregnated MWCNTs/TiO_2 Based Photoanode for Dye-Sensitized Solar Cells, *Electrochim. Acta*, 2016, **203**, 162–170.

15 V. Rondán-Gómez, I. Montoya De Los Santos, D. Seuret-Jiménez, F. Ayala-Mató, A. Zamudio-Lara, T. Robles-Bonilla and M. Courel, Recent Advances in Dye-Sensitized Solar Cells, *Appl. Phys. A: Mater. Sci. Process.*, 2019, **125**(12), 1–24.

16 M. Freitag, J. Teuscher, Y. Saygili, X. Zhang, F. Giordano, P. Liska, J. Hua, S. M. Zakeeruddin, J.-E. Moser and

M. Grätzel, *et al.*, Dye-Sensitized Solar Cells for Efficient Power Generation under Ambient Lighting, *Nat. Photonics*, 2017, **11**(6), 372–378.

17 C. Arrouvel and S. C. Parker, Investigating Surface Properties and Lithium Diffusion in Brookite-TiO$_2$, *J. Braz. Chem. Soc.*, 2020, **31**(1), 51–65.

18 B. O'regan and M. Grätzel, A Low-Cost, High-Efficiency Solar Cell Based on Dye-Sensitized Colloidal TiO$_2$ Films, *Lett. Nat.*, 1991, **353**, 737–740.

19 J. J. Cid, J. H. Yum, S. R. Jang, M. K. Nazeeruddin, E. Martínez-Ferrero, E. Palomares, J. Ko, M. Grätzel and T. Torres, Molecular Cosensitization for Efficient Panchromatic Dye-Sensitized Solar Cells, *Angew. Chem., Int. Ed.*, 2007, **46**(44), 8358–8362.

20 H. J. Snaith, Estimating the Maximum Attainable Efficiency in Dye-Sensitized Solar Cells, *Adv. Funct. Mater.*, 2010, **20**(1), 13–19.

21 S. Ardo and G. J. Meyer, Photodriven Heterogeneous Charge Transfer with Transition-Metal Compounds Anchored to TiO$_2$ Semiconductor Surfaces, *Chem. Soc. Rev.*, 2009, **38**(1), 115–164.

22 A. Hagfeldt and M. Grätzel, Light-Induced Redox Reactions in Nanocrystalline Systems, *Chem. Rev.*, 1995, **95**(1), 49–68.

23 *Nanostructured and Photoelectrochemical Systems for Solar Photon Conversion*, ed. M. D. Archer and A. J. Nozik, Imperial College Press, 2008.

24 J. R. Durrant, S. A. Haque and E. Palomares, Towards Optimisation of Electron Transfer Processes in Dye Sensitised Solar Cells, *Coord. Chem. Rev.*, 2004, **248**(13–14), 1247–1257.

25 S. A. Haque, E. Palomares, B. M. Cho, A. N. M. Green, N. Hirata, D. R. Klug and J. R. Durrant, Charge Separation versus Recombination in Dye-Sensitized Nanocrystalline Solar Cells: The Minimization of Kinetic Redundancy, *J. Am. Chem. Soc.*, 2005, **127**(10), 3456–3462.

26 N. A. Andersen and T. Lian, Ultrafast Electron Transfer at the Molecule-Semiconductor Nanoparticle Interface, *Annu. Rev. Phys. Chem.*, 2005, **56**(78), 491–519.

27 A. Listorti, B. O'Regan and J. R. Durrant, Electron Transfer Dynamics in Dye-Sensitized Solar Cells, *Chem. Mater.*, 2011, **23**(15), 3381–3399.

28 Y. Q. Gao and R. Marcus, On the theory of electron transfer reactions at semiconductor/liquid interfaces. II. A free electron model, *J. Chem. Phys.*, 2000, **113**(15), 1–3.

29 R. Katoh, A. Furube, A. V. Barzykin, H. Arakawa and M. Tachiya, Kinetics and Mechanism of Electron Injection and Charge Recombination in Dye-Sensitized Nanocrystalline Semiconductors, *Coord. Chem. Rev.*, 2004, **248**(13–14), 1195–1213, DOI: 10.1016/j.ccr.2004.03.017.

30 X. Zhang, J. J. Zhang and Y. Y. Xia, Molecular Design of Coumarin Dyes with High Efficiency in Dye-Sensitized Solar Cells, *J. Photochem. Photobiol., A*, 2008, **194**(2–3), 167–172.

31 K. Hara, T. Sato, R. Katoh, A. Furube, Y. Ohga, A. Shinpo, S. Suga, K. Sayama, H. Sugihara and H. Arakawa, Molecular Design of Coumarin Dyes for Efficient Dye-Sensitized Solar Cells, *J. Phys. Chem. B*, 2003, **107**(2), 597–606.

32 T. Santos, A. Dos Morandeira, S. Koops, A. J. Mozer, G. Tsekouras, Y. Dong, P. Wagner, G. Wallace, J. C. Earles and K. C. Gordon, *et al.*, Injection Limitations in a Series of Porphyrin Dye-Sensitized Solar Cells, *J. Phys. Chem. C*, 2010, **114**(7), 3276–3279.

33 K. Hara, Z. S. Wang, T. Sato, A. Furube, R. Katoh, H. Sugihara, Y. Dan-Oh, C. Kasada, A. Shinpo and S. Suga, Oligothiophene-Containing Coumarin Dyes for Efficient Dye-Sensitized Solar Cells, *J. Phys. Chem. B*, 2005, **109**(32), 15476–15482.

34 A. Morandeira, I. López-Duarte, M. V. Martínez-Díaz, B. O'Regan, C. Shuttle, N. A. Haji-Zainulabidin, T. Torres, E. Palomares and J. R. Durrant, Slow Electron Injection on Ru-Phthalocyanine Sensitized TiO$_2$, *J. Am. Chem. Soc.*, 2007, **129**(30), 9250–9251.

35 S. E. Koops, B. C. O'Regan, P. R. F. Barnes and J. R. Durrant, Parameters Influencing the Efficiency of Electron Injection in Dye-Sensitized Solar Cells, *J. Am. Chem. Soc.*, 2009, **131**(13), 4808–4818.

36 H. N. Ghosh, J. B. Asbury and T. Lian, Direct Observation of Ultrafast Electron Injection from Coumarin 343 to TiO$_2$ Nanoparticles by Femtosecond Infrared Spectroscopy, *J. Phys. Chem. B*, 1998, **102**(34), 6482–6486.

37 S. Pelet, M. Grätzel and J. E. Moser, Femtosecond Dynamics of Interfacial and Intermolecular Electron Transfer at Eosin-Sensitized Metal Oxide Nanoparticles, *J. Phys. Chem. B*, 2003, **107**(14), 3215–3224.

38 R. J. Ellingson, J. B. Asbury, S. Ferrere, H. N. Ghosh, J. R. Sprague, T. Lian and A. J. Nozik, Dynamics of Electron Injection in Nanocrystalline Titanium Dioxide Films Sensitized with [Ru(4,4′-Dicarboxy-2,2′-Bipyridine)$_2$(NCS)$_2$] by Infrared Transient Absorption, *J. Phys. Chem. B*, 1998, **102**(34), 6455–6458.

39 Y. Tachibana, J. E. Moser, M. Grätzel, D. R. Klug and J. R. Durrant, Subpicosecond Interfacial Charge Separation in Dye-Sensitized Nanocrystalline Titanium Dioxide Films, *J. Phys. Chem.*, 1996, **100**(51), 20056–20062.

40 J. B. Asbury, E. Hao, Y. Wang, H. N. Ghosh and T. Lian, Ultrafast Electron Transfer Dynamics from Molecular Adsorbates to Semiconductor Nanocrystalline Thin Films, *J. Phys. Chem. B*, 2001, **105**(20), 4545–4557.

41 J. Kallioinen, G. Benkö, V. Sundström, J. E. I. Korppi-Tommola and A. P. Yartsev, Electron Transfer from the Singlet and Triplet Excited States of Ru(Dcbpy)$_2$(NCS)$_2$ into Nanocrystalline TiO$_2$ Thin Films, *J. Phys. Chem. B*, 2002, **106**(17), 4396–4404.

42 J. E. Moser and M. Grätzel, Observation of Temperature Independent Heterogeneous Electron Transfer Reactions in the Inverted Marcus Region, *Chem. Phys.*, 1993, **176**(2–3), 493–500.

43 D. Kuciauskas, J. E. Monat, R. Villahermosa, H. B. Gray, N. S. Lewis and J. K. McCusker, Transient Absorption Spectroscopy of Ruthenium and Osmium Polypyridyl Complexes Adsorbed onto Nanocrystalline TiO$_2$ Photoelectrodes, *J. Phys. Chem. B*, 2002, **106**(36), 9347–9358.

44 Y. Tachibana, S. A. Haque, I. P. Mercer, J. E. Moser, D. R. Klug and J. R. Durrant, Modulation of the Rate of

Electron Injection in Dye-Sensitized Nanocrystalline TiO_2 Films by Externally Applied Bias, *J. Phys. Chem. B*, 2001, **105**(31), 7424–7431.

45 F. Werner, J. F. Gnichwitz, R. Marczak, E. Palomares, W. Peukert, A. Hirsch and D. M. Guldi, Grafting Porphyrins (Face-to-Edge/Orthogonal versus Face-to-Face/Parallel) to ZnO En Route toward Dye-Sensitized Solar Cells, *J. Phys. Chem. B*, 2010, **114**(45), 14671–14678.

46 M. Planells, F. J. Céspedes-Guirao, L. Gonçalves, A. Sastre-Santos, F. Fernández-Lázaro and E. Palomares, Supramolecular Interactions in Dye-Sensitised Solar Cells, *J. Mater. Chem.*, 2009, **19**(32), 5818–5825.

47 J. J. Cid, M. García-Iglesias, J. H. Yum, A. Forneli, J. Albero, E. Martínez-Ferrero, P. Vázquez, M. Grätzel, M. K. Nazeeruddin and E. Palomares, *et al.*, Structure-Function Relationships in Unsymmetrical Zinc Phthalocyanines for Dye-Sensitized Solar Cells, *Chem. – Eur. J.*, 2009, **15**(20), 5130–5137.

48 A. Reynal, A. Forneli and E. Palomares, Dye Structure-Charge Transfer Process Relationship in Efficient Ruthenium-Dye Based Dye Sensitized Solar Cells, *Energy Environ. Sci.*, 2010, **3**(6), 805–812.

49 H. J. Snaith, A. Petrozza, S. Ito, H. Miura and M. Graätzel, Charge Generation and Photovoltaic Operation of Solid-State Dye-Sensitized Solar Cells Incorporating a High Extinction Coefficient Indolene-Based Sensitizer, *Adv. Funct. Mater.*, 2009, **19**(11), 1810–1818.

50 H. K. Ardakani, Electrical and Optical Properties of *in Situ* "Hydrogen-Reduced" Titanium Dioxide Thin Films Deposited by Pulsed Excimer Laser Ablation, *Thin Solid Films*, 1994, **248**(2), 234–239.

51 *CRC Handbook of Chemistry and Physics 95th Edition*, ed. W. M. Haynes, R. David and T. J. B. Lide, CRC Press, 95th edn, 1942.

52 R. Asahi, Y. Taga and W. Mannstadt, Electronic and Optical Properties of Anatase, *Phys. Rev. B: Condens. Matter Mater. Phys.*, 2000, **61**(11), 7459–7465.

53 M. A. Othman, N. F. Amat, B. H. Ahmad and J. Rajan, Electrical Conductivity Characteristic of TiO_2 Nanowires from Hydrothermal Method., *J. Phys.: Conf. Ser.*, 2014, **495**(1), 012027, DOI: 10.1088/1742-6596/495/1/012027.

54 M. C. K. Sellers and E. G. Seebauer, Measurement Method for Carrier Concentration in TiO_2 *via* the Mott–Schottky Approach, *Thin Solid Films*, 2011, **519**(7), 2103–2110.

55 G. Murali, M. Reddeppa, C. Seshendra Reddy, S. Park, T. Chandrakalavathi, M. D. Kim and I. In, Enhancing the Charge Carrier Separation and Transport *via* Nitrogen-Doped Graphene Quantum Dot-TiO_2 Nanoplate Hybrid Structure for an Efficient NO Gas Sensor, *ACS Appl. Mater. Interfaces*, 2020, **12**(11), 13428–13436.

56 A. K. Chandiran, F. Sauvage, M. Casas-Cabanas, P. Comte, S. M. Zakeeruddin and M. Graetzel, Doping a TiO_2 Photoanode with Nb^{5+} to Enhance Transparency and Charge Collection Efficiency in Dye-Sensitized Solar Cells., *J. Phys. Chem. C*, 2010, **114**(37), 15849–15856.

57 K. Subalakshmi and J. Senthilselvan, Effect of Fluorine-Doped TiO_2 Photoanode on Electron Transport, Recombination

Dynamics and Improved DSSC Efficiency., *Sol. Energy*, 2018, **171**, 914–928.

58 A. Paxton and L. Thiên-Nga, Electronic Structure of Reduced Titanium Dioxide, *Phys. Rev. B: Condens. Matter Mater. Phys.*, 1998, **57**(3), 1579–1584.

59 H. J. Snaith and L. Schmidt-Mende, Advances in Liquid-Electrolyte and Solid-State Dye-Sensitized Solar Cells, *Adv. Mater.*, 2007, **19**(20), 3187–3200.

60 M. Radecka, M. Rekas, A. Trenczek-Zajac and K. Zakrzewska, Importance of the Band Gap Energy and Flat Band Potential for Application of Modified TiO_2 Photoanodes in Water Photolysis, *J. Power Sources*, 2008, **181**(1), 46–55.

61 V. Kumar, S. K. Swami, A. Kumar, O. M. Ntwaeaborwa, V. Dutta and H. C. Swart, Eu^{3+} Doped down Shifting TiO_2 Layer for Efficient Dye-Sensitized Solar Cells, *J. Colloid Interface Sci.*, 2016, **484**, 24–32.

62 B. Roose, S. Pathak and U. Steiner, Doping of TiO_2 for Sensitized Solar Cells, *Chem. Soc. Rev.*, 2015, **44**(22), 8326–8349.

63 A. A. Awsha, S. H. Alazoumi and B. Elhub, A Review on the Development of TiO_2 Photoanode for Solar Applications, 2021, **6**(2), 1–9.

64 X. Hou, K. Aitola and P. D. Lund, TiO_2 Nanotubes for Dye-Sensitized Solar Cells—A Review., *Energy Sci. Eng.*, 2020, 921–937.

65 H. H. Nguyen, G. Gyawali, J. S. Hoon, T. Sekino and S. W. Lee, Cr-Doped TiO_2 Nanotubes with a Double-Layer Model: An Effective Way to Improve the Efficiency of Dye-Sensitized Solar Cells, *Appl. Surf. Sci.*, 2018, **458**, 523–528.

66 M.-C. Wu, W.-C. Chen, T.-H. Lin, K.-C. Hsiao, K.-M. Lee and C.-G. Wu, Enhanced Open-Circuit Voltage of Dye-Sensitized Solar Cells Using Bi-Doped TiO_2 Nanofibers as Working Electrode and Scattering Layer, *Sol. Energy*, 2016, **135**, 22–28.

67 D. Dahlan, S. K. Md Saad, A. U. Berli, A. Bajili and A. A. Umar, Synthesis of Two-Dimensional Nanowall of Cu-Doped TiO_2 and Its Application as Photoanode in DSSCs., *Phys. E*, 2017, **91**, 185–189.

68 S. Shalini, R. Balasundaraprabhu, T. Satish Kumar, N. Muthukumarasamy, S. Prasanna, K. Sivakumaran and M. D. Kannan, Enhanced Performance of Sodium Doped TiO_2 Nanorods Based Dye Sensitized Solar Cells Sensitized with Extract from Petals of Hibiscus SABDARIFFA (Roselle), *Mater. Lett.*, 2018, **221**, 192–195.

69 Y. Duan, N. Fu, Q. Zhang, Y. Fang, X. Zhou and Y. Lin, Influence of Sn Source on the Performance of Dye-Sensitized Solar Cells Based on Sn-Doped TiO_2 Photoanodes: A Strategy for Choosing an Appropriate Doping Source, *Electrochim. Acta*, 2013, **107**, 473–480.

70 V. Kumar, S. K. Swami, A. Kumar, O. M. Ntwaeaborwa, V. Dutta and H. C. Swart, Eu^{3+} Doped down Shifting TiO_2 Layer for Efficient Dye-Sensitized Solar Cells, *J. Colloid Interface Sci.*, 2016, **484**, 24–32.

71 E. Jalali-Moghadam and Z. Shariatinia, Al^{3+} Doping into TiO_2 Photoanodes Improved the Performances of Amine Anchored CdS Quantum Dot Sensitized Solar Cells, *Mater. Res. Bull.*, 2018, **98**, 121–132.

72 F. A. Unal, S. Ok, M. Unal, S. Topal, K. Cellat and F. Şen, Synthesis, Characterization, and Application of Transition Metals (Ni, Zr, and Fe) Doped TiO_2 Photoelectrodes for Dye-Sensitized Solar Cells, *J. Mol. Liq.*, 2020, **299**, 112177.

73 M. N. An'amt, S. Radiman, N. M. Huang, M. A. Yarmo, N. P. Ariyanto, H. N. Lim and M. R. Muhamad, Sol–Gel Hydrothermal Synthesis of Bismuth–TiO_2 Nanocubes for Dye-Sensitized Solar Cell, *Ceram. Int.*, 2010, **36**(7), 2215–2220.

74 M. I. Khan, M. Sabir, G. M. Mustafa, M. Fatima, A. Mahmood, S. A. Abubshait, H. A. Abubshait and M. Iqbal, 300 keV Cobalt Ions Irradiations Effect on the Structural, Morphological, Optical and Photovoltaic Properties of Zn Doped TiO_2 Thin Films Based Dye Sensitized Solar Cells., *Ceram. Int.*, 2020, **46**(10, Part B), 16813–16819.

75 Y. Zhang, N. Zhou, K. Zhang and F. Yan, Plasmonic Copper Nanowire@TiO_2 Nanostructures for Improving the Performance of Dye-Sensitized Solar Cells, *J. Power Sources*, 2017, **342**, 292–300.

76 Q. Ma and Y. M. Huang, Improved Photovoltaic Performance of Dye Sensitized Solar Cell by Decorating TiO_2 Photoanode with Li-Doped ZnO Nanorods, *Mater. Lett.*, 2015, **148**, 171–173.

77 A. I. Rafieh, P. Ekanayake, A. L. Tan and C. M. Lim, Effects of Ionic Radii of Co-Dopants (Mg, Ca, Al and La) in TiO_2 on Performance of Dye-Sensitized Solar Cells, *Sol. Energy*, 2017, **141**, 249–255.

78 A. A. Qureshi, H. M. A. Javed, S. Javed, A. Bashir, M. Usman, A. Akram, M. I. Ahmad, U. Ali, M. Shahid and M. Rizwan, *et al.*, Incorporation of Zr-Doped TiO_2 Nanoparticles in Electron Transport Layer for Efficient Planar Perovskite Solar Cells, *Surf. Interfaces*, 2021, **25**, 101299.

79 K. Sahu Dhonde, M. Dhonde and V. V. S. Murty, Novel Synergistic Combination of Al/N Co-Doped TiO_2 Nanoparticles for Highly Efficient Dye-Sensitized Solar Cells, *Sol. Energy*, 2018, **173**, 551–557.

80 V. S. Katta, A. Das, K. R. Dileep, G. Cilaveni, S. Pulipaka, G. Veerappan, E. Ramasamy, P. Meduri, S. Asthana and D. Melepurath, *et al.*, Vacancies Induced Enhancement in Neodymium Doped Titania Photoanodes Based Sensitized Solar Cells and Photo-Electrochemical Cells, *Sol. Energy Mater. Sol. Cells*, 2021, **220**, 110843.

81 Y. Akila, N. Muthukumarasamy, S. Agilan, S. Senthilarasu and D. Velauthapillai, Zirconium Oxide Post Treated Tin Doped TiO_2 for Dye Sensitized Solar Cells, *Mater. Sci. Semicond. Process.*, 2017, **57**, 24–31.

82 M. Dhonde, K. Sahu, V. V. S. Murty, S. S. Nemala, P. Bhargava and S. Mallick, Enhanced Photovoltaic Performance of a Dye Sensitized Solar Cell with Cu/N Co-Doped TiO_2 Nanoparticles, *J. Mater. Sci.: Mater. Electron.*, 2018, **29**(8), 6274–6282.

83 V. M. Ramakrishnan, Microwave Assisted Solvothermal Synthesis of Quasi Cubic F Doped TiO_2 Nanostructures and Its Performance as Dye Sensitized Solar Cell Photoanode, *Int. J. Energy Res.*, 2021, **45**(12), 17259–17268.

84 K. Subalakshmi and J. Senthilselvan, Effect of Fluorine-Doped TiO_2 Photoanode on Electron Transport, Recombination

Dynamics and Improved DSSC Efficiency, *Sol. Energy*, 2018, **171**, 914–928.

85 S. Nakade, S. Kambe, T. Kitamura, Y. Wada and S. Yanagida, Effects of Lithium Ion Density on Electron Transport in Nanoporous TiO_2 Electrodes, *J. Phys. Chem. B*, 2001, **105**(38), 9150–9152.

86 D. F. Watson and G. J. Meyer, Cation Effects in Nanocrystalline Solar Cells, *Coord. Chem. Rev.*, 2004, **248**(13–14), 1391–1406.

87 A. Subramanian, J. S. Bow and H. W. Wang, The Effect of Li^+ Intercalation on Different Sized TiO_2 Nanoparticles and the Performance of Dye-Sensitized Solar Cells, *Thin Solid Films*, 2012, **520**(23), 7011–7017.

88 J. Manju and S. M. J. Jawhar, Synthesis of Magnesium-Doped TiO_2 Photoelectrodes for Dye-Sensitized Solar Cell Applications by Solvothermal Microwave Irradiation Method, *J. Mater. Res.*, 2018, **33**(11), 1534–1542.

89 Q. Liu, Photovoltaic Performance Improvement of Dye-Sensitized Solar Cells Based on Mg-Doped TiO_2 Thin Films, *Electrochim. Acta*, 2014, **129**, 459–462.

90 M. I. Khan, W. A. Farooq, M. Saleem, K. A. Bhatti, M. Atif and A. Hanif, Phase Change, Band Gap Energy and Electrical Resistivity of Mg Doped TiO_2 Multilayer Thin Films for Dye Sensitized Solar Cells Applications., *Ceram. Int.*, 2019, **45**(17, Part A), 21436–21439.

91 K. Kakiage, T. Tokutome, S. Iwamoto, T. Kyomen and M. Hanaya, Fabrication of a Dye-Sensitized Solar Cell Containing a Mg-Doped TiO_2 Electrode and a Br^{3-}/Br^- Redox Mediator with a High Open-Circuit Photovoltage of 1.21 V, *Chem. Commun.*, 2013, **49**(2), 179–180.

92 S. Iwamoto, Y. Sazanami, M. Inoue, T. Inoue, T. Hoshi, K. Shigaki, M. Kaneko and A. Maenosono, Fabrication of Dye-Sensitized Solar Cells with an Open-Circuit Photovoltage of 1 V, *ChemSusChem*, 2008, **1**(5), 401–403.

93 C. Zhang, S. Chen, L. E. Mo, Y. Huang, H. Tian, L. Hu, Z. Huo, S. Dai, F. Kong and X. Pan, Charge Recombination and Band-Edge Shift in the Dye-Sensitized Mg^{2+}-Doped TiO_2 Solar Cells, *J. Phys. Chem. C*, 2011, **115**(33), 16418–16424.

94 W. Li, J. Yang, J. Zhang, S. Gao, Y. Luo and M. Liu, Improve Photovoltaic Performance of Titanium Dioxide Nanorods Based Dye-Sensitized Solar Cells by Ca-Doping, *Mater. Res. Bull.*, 2014, **57**, 177–183.

95 M. Pan, H. Liu, Z. Yao and X. Zhong, Enhanced Efficiency of Dye-Sensitized Solar Cells by Trace Amount ca-Doping in TiO_2 Photoelectrodes, *J. Nanomater.*, 2015, 2015.

96 Q. Liu, Y. Zhou, Y. Duan, M. Wang, X. Zhao and Y. Lin, Enhanced Conversion Efficiency of Dye-Sensitized Titanium Dioxide Solar Cells by Ca-Doping., *J. Alloys Compd.*, 2013, **548**, 161–165.

97 S. Shakir, H. M. Abd-ur-Rehman, K. Yunus, M. Iwamoto and V. Periasamy, Fabrication of Un-Doped and Magnesium Doped TiO_2 Films by Aerosol Assisted Chemical Vapor Deposition for Dye Sensitized Solar Cells, *J. Alloys Compd.*, 2018, **737**, 740–747.

98 N. Rajamanickam and K. Ramachandran, Improved Photovoltaic Performance in Nano TiO_2 Based Dye Sensitized

Solar Cells: Effect of TiCl4 Treatment and Sr Doping, *J. Colloid Interface Sci.*, 2020, **580**, 407–418.

99 H. F. Mehnane, C. Wang, K. K. Kondamareddy, W. Yu, W. Sun, H. Liu, S. Bai, W. Liu, S. Guo and X.-Z. Zhao, Hydrothermal Synthesis of TiO_2 Nanoparticles Doped with Trace Amounts of Strontium, and Their Application as Working Electrodes for Dye Sensitized Solar Cells: Tunable Electrical Properties & Enhanced Photo-Conversion Performance, *RSC Adv.*, 2017, **7**(4), 2358–2364.

100 N. Rajamanickam and K. Ramachandran, Improved Photovoltaic Performance in Nano TiO(2) Based Dye Sensitized Solar Cells: Effect of TiCl(4) Treatment and Sr Doping, *J. Colloid Interface Sci.*, 2020, **580**, 407–418.

101 X. H. Wu, S. Wang, Y. Guo, Z. Y. Xie, L. Han and Z. H. Jiang, Enhanced Energy Conversion Efficiency of La^{3+}-Modified Nanoporous TiO_2 Electrode Sensitized with a Ruthenium Complex, *Chin. J. Chem.*, 2008, **26**(10), 1939–1943.

102 S. Yahav, S. Rühle, S. Greenwald, H. N. Barad, M. Shalom and A. Zaban, Strong Efficiency Enhancement of Dye-Sensitized Solar Cells Using a La-Modified $TiCl_4$ Treatment of Mesoporous TiO_2 Electrodes, *J. Phys. Chem. C*, 2011, **115**(43), 21481–21486.

103 J. Zhang, Z. Zhao, X. Wang, T. Yu, J. Guan, Z. Yu, Z. Li and Z. Zou, Increasing the Oxygen Vacancy Density on the TiO_2 Surface by La-Doping for Dye-Sensitized Solar Cells, *J. Phys. Chem. C*, 2010, **114**(43), 18396–18400.

104 M. Liu, Y. Hou and X. Qu, Enhanced Power Conversion Efficiency of Dye-Sensitized Solar Cells with Samarium Doped TiO_2 Photoanodes, *J. Mater. Res.*, 2017, **32**(18), 3469–3476.

105 H. Hafez, M. Saif and M. S. A. Abdel-Mottaleb, Down-Converting Lanthanide Doped TiO_2 Photoelectrodes for Efficiency Enhancement of Dye-Sensitized Solar Cells, *J. Power Sources*, 2011, **196**(13), 5792–5796.

106 K. Singh, S. Harish, J. Archana, M. Navaneethan, M. Shimomura and Y. Hayakawa, Investigation of Gd-Doped Mesoporous TiO_2 Spheres for Environmental Remediation and Energy Applications, *Appl. Surf. Sci.*, 2019, **489**, 883–892.

107 E. Akman, S. Akin, T. Ozturk, B. Gulveren and S. Sonmezoglu, Europium and Terbium Lanthanide Ions Co-Doping in TiO_2 Photoanode to Synchronously Improve Light-Harvesting and Open-Circuit Voltage for High-Efficiency Dye-Sensitized Solar Cells, *Sol. Energy*, 2020, **202**, 227–237.

108 J. Wang, J. Lin, J. Wu, M. Huang, Z. Lan, Y. Chen, S. Tang, L. Fan and Y. Huang, Application of Yb^{3+}, Er^{3+}-Doped Yttrium Oxyfluoride Nanocrystals in Dye-Sensitized Solar Cells, *Electrochim. Acta*, 2012, **70**, 131–135.

109 J. Wu, J. Wang, J. Lin, Z. Lan, Q. Tang, M. Huang, Y. Huang, L. Fan, Q. Li and Z. Tang, Enhancement of the Photovoltaic Performance of Dye-Sensitized Solar Cells by Doping $Y_{0.78}Yb_{0.20}Er_{0.02}F_3$ in the Photoanode, *Adv. Energy Mater.*, 2012, **2**(1), 78–81.

110 J. Yu, Y. Yang, R. Fan, H. Zhang, L. Li, L. Wei, Y. Shi, K. Pan and H. Fu, Er^{3+} and Yb^{3+} Co-Doped TiO_2-XFx up-Conversion Luminescence Powder as a Light Scattering Layer with

Enhanced Performance in Dye Sensitized Solar Cells, *J. Power Sources*, 2013, **243**, 436–443.

111 Q. Li, J. Lin, J. Wu, Z. Lan, Y. Wang, F. Peng and M. Huang, Enhancing Photovoltaic Performance of Dye-Sensitized Solar Cell by Rare-Earth Doped Oxide of Lu_2O_3:(Tm^{3+}, Yb^{3+}), *Electrochim. Acta*, 2011, **56**(14), 4980–4984.

112 G. Xie, Y. Wei, L. Fan and J. Wu, Application of Doped Rare-Earth Oxide TiO_2:(Tm^{3+}, Yb^{3+}) in Dye-Sensitized Solar Cells., *J. Phys.: Conf. Ser.*, 2012, **339**(1), 012010, DOI: **10.1088/1742-6596/339/1/012010**.

113 X. Wei-Wei, D. Son-yuan, H. Lin-Hua, L. L. Yun and W. Kong-Jia, Influence of Yb Doped Nanoporous TiO_2 Films on Photovoltaic Performance of Dye Sensitized Solar Cells., *Chin. Phys. Lett.*, 2006, **23**(8), 2288–2291.

114 R. T. Ako, P. Ekanayake, A. L. Tan and D. J. Young, La Modified TiO_2 Photoanode and Its Effect on DSSC Performance: A Comparative Study of Doping and Surface Treatment on Deep and Surface Charge Trapping, *Mater. Chem. Phys.*, 2016, **172**, 105–112.

115 A. R. Tanyi, A. I. Rafieh, P. Ekaneyaka, A. L. Tan, D. J. Young, Z. Zheng, V. Chellappan, G. S. Subramanian and R. L. N. Chandrakanthi, Enhanced Efficiency of Dye-Sensitized Solar Cells Based on Mg and La Co-Doped TiO_2 Photoanodes, *Electrochim. Acta*, 2015, **178**, 240–248.

116 J. Liqiang, S. Xiaojun, X. Baifu, W. Baiqi, C. Weimin and F. Honggang, The Preparation and Characterization of La Doped TiO_2 Nanoparticles and Their Photocatalytic Activity, *J. Solid State Chem.*, 2004, **177**(10), 3375–3382.

117 Neetu, S. Singh, P. Srivastava and L. Bahadur, Hydrothermal Synthesized Nd-Doped TiO_2 with Anatase and Brookite Phases as Highly Improved Photoanode for Dye-Sensitized Solar Cell., *Sol. Energy*, 2020, **208**, 173–181.

118 L. Li, X. Yang, W. Zhang, H. Zhang and X. Li, Boron and Sulfur Co-Doped TiO_2 nanofilm as Effective Photoanode for High Efficiency CdS Quantum-Dot-Sensitized Solar Cells, *J. Power Sources*, 2014, **272**, 508–512.

119 E. Finazzi, C. Valentin and G. Di Pacchioni, Boron-Doped Anatase TiO_2: Pure and Hybrid DFT Calculations, *J. Phys. Chem. C*, 2009, **113**(1), 220–228.

120 M. Wang, S. Bai, A. Chen, Y. Duan, Q. Liu, D. Li and Y. Lin, Improved Photovoltaic Performance of Dye-Sensitized Solar Cells by Sb-Doped TiO_2 Photoanode, *Electrochim. Acta*, 2012, **77**, 54–59.

121 H. Imahori, S. Hayashi, T. Umeyama, S. Eu, A. Oguro, S. Kang, Y. Matano, T. Shishido, S. Ngamsinlapasathian and S. Yoshikawa, Comparison of Electrode Structures and Photovoltaic Properties of Porphyrin-Sensitized Solar Cells with TiO_2 and Nb, Ge, Zr-Added TiO_2 Composite Electrodes, *Langmuir*, 2006, **22**(26), 11405–11411.

122 A. Subramanian and H. W. Wang, Effects of Boron Doping in TiO_2 Nanotubes and the Performance of Dye-Sensitized Solar Cells, *Appl. Surf. Sci.*, 2012, **258**(17), 6479–6484.

123 H. Tian, L. Hu, W. Li, J. Sheng, S. Xu and S. Dai, A Facile Synthesis of Anatase N,B Codoped TiO_2 Anodes for Improved-Performance Dye-Sensitized Solar Cells, *J. Mater. Chem.*, 2011, **21**(20), 7074–7077.

124 H. Tian, L. Hu, C. Zhang, S. Chen, J. Sheng, L. Mo, W. Liu and S. Dai, Enhanced Photovoltaic Performance of Dye-Sensitized Solar Cells Using a Highly Crystallized Mesoporous TiO_2 Electrode Modified by Boron Doping, *J. Mater. Chem.*, 2011, **21**(3), 863–868.

125 J. S. Im, J. Yun, S. K. Lee and Y. S. Lee, Effects of Multi-Element Dopants of TiO_2 for High Performance in Dye-Sensitized Solar Cells, *J. Alloys Compd.*, 2012, **513**, 573–579.

126 D. Chen, D. Yang, Q. Wang and Z. Jiang, Effects of Boron Doping on Photocatalytic Activity and Microstructure of Titanium Dioxide Nanoparticles, *Ind. Eng. Chem. Res.*, 2006, **45**(12), 4110–4116.

127 A. Latini, C. Cavallo, F. K. Aldibaja, D. Gozzi, D. Carta, A. Corrias, L. Lazzarini and G. Salviati, Efficiency Improvement of DSSC Photoanode by Scandium Doping of Mesoporous Titania Beads, *J. Phys. Chem. C*, 2013, **117**(48), 25276–25289.

128 A. Ray, A. Roy, P. Sadhukhan, S. R. Chowdhury, P. Maji, S. K. Bhattachrya and S. Das, Electrochemical Properties of TiO_2–V_2O_5 Nanocomposites as a High Performance Supercapacitors Electrode Material, *Appl. Surf. Sci.*, 2018, **443**, 581–591.

129 C. Kim, K. S. Kim, H. Y. Kim and Y. S. Han, Modification of a TiO_2 Photoanode by Using Cr-Doped TiO_2 with an Influence on the Photovoltaic Efficiency of a Dye-Sensitized Solar Cell, *J. Mater. Chem.*, 2008, **18**(47), 5809–5814.

130 L. C. K. Liau and C. C. Lin, Semiconductor Characterization of Cr^{3+}-Doped Titania Electrodes with p-n Homojunction Devices, *Thin Solid Films*, 2008, **516**(8), 1998–2002.

131 Y. Liu, H. Ran, J. Fan, X. Zhang, J. Mao and G. Shao, Fabrication and Photovoltaic Performance of Niobium Doped TiO_2 Hierarchical Microspheres with Exposed {001} Facets and High Specific Surface Area, *Appl. Surf. Sci.*, 2017, **410**, 241–248.

132 L. B. Patle, V. R. Huse and A. L. Chaudhari, Band Edge Movement and Structural Modifications in Transition Metal Doped TiO_2 Nanocrystals for the Application of DSSC., *Mater. Res. Express*, 2017, **4**(10), 105045.

133 B. Yacoubi, L. Samet, J. Bennaceur, A. Lamouchi and R. Chtourou, Properties of Transition Metal Doped-Titania Electrodes: Impact on Efficiency of Amorphous and Nanocrystalline Dye-Sensitized Solar Cells, *Mater. Sci. Semicond. Process.*, 2015, **30**, 361–367.

134 C. T. Wang, W. P. Wang and H. S. Lin, Niobium and Iron Co-Doped Titania Nanobelts for Improving Charge Collection in Dye-Sensitized TiO_2 Solar Cells, *Ceram. Int.*, 2018, **44**(15), 18032–18038.

135 A. E. Shalan and M. M. Rashad, Incorporation of Mn^{2+} and Co^{2+} to TiO_2 Nanoparticles and the Performance of Dye-Sensitized Solar Cells, *Appl. Surf. Sci.*, 2013, **283**, 975–981.

136 P. S. Archana, E. N. Kumar, C. Vijila, S. Ramakrishna, M. M. Yusoff and R. Jose, Random Nanowires of Nickel Doped TiO_2 with High Surface Area and Electron Mobility for High Efficiency Dye-Sensitized Solar Cells, *Dalton Trans.*, 2013, **42**, 1024–1032.

137 J. Y. Park, C. S. Kim, K. Okuyama, H. M. Lee, H. D. Jang, S. E. Lee and T. O. Kim, Copper and Nitrogen Doping on TiO_2 Photoelectrodes and Their Functions in Dye-Sensitized Solar Cells, *J. Power Sources*, 2016, **306**, 764–771.

138 W. Liu, H. G. Wang, X. Wang, M. Zhang and M. Guo, Titanium Mesh Supported TiO_2 Nanowire Arrays/Nb-Doped TiO_2 Nanoparticles for Fully Flexible Dye-Sensitized Solar Cells with Improved Photovoltaic Properties, *J. Mater. Chem. C*, 2016, **4**(47), 11118–11128.

139 A. Khlyustova, N. Sirotkin, T. Kusova, A. Kraev, V. Titov and A. Agafonov, Doped TiO_2: The Effect of Doping Elements on Photocatalytic Activity, *Mater. Adv.*, 2020, **1**(5), 1193–1201.

140 T. S. Bramhankar, S. S. Pawar, J. S. Shaikh, V. C. Gunge, N. I. Beedri, P. K. Baviskar, H. M. Pathan, P. S. Patil, R. C. Kambale and R. S. Pawar, Effect of Nickel–Zinc Co-Doped TiO_2 Blocking Layer on Performance of DSSCs., *J. Alloys Compd.*, 2020, **817**(xxxx), 152810.

141 A. K. Chandiran, F. Sauvage, L. Etgar and M. Graetzel, Ga^{3+} and Y^{3+} Cationic Substitution in Mesoporous TiO_2 Photoanodes for Photovoltaic Applications, *J. Phys. Chem. C*, 2011, **115**(18), 9232–9240.

142 H. Su, Y. T. Huang, Y. H. Chang, P. Zhai, N. Y. Hau, P. C. H. Cheung, W. T. Yeh, T. C. Wei and S. P. Feng, The Synthesis of Nb-Doped TiO_2 Nanoparticles for Improved-Performance Dye Sensitized Solar Cells, *Electrochim. Acta*, 2015, **182**, 230–237.

143 S. Rabhi, H. Belkacemi, M. Bououdina, A. Kerrami, L. Ait Brahem and E. Sakher, Effect of Ag Doping of TiO_2 Nanoparticles on Anatase-Rutile Phase Transformation and Excellent Photodegradation of Amlodipine Besylate, *Mater. Lett.*, 2019, **236**, 640–643.

144 M. Motlak, A. M. Hamza, M. G. Hammed and N. A. M. Barakat, Cd-Doped TiO_2 Nanofibers as Effective Working Electrode for the Dye Sensitized Solar Cells, *Mater. Lett.*, 2019, **246**, 206–209.

145 J. Liu, Y. Duan, X. Zhou and Y. Lin, Influence of VB Group Doped TiO_2 on Photovoltaic Performance of Dye-Sensitized Solar Cells, *Appl. Surf. Sci.*, 2013, **277**, 231–236.

146 X. Zhang, F. Liu, Q. L. Huang, G. Zhou and Z. S. Wang, Dye-Sensitized W-Doped TiO_2 Solar Cells with a Tunable Conduction Band and Suppressed Charge Recombination, *J. Phys. Chem. C*, 2011, **115**(25), 12665–12671.

147 H. Seo, Y. Wang, D. Ichida, G. Uchida, N. Itagaki, K. Koga, M. Shiratani, S. H. Nam and J. H. Boo, Improvement on the Electron Transfer of Dye-Sensitized Solar Cell Using Vanadium Doped TiO_2, *Jpn. J. Appl. Phys.*, 2013, **52**(11 PART 2), 2–6.

148 X. Li, Z. Guo and T. He, The Doping Mechanism of Cr into TiO_2 and Its Influence on the Photocatalytic Performance, *Phys. Chem. Chem. Phys.*, 2013, **15**(46), 20037–20045.

149 Y. Xie, N. Huang, S. You, Y. Liu, B. Sebo, L. Liang, X. Fang, W. Liu, S. Guo and X. Z. Zhao, Improved Performance of Dye-Sensitized Solar Cells by Trace Amount Cr-Doped TiO_2 Photoelectrodes, *J. Power Sources*, 2013, **224**, 168–173.

150 H. H. Nguyen, G. Gyawali, A. Martinez-Oviedo, Y. K. Kshetri and S. W. Lee, Physicochemical Properties of Cr-Doped TiO_2 Nanotubes and Their Application in Dye-Sensitized Solar Cells, *J. Photochem. Photobiol., A*, 2020, **397**, 112514.

151 B. Ünlü and M. Özacar, Effect of Cu and Mn Amounts Doped to TiO$_2$ on the Performance of DSSCs, *Sol. Energy*, 2020, **196**, 448–456.

152 S. Shah, N. N. S. Baharun, S. N. F. Yusuf and A. K. Arof, Efficiency Enhancement of Dye-Sensitized Solar Cells (DSSCs) Using Copper Nanopowder (CuNW) in TiO$_2$ as Photoanode, *IOP Conf. Ser.: Mater. Sci. Eng.*, 2019, **515**(1), 012002, DOI: 10.1088/1757-899X/515/1/012002.

153 B. Ünlü, S. Çakar and M. Özacar, The Effects of Metal Doped TiO$_2$ and Dithizone-Metal Complexes on DSSCs Performance, *Sol. Energy*, 2018, **166**, 441–449.

154 R. T. Ako, P. Ekanayake, D. J. Young, J. Hobley, V. Chellappan, A. L. Tan, S. Gorelik, G. S. Subramanian and C. M. Lim, Evaluation of Surface Energy State Distribution and Bulk Defect Concentration in DSSC Photoanodes Based on Sn, Fe, and Cu Doped TiO$_2$, *Appl. Surf. Sci.*, 2015, **351**, 950–961.

155 L. C. K. Liau and C. C. Lin, Fabrication and Characterization of Fe^{3+}-Doped Titania Semiconductor Electrodes with p–n Homojunction Devices, *Appl. Surf. Sci.*, 2007, **253**(21), 8798–8801.

156 M. I. Khan, Synthesis, Characterization and Application of Co Doped TiO$_2$ Multilayer Thin Films, *Results Phys.*, 2018, **9**, 359–363.

157 B. Ünlü, S. Çakar and M. Özacar, The Effects of Metal Doped TiO$_2$ and Dithizone-Metal Complexes on DSSCs Performance, *Sol. Energy*, 2018, **166**, 441–449.

158 A. Malik, S. Hameed, M. J. Siddiqui, M. M. Haque, K. Umar, A. Khan and M. Muneer, Electrical and Optical Properties of Nickel- and Molybdenum-Doped Titanium Dioxide Nanoparticle: Improved Performance in Dye-Sensitized Solar Cells, *J. Mater. Eng. Perform.*, 2014, **23**, 3184–3192.

159 K. Sahu, M. Dhonde and V. V. S. Murty, Microwave-Assisted Hydrothermal Synthesis of Cu-Doped TiO$_2$ Nanoparticles for Efficient Dye-Sensitized Solar Cell with Improved Open-Circuit Voltage, *Int. J. Energy Res.*, 2021, **45**(4), 5423–5432.

160 Y. Wang, Y. Hao, H. Cheng, J. Ma and B. I. N. Xu, The Photoelectrochemistry of Transition Metal-Ion-Doped TiO$_2$ Nanocrystalline Electrodes and Higher Solar Cell Conversion Efficiency Based on Zn^{2+}-Doped TiO$_2$ Electrode, *J. Mater. Sci.*, 1999, **34**, 2773–2779.

161 T. N. D. S. Cells, F. Zhu, P. Zhang, X. Wu, L. Fu and J. Zhang, The Origin of Higher Open-Circuit Voltage in Zn-Doped, *ChemPhysChem*, 2012, **13**(16), 1439–4235.

162 P. Taylor, H. Chen, L. Zhao, Y. Xiang, Y. He, G. Song, X. Wang and F. Liang, A Novel Zn–TiO$_2$/C@SiO$_2$ Nanoporous Material on Rice Husk for Photocatalytic Applications under Visible Light, *Desalin. Water Treat.*, 2015, **57**(21), 9660–9670.

163 K. Wang and H. Teng, Zinc-Doping in TiO$_2$ Films to Enhance Electron Transport in Dye-Sensitized Solar Cells under Low-Intensity Illumination, *Phys. Chem. Chem. Phys.*, 2009, **11**, 9489–9496.

164 J. Zhang, Z. Han, Z. Fu, Y. Wen and F. Zhao, Study of N–Ag–Zn/TiO$_2$, N–Ag–Zr/TiO$_2$ with N719 and P3OT Co-Sensitization Effect on the Performance of Dye-Sensitized Solar Cell, *J. Sol-Gel Sci. Technol.*, 2016, **78**(1), 207–217.

165 B. Zhao, J. Wang, H. Li, H. Wang, X. Jia and P. Su, The Influence of Yttrium Dopant on the Properties of Anatase Nanoparticles and the Performance of Dye-Sensitized Solar Cells, *Phys. Chem. Chem. Phys.*, 2015, **17**(22), 14836–14842.

166 X. Qu, Y. Hou, M. Liu, L. Shi, M. Zhang, H. Song and F. Du, Yttrium Doped TiO$_2$ Porous Film Photoanode for Dye-Sensitized Solar Cells with Enhanced Photovoltaic Performance, *Results Phys.*, 2016, **6**, 1051–1058.

167 M. Moradzaman, M. R. Mohammadi and H. Nourizadeh, Efficient Dye-Sensitized Solar Cells Based on CNTs and Zr-Doped TiO$_2$ Nanoparticles, *Mater. Sci. Semicond. Process.*, 2015, **40**, 383–390.

168 N. Tsvetkov, L. Larina, O. Shevaleevskiy and B. T. Ahn, Effect of Nb Doping of TiO$_2$ Electrode on Charge Transport in Dye-Sensitized Solar Cells, *J. Electrochem. Soc.*, 2011, **158**(11), B1281.

169 L. Long, L. Wu, X. Yang and X. Li, Photoelectrochemical Performance of Nb-Doped TiO$_2$ Nanoparticles Fabricated by Hydrothermal Treatment of Titanate Nanotubes in Niobium Oxalate Aqueous Solution, *J. Mater. Sci. Technol.*, 2014, **30**(8), 765–769.

170 N. Yamada, T. Hitosugi, J. Kasai, N. L. H. Hoang, S. Nakao, Y. Hirose, T. Shimada and T. Hasegawa, Direct Growth of Transparent Conducting Nb-Doped Anatase TiO$_2$ Polycrystalline Films on Glass, *J. Appl. Phys.*, 2009, **105**(12), 123702, DOI: 10.1063/1.3148267.

171 T. Nikolay, L. Larina, O. Shevaleevskiy and B. T. Ahn, Electronic Structure Study of Lightly Nb-Doped TiO$_2$ Electrode for Dye-Sensitized Solar Cells, *Energy Environ. Sci.*, 2011, **4**(4), 1480–1486.

172 Y. Liu, H. Ran, J. Fan, X. Zhang, J. Mao and G. Shao, Fabrication and Photovoltaic Performance of Niobium Doped TiO$_2$ Hierarchical Microspheres with Exposed {001} Facets and High Specific Surface Area, *Appl. Surf. Sci.*, 2017, **410**, 241–248.

173 W. Liu, H. Wang, X. Wang, M. Zhang and M. Guo, Titanium Mesh Supported TiO$_2$ Nanowire Arrays/Nb-Doped TiO$_2$ Nanoparticles for Fully Flexible Dye-Sensitized Solar Cells with Improved Photovoltaic Properties, *J. Mater. Chem. C*, 2016, **4**(47), 11118–11128.

174 B.-R. Koo, D.-H. Oh and H.-J. Ahn, Influence of Nb-Doped TiO$_2$ Blocking Layers as a Cascading Band Structure for Enhanced Photovoltaic Properties, *Appl. Surf. Sci.*, 2018, **433**, 27–34.

175 J.-M. Song, P.-J. Wang, L.-H. Chan, C.-M. Chen, W.-F. Ho and S.-Y. Chen, Efficiency Enhancement of Dye-Sensitized Solar Cells Using Ti–Nb Alloy Photoanodes with Mesoporous Oxide Surface, *J. Electrochem. Soc.*, 2020, **167**(4), 046501.

176 P. Nbelayim, G. Kawamura, W. Kian Tan, H. Muto and A. Matsuda, Systematic Characterization of the Effect of Ag@TiO$_2$ Nanoparticles on the Performance of Plasmonic Dye-Sensitized Solar Cells, *Sci. Rep.*, 2017, **7**(1), 1–12.

177 K. Usha, P. Kumbhakar and B. Mondal, Effect of Ag-Doped TiO$_2$ Thin Film Passive Layers on the Performance of Photo-Anodes for Dye-Sensitized Solar Cells, *Mater. Sci. Semicond. Process.*, 2016, **43**, 17–24.

178 J. Liu, H. Yang, W. Tan, X. Zhou and Y. Lin, Photovoltaic Performance Improvement of Dye-Sensitized Solar Cells Based on Tantalum-Doped TiO_2 Thin Films, *Electrochim. Acta*, 2010, **56**(1), 396–400.

179 J.-H. Choi, S.-H. Kwon, Y.-K. Jeong, I. Kim and K.-H. Kim, Atomic Layer Deposition of Ta-Doped TiO_2 Electrodes for Dye-Sensitized Solar Cells, *J. Electrochem. Soc.*, 2011, **158**(6), B749.

180 I. M. A. Mohamed, V.-D. Dao, N. A. M. Barakat, A. S. Yasin, A. Yousef and H.-S. Choi, Efficiency Enhancement of Dye-Sensitized Solar Cells by Use of ZrO_2-Doped TiO_2 Nanofibers Photoanode, *J. Colloid Interface Sci.*, 2016, **476**, 9–19.

181 L. Zhao, C. Zhong, Y. Wang, S. Wang, B. Dong and L. Wan, Ag Nanoparticle-Decorated 3D Flower-like TiO_2 Hierarchical Microstructures Composed of Ultrathin Nanosheets and Enhanced Photoelectrical Conversion Properties in Dye-Sensitized Solar Cells, *J. Power Sources*, 2015, **292**, 49–57.

182 N. Massihi, M. R. Mohammadi, A. M. Bakhshayesh and M. Abdi-Jalebi, Controlling Electron Injection and Electron Transport of Dye-Sensitized Solar Cells Aided by Incorporating CNTs into a Cr-Doped TiO_2 Photoanode, *Electrochim. Acta*, 2013, **111**, 921–929.

183 R. Ghosh, Y. Hara, L. Alibabaei, K. Hanson, S. Rangan, R. Bartynski, T. J. Meyer and R. Lopez, Increasing Photocurrents in Dye Sensitized Solar Cells with Tantalum-Doped Titanium Oxide Photoanodes Obtained by Laser Ablation, *ACS Appl. Mater. Interfaces*, 2012, **4**(9), 4566–4570.

184 P. Zhong, X. Chen, B. Niu, C. Li, Y. Wang, H. Xi, Y. Lei, Z. Wang and X. Ma, Niobium Doped TiO_2 Nanorod Arrays as Efficient Electron Transport Materials in Photovoltaic, *J. Power Sources*, 2020, **450**, 227715, DOI: 10.1016/j.jpowsour.2020.227715.

185 S. K. M. Saad, A. A. Umar, M. Y. A. Rahman and M. M. Salleh, Porous Zn-Doped TiO_2 Nanowall Photoanode: Effect of Zn^{2+} Concentration on the Dye-Sensitized Solar Cell Performance., *Appl. Surf. Sci.*, 2015, **353**, 835–842.

186 R. Bendoni, E. Mercadelli, N. Sangiorgi, A. Strini, A. Sangiorgi and A. Sanson, Alternative Route for the Preparation of Zr-Doped TiO_2 Layers for Energy and Environmental Applications, *Ceram. Int.*, 2015, **41**(8), 9899–9909.

187 B. Sebo, N. Huang, Y. Liu, Q. Tai, L. Liang, H. Hu, S. Xu and X. Z. Zhao, Dye-Sensitized Solar Cells Enhanced by Optical Absorption, Mediated by TiO_2 Nanofibers and Plasmonic Ag Nanoparticles, *Electrochim. Acta*, 2013, **112**, 458–464.

188 M. Dhonde, K. Sahu, V. V. S. Murty, S. S. Nemala and P. Bhargava, Surface Plasmon Resonance Effect of Cu Nanoparticles in a Dye Sensitized Solar Cell, *Electrochim. Acta*, 2017, **249**, 89–95.

189 R. Tanyi, P. Ekanayake, D. James, J. Hobley, V. Chellappan, A. Ling, S. Gorelik and G. Sandhya, Evaluation of Surface Energy State Distribution and Bulk Defect Concentration in DSSC Photoanodes Based on Sn, Fe, and Cu Doped TiO_2, *Appl. Surf. Sci.*, 2015, **351**, 950–961.

190 J. Du, J. Qi, D. Wang and Z. Tang, Facile Synthesis of $Au@TiO_2$ Core-Shell Hollow Spheres for Dye-Sensitized Solar Cells with Remarkably Improved Efficiency, *Energy Environ. Sci.*, 2012, **5**(5), 6914–6918.

191 Y. Y. Li, J. G. Wang, X. R. Liu, C. Shen, K. Xie and B. Wei, Au/TiO_2 Hollow Spheres with Synergistic Effect of Plasmonic Enhancement and Light Scattering for Improved Dye-Sensitized Solar Cells, *ACS Appl. Mater. Interfaces*, 2017, **9**(37), 31691–31698.

192 B. R. Koo, D. H. Oh and H. J. Ahn, Influence of Nb-Doped TiO_2 Blocking Layers as a Cascading Band Structure for Enhanced Photovoltaic Properties, *Appl. Surf. Sci.*, 2018, **433**, 27–34.

193 X. Lü, X. Mou, J. Wu, D. Zhang, L. Zhang, F. Huang, F. Xu and S. Huang, Improved-Performance Dye-Sensitized Solar Cells Using Nb-Doped TiO_2 Electrodes: Efficient Electron Injection and Transfer, *Adv. Funct. Mater.*, 2010, **20**(3), 509–515.

194 P. Xiang, W. Ma, T. Xiao, L. Jiang, X. Tan and T. Shu, Ta-Doped Hierarchical TiO_2 Spheres for Dye-Sensitized Solar Cells, *J. Alloys Compd.*, 2016, **656**, 45–50.

195 S. K. M. Saad, A. A. Umar, M. Y. A. Rahman and M. M. Salleh, Porous Zn-Doped TiO_2 Nanowall Photoanode: Effect of Zn^{2+} Concentration on the Dye-Sensitized Solar Cell Performance, *Appl. Surf. Sci.*, 2015, **353**, 835–842.

196 I. M. A. Mohamed, V. Dao, N. A. M. Barakat, A. S. Yasin, A. Yousef and H. Choi, Efficiency Enhancement of Dye-Sensitized Solar Cells by Use of ZrO_2-Doped TiO_2 Nanofibers Photoanode, *J. Colloid Interface Sci.*, 2016, **476**, 9–19.

197 E. Jalali-moghadam and Z. Shariatinia, Al^{3+} Doping into TiO_2 Photoanodes Improved the Performances of Amine Anchored CdS Quantum Dot Sensitized Solar Cells, *Mater. Res. Bull.*, 2018, **98**, 121–132.

198 A. K. Chandiran, F. Sauvage, L. Etgar and M. Graetzel, Ga^{3+} and Y^{3+} Cationic Substitution in Mesoporous TiO_2 Photoanodes for Photovoltaic Applications, *J. Phys. Chem. C*, 2011, **115**(18), 9232–9240.

199 B. Baptayev, S. Adilov and M. P. Balanay, Surface Modification of TiO_2 Photoanodes with In^{3+} Using a Simple Soaking Technique for Enhancing the Efficiency of Dye-Sensitized Solar Cells, *J. Photochem. Photobiol., A*, 2020, **394**, 112468, DOI: 10.1016/j.jphotochem.2020.112468.

200 M. I. Khan, G. Hassan, M. S. Hasan, S. A. Abubshait, H. A. Abubshait, W. Al-Masry, Q. Mahmood, A. Mahmood and S. M. Ramay, Investigations on the Efficiency Variation of Zinc and Gallium Co-Doped TiO_2 Based Dye Sensitized Solar Cells, *Ceram. Int.*, 2020, **46**(16), 24844–24849.

201 M. N. An, S. Radiman, N. M. Huang and M. A. Yarmo, Sol–Gel Hydrothermal Synthesis of Bismuth–TiO_2 Nanocubes for Dye-Sensitized Solar Cell, *Ceram. Int.*, 2010, **36**(7), 2215–2220.

202 F. Huang, B. Y. Cheng and R. A. Caruso, Al-Doped TiO_2 Photoanode for Dye-Sensitized Solar Cells, *Aust. J. Chem.*, 2011, **64**, 820–824.

203 A. M. Bakhshayesh and N. Farajisafiloo, Anatase-Stabilised $Al_xTi_{1-x}O_2$ Photoanodes Containing Uniform Spherical Particles for Efficient Dye-Sensitized Solar Cells, *Appl. Surf. Sci.*, 2015, **331**, 58–65.

204 K. Manoharan and P. Venkatachalam, Photoelectrochemical Performance of Dye Sensitized Solar Cells Based on

Aluminum-Doped Titanium Dioxide Structures, *Mater. Sci. Semicond. Process.*, 2015, **30**, 208–217.

205 R. Li, Y. Zhao, R. Hou, X. Ren, S. Yuan, Y. Lou, Z. Wang, D. Li and L. Shi, Enhancement of Power Conversion Efficiency of Dye Sensitized Solar Cells by Modifying Mesoporous TiO_2 Photoanode with Al-Doped TiO_2 Layer, *J. Photochem. Photobiol., A*, 2016, **319–320**, 62–69.

206 J. Chae, D. Y. Kim, S. Kim and M. Kang, Photovoltaic Efficiency on Dye-Sensitized Solar Cells (DSSC) Assembled Using Ga-Incorporated TiO_2 Materials, *J. Ind. Eng. Chem.*, 2010, **16**(6), 906–911.

207 X. Sun, Q. Zhang, Y. Liu, N. Huang, P. Sun, T. Peng, T. Peng and X. Z. Zhao, Photovoltaic Performance Improvement of Dye-Sensitized Solar Cells through Introducing In-Doped TiO_2 Film at Conducting Glass and Mesoporous TiO_2 Interface as an Efficient Compact Layer, *Electrochim. Acta*, 2014, **129**, 276–282.

208 Y. Duan, N. Fu, Q. Liu, Y. Fang, X. Zhou, J. Zhang and Y. Lin, Sn-Doped TiO_2 Photoanode for Dye-Sensitized Solar Cells, *J. Phys. Chem. C*, 2012, 8–13.

209 J. Chae, D. Y. Kim, S. Kim and M. Kang, Photovoltaic Efficiency on Dye-Sensitized Solar Cells (DSSC) Assembled Using Ga-Incorporated TiO_2 Materials., *J. Ind. Eng. Chem.*, 2010, **16**(6), 906–911.

210 Y. Duan, N. Fu, Q. Zhang, Y. Fang, X. Zhou and Y. Lin, Influence of Sn Source on the Performance of Dye-Sensitized Solar Cells (Based on Sn-Doped TiO_2 Photoanodes: A Strategy for Choosing an Appropriate Doping Source), *Electrochim. Acta*, 2013, **107**, 473–480.

211 S. P. Berglund, S. Hoang, R. L. Minter, R. R. Fullon and C. B. Mullins, Investigation of 35 Elements as Single Metal Oxides, Mixed Metal Oxides, or Dopants for Titanium Dioxide for Dye-Sensitized Solar Cells, *J. Phys. Chem. C*, 2013, **117**(48), 25248–25258.

212 Q. Hou, Y. Zheng, J. F. Chen, W. Zhou, J. Deng and X. Tao, Visible-Light-Response Iodine-Doped Titanium Dioxide Nanocrystals for Dye-Sensitized Solar Cells, *J. Mater. Chem.*, 2011, **21**(11), 3877–3883.

213 Z. He, L. Zhan, F. Hong, S. Song, Z. Lin, J. Chen and M. Jin, A Visible Light-Responsive Iodine-Doped Titanium Dioxide Nanosphere, *J. Environ. Sci.*, 2011, **23**(1), 166–170.

214 G. Liu, C. Sun, X. Yan, L. Cheng, Z. Chen, X. Wang, L. Wang, S. C. Smith, G. Q. Lu and H. M. Cheng, Iodine Doped Anatase TiO_2 Photocatalyst with Ultra-Long Visible Light Response: Correlation between Geometric/Electronic Structures and Mechanisms, *J. Mater. Chem.*, 2009, **19**(18), 2822–2829.

215 J. Song, H. B. Yang, X. Wang, S. Y. Khoo, C. C. Wong, X. W. Liu and C. M. Li, Improved Utilization of Photo-generated Charge Using Fluorine-Doped TiO_2 Hollow Spheres Scattering Layer in Dye-Sensitized Solar Cells, *ACS Appl. Mater. Interfaces*, 2012, **4**(7), 3712–3717.

216 S. In, K. Bae, H. Ahn and T. Seong, Improved Efficiency of Dye-Sensitized Solar Cells through Fluorine-Doped TiO_2 Blocking Layer, *Ceram. Int.*, 2013, **39**(7), 8097–8101.

217 K. Subalakshmi and J. Senthilselvan, Effect of Fluorine-Doped TiO_2 Photoanode on Electron Transport, Recombination

Dynamics and Improved DSSC Efficiency, *Sol. Energy*, 2018, **171**, 914–928.

218 S. I. Noh, K. N. Bae, H. J. Ahn and T. Y. Seong, Improved Efficiency of Dye-Sensitized Solar Cells through Fluorine-Doped TiO_2 Blocking Layer, *Ceram. Int.*, 2013, **39**(7), 8097–8101.

219 V. Madurai Ramakrishnan, M. Natarajan, S. Pitchaiya, A. Santhanam, D. Velauthapillai and A. Pugazhendhi, Microwave Assisted Solvothermal Synthesis of Quasi Cubic F Doped TiO_2 Nanostructures and Its Performance as Dye Sensitized Solar Cell Photoanode, *Int. J. Energy Res.*, 2021, **45**(12), 17259–17268.

220 P. Xiang, F. Lv, T. Xiao, L. Jiang, X. Tan and T. Shu, Improved Performance of Quasi-Solid-State Dye-Sensitized Solar Cells Based on Iodine-Doped TiO_2 Spheres Photoanodes, *J. Alloys Compd.*, 2018, **741**, 1142–1147.

221 C. Y. Neo and J. Ouyang, LiF-Doped Mesoporous TiO_2 as the Photoanode of Highly Efficient Dye-Sensitized Solar Cells, *J. Power Sources*, 2013, **241**, 647–653.

222 P. Xiang, F. Lv, T. Xiao, L. Jiang, X. Tan and T. Shu, Improved Performance of Quasi-Solid-State Dye-Sensitized Solar Cells Based on Iodine-Doped TiO_2 Spheres Photo-anodes, *J. Alloys Compd.*, 2018, **741**, 1142–1147.

223 M. S. Mahmoud, M. S. Akhtar, I. M. A. Mohamed, R. Hamdan, Y. A. Dakka and N. A. M. Barakat, Demonstrated Photons to Electron Activity of S-Doped TiO_2 Nanofibers as Photoanode in the DSSC, *Mater. Lett.*, 2018, **225**, 77–81.

224 T. Shu, P. Xiang, Z. M. Zhou, H. Wang, G. H. Liu, H. W. Han and Y. D. Zhao, Mesoscopic Nitrogen-Doped TiO_2 Spheres for Quantum Dot-Sensitized Solar Cells, *Electrochim. Acta*, 2012, **68**, 166–171.

225 M. Motlak, M. S. Akhtar, N. A. M. Barakat, A. M. Hamza, O. B. Yang and H. Y. Kim, High-Efficiency Electrode Based on Nitrogen-Doped TiO_2 Nanofibers for Dye-Sensitized Solar Cells, *Electrochim. Acta*, 2014, **115**, 493–498.

226 H. Wang, H. Li, J. Wang, J. Wu, D. Li, M. Liu and P. Su, Nitrogen-Doped TiO_2 Nanoparticles Better TiO_2 Nanotube Array Photo-Anodes for Dye Sensitized Solar Cells, *Electrochim. Acta*, 2014, **137**, 744–750.

227 Z. S. Seddigi, S. A. Ahmed, S. Sardar and S. K. Pal, Carbonate Doping in TiO_2 Microsphere: The Key Parameter Influencing Others for Efficient Dye Sensitized Solar Cell, *Sci. Rep.*, 2016, **6**, 1–9.

228 M. Zhu, Y. Dong, J. Xu, B. Zhang and Y. Feng, Enhanced Photovoltaic Performance of Dye-Sensitized Solar Cells (DSSCs) Using Graphdiyne-Doped TiO_2 Photoanode, *J. Mater. Sci.*, 2018, **54**(6), 4893–4904.

229 S. Shogh, R. Mohammadpour, A. Iraji zad and N. Taghavinia, A New Strategy on Utilizing Nitrogen Doped TiO_2 in Nanostructured Solar Cells: Embedded Multifunctional N-TiO_2 Scattering Particles in Mesoporous Photoanode, *Mater. Res. Bull.*, 2015, **72**, 64–69.

230 S. H. Kang, H. S. Kim, J. Y. Kim and Y. E. Sung, Enhanced Photocurrent of Nitrogen-Doped TiO_2 Film for Dye-Sensitized Solar Cells, *Mater. Chem. Phys.*, 2010, **124**(1), 422–426.

231 M. A. K. L. Dissanayake, J. M. K. W. Kumari, G. K. R. Senadeera, C. A. Thotawatthage, B. E. Mellander and

I. Albinsson, A Novel Multilayered Photoelectrode with Nitrogen Doped TiO_2 for Efficiency Enhancement in Dye Sensitized Solar Cells, *J. Photochem. Photobiol., A*, 2017, **349**, 63–72.

232 Y. Gao, Y. Feng, B. Zhang, F. Zhang, X. Peng, L. Liu and S. Meng, Double-N Doping: A New Discovery about N-Doped TiO_2 Applied in Dye-Sensitized Solar Cells, *RSC Adv.*, 2014, **4**(33), 16992–16998.

233 T. Lindgren, J. M. Mwabora, E. Avandaño, J. Jonsson, A. Hoel, C. G. Granqvist and S. E. Lindquist, Photoelectrochemical and Optical Properties of Nitrogen Doped Titanium Dioxide Films Prepared by Reactive DC Magnetron Sputtering, *J. Phys. Chem. B*, 2003, **107**(24), 5709–5716.

234 X. Wang, Y. Yang, Z. Jiang and R. Fan, Preparation of TiN_xO_{2-x} Photoelectrodes with NH_3 under Controllable Middle Pressures for Dye-Sensitized Solar Cells, *Eur. J. Inorg. Chem.*, 2009, 3481–3487.

235 F. Guo, H. Hu, Q. D. Tai, B. L. Chen, B. Sebo, C. H. Bu, J. H. Xu and X. Z. Zhao, Facile Preparation of Nanofibrous Polyaniline Thin Film as Counter Electrodes for Dye Sensitized Solar Cells, *J. Renewable Sustainable Energy*, 2012, **4**(2), 023109, DOI: 10.1063/1.3699618.

236 W. Liu, Z. Feng and W. Cao, Preparation of Large-Area Dye-Sensitized Solar Cells Based on Hydrothermally Synthesized Nitrogen-Doped TiO_2 Powders, *Res. Chem. Intermed.*, 2013, **39**(4), 1623–1631.

237 D. A. Duarte, M. Massi and A. S. Da Silva Sobrinho, Development of Dye-Sensitized Solar Cells with Sputtered N-Doped TiO_2 Thin Films: From Modeling the Growth Mechanism of the Films to Fabrication of the Solar Cells, *Int. J. Photoenergy*, 2014, 2014.

238 S. P. Lim, A. Pandikumar, N. M. Huang, H. N. Lim, G. Gu and T. L. Ma, Promotional Effect of Silver Nanoparticles on the Performance of N-Doped TiO_2 Photoanode-Based Dye-Sensitized Solar Cells, *RSC Adv.*, 2014, **4**(89), 48236–48244.

239 W. Mekprasart, S. Suphankij, T. Tangcharoen, A. Simpraditpan and W. Pecharapa, Modification of Dye-Sensitized Solar Cell Working Electrode Using TiO_2 Nanoparticle/N-Doped TiO_2 Nanofiber Composites., *Phys. Status Solidi A*, 2014, **211**(8), 1745–1751.

240 A. Bjelajac, R. Petrović, M. Popović, Z. Rakočević, G. Socol, I. N. Mihailescu and D. Janaćković, Doping of TiO_2 Nanotubes with Nitrogen by Annealing in Ammonia for Visible Light Activation: Influence of Pre- and Post-Annealing in Air, *Thin Solid Films*, 2019, **692**, 137598.

241 W. Guo, Y. Shen, G. Boschloo, A. Hagfeldt and T. Ma, Influence of Nitrogen Dopants on N-Doped TiO_2 Electrodes and Their Applications in Dye-Sensitized Solar Cells, *Electrochim. Acta*, 2011, **56**(12), 4611–4617.

242 L. Qi, C. Li and Y. Chen, Dye-Sensitized Solar Cells Based on Nitrogen-Doped TiO_2-B Nanowire/TiO_2 Nanoparticle Composite Photoelectrode, *Chem. Phys. Lett.*, 2012, **539–540**, 128–132.

243 C. K. Lim, H. Huang, C. L. Chow, P. Y. Tan, X. Chen, M. S. Tse and O. K. Tan, Enhanced Charge Transport Properties of Dye-Sensitized Solar Cells Using TiN_xO_y Nanostructure Composite Photoanode, *J. Phys. Chem. C*, 2012, **116**(37), 16659–19664.

244 J. Zhang, Z. Fu, Q. Lv, X. Yang and W. Cao, Technology of Preparing Anode Films and the Effect of Co-Sensitization in Dye-Sensitized Solar Cells, *J. Sol-Gel Sci. Technol.*, 2012, **63**(3), 554–562.

245 T. Sano, N. Mera, Y. Kanai, C. Nishimoto, S. Tsutsui, T. Hirakawa and N. Negishi, Origin of Visible-Light Activity of N-Doped TiO_2 Photocatalyst: Behaviors of N and S Atoms in a Wet N-Doping Process., *Appl. Catal., B*, 2012, **128**, 77–83.

246 T. Ohno, M. Akiyoshi, T. Umebayashi, K. Asai, T. Mitsui and M. Matsumura, Preparation of S-Doped TiO_2 Photocatalysts and Their Photocatalytic Activities under Visible Light, *Appl. Catal., A*, 2004, **265**(1), 115–121.

247 Z. Xing, Z. Li, X. Wu, G. Wang and W. Zhou, In-Situ S-Doped Porous Anatase TiO_2 Nanopillars for High-Efficient Visible-Light Photocatalytic Hydrogen Evolution, *Int. J. Hydrogen Energy*, 2016, **41**(3), 1535–1541.

248 B. A. D. Williamson, J. Buckeridge, N. P. Chadwick, S. Sathasivam, C. J. Carmalt, I. P. Parkin and D. O. Scanlon, Dispelling the Myth of Passivated Codoping in TiO_2, *Chem. Mater.*, 2019, **31**(7), 2577–2589.

249 B. S. Constantino, C. H. Gonzalez, N. L. Gomes, N. D. G. Silva, R. O. Domingues, R. A. S. Ferreira and Y. P. Yadava, Effect of TiO_2 Doping on the Sintering Behavior of Zr-Based Ceramic for Use as TBC, *J. Aust. Ceram. Soc.*, 2021, **57**(5), 1425–1434.

250 A. M. Bakhshayesh and N. Bakhshayesh, Enhanced Short Circuit Current Density of Dye-Sensitized Solar Cells Aided by Sr,V Co-Doped TiO_2 Particles, *Mater. Sci. Semicond. Process.*, 2016, **41**, 92–101.

251 Y. Li, L. Jia, C. Wu, S. Han, Y. Gong, B. Chi, J. Pu and L. Jian, Mesoporous (N, S)-Codoped TiO_2 Nanoparticles as Effective Photoanode for Dye-Sensitized Solar Cells, *J. Alloys Compd.*, 2012, **512**(1), 23–26.

252 S. P. Lim, A. Pandikumar, H. N. Lim, R. Ramaraj and N. M. Huang, Boosting Photovoltaic Performance of Dye-Sensitized Solar Cells Using Silver Nanoparticle-Decorated N,S-Co-Doped-TiO_2 Photoanode, *Sci. Rep.*, 2015, **5**, 1–14.

253 F. Lv, Y. Ma, P. Xiang, T. Shu, X. Tan, L. Qiu, L. Jiang, T. Xiao and X. Chen, N–I Co-Doped TiO_2 Compact Film as a Highly Effective n-Type Electron Blocking Layer for Solar Cells, *J. Alloys Compd.*, 2020, **837**, 155555.

254 S. Yang, H. Xue, H. Wang, H. Kou, J. Wang and G. Zhu, Improved Efficiency of Dye-Sensitized Solar Cells Applied with Nanostructured N–F Doped TiO_2 Electrode, *J. Phys. Chem. Solids*, 2012, **73**(7), 911–916.

255 Y. Duan, J. Zheng, M. Xu, X. Song, N. Fu, Y. Fang, X. Zhou, Y. Lin and F. Pan, Metal and F Dual-Doping to Synchronously Improve Electron Transport Rate and Lifetime for TiO_2 Photoanode to Enhance Dye-Sensitized Solar Cells Performances, *J. Mater. Chem. A*, 2015, **3**(10), 5692–5700.

256 A. Gupta, K. Sahu, M. Dhonde and V. V. S. Murty, Novel Synergistic Combination of Cu/S Co-Doped TiO_2 Nanoparticles Incorporated as Photoanode in Dye Sensitized Solar Cell., *Sol. Energy*, 2020, **203**, 296–303.

257 Y. F. Jiang, Y. Y. Chen, B. Zhang and Y. Q. Feng, N, La Co-Doped TiO$_2$ for Use in Low-Temperature-Based Dye-Sensitized Solar Cells, *J. Electrochem. Soc.*, 2016, **163**(10), F1133–F1138.

258 W. Wang, Y. Liu, J. Sun and L. Gao, Nitrogen and Yttrium Co-Doped Mesoporous Titania Photoanodes Applied in DSSCs, *J. Alloys Compd.*, 2016, **659**, 15–22.

259 L. Wang, L. Jia and Q. Li, A Novel Sulfur Source for Biosynthesis of (Ag, S)-Modified TiO$_2$ Photoanodes in DSSC, *Mater. Lett.*, 2014, **123**, 83–86.

260 Y. Duan, J. Zheng, M. Xu, X. Song, N. Fu, Y. Fang, X. Zhou, Y. Lin and F. Pan, Metal and F Dual-Doping to Synchronously Improve Electron Transport Rate and Lifetime for TiO$_2$ Photoanode to Enhance Dye-Sensitized Solar Cells Performances, *J. Mater. Chem. A*, 2015, **3**(10), 5692–5700.

261 J. Y. Park, K. H. Lee, B. S. Kim, C. S. Kim, S. E. Lee, K. Okuyama, H. D. Jang and T. O. Kim, Enhancement of Dye-Sensitized Solar Cells Using Zr/N-Doped TiO$_2$ Composites as Photoelectrodes, *RSC Adv.*, 2014, **4**(20), 9946–9952.

262 S. Munir, S. M. Shah, H. Hussain and R. Ali Khan, Effect of Carrier Concentration on the Optical Band Gap of TiO$_2$ Nanoparticles., *Mater. Des.*, 2016, **92**, 64–72.

263 C. T. Wang, H. S. Lin and W. P. Wang, Hydrothermal Synthesis of Fe[Sbnd] and Nb-Doped Titania Nanobelts and Their Tunable Electronic Structure toward Photovoltaic Application, *Mater. Sci. Semicond. Process.*, 2019, **99**, 85–91.

264 A. R. Tanyi, A. I. Rafieh, P. Ekaneyaka, A. L. Tan, D. J. Young, Z. Zheng, V. Chellappan, G. S. Subramanian and R. L. N. Chandrakanthi, Enhanced Efficiency of Dye-Sensitized Solar Cells Based on Mg and La Co-Doped TiO$_2$ Photoanodes, *Electrochim. Acta*, 2015, **178**, 240–248.

265 A. M. Bakhshayesh and N. Bakhshayesh, Enhanced Performance of Dye-Sensitized Solar Cells Aided by Sr,Cr Co-Doped TiO$_2$ Xerogel Films Made of Uniform Spheres, *J. Colloid Interface Sci.*, 2015, **460**, 18–28.

266 M. Mohammadnezhad, G. S. Selopal, O. Cavuslar, D. Barba, E. G. Durmusoglu, H. Y. Acar, Z. M. Wang, G. P. Lopinski, B. Stansfield and H. Zhao, *et al.*, Gold Nanoparticle Decorated Carbon Nanotube Nanocomposite for Dye-Sensitized Solar Cell Performance and Stability Enhancement, *Chem. Eng. J.*, 2021, **421**, 127756.

267 T. R. Naveen Kumar, S. Yuvaraj, P. Kavitha, V. Sudhakar, K. Krishnamoorthy and B. Neppolian, Aromatic Amine Passivated TiO$_2$ for Dye-Sensitized Solar Cells (DSSC) with ∼9.8% Efficiency, *Sol. Energy*, 2020, **201**, 965–971.

268 J. Men, Q. Gao, S. Sun, X. Zhang, L. Duan and W. Lü, Carbon Nitride Doped TiO$_2$ Photoelectrodes for Photocatalysts and Quantum Dot Sensitized Solar Cells, *Mater. Res. Bull.*, 2017, **85**, 209–215.

269 H. Lu, W. Tian, J. Guo and L. Li, Interface Engineering through Atomic Layer Deposition towards Highly Improved Performance of Dye-Sensitized Solar Cells, *Sci. Rep.*, 2015, **5**, 1–12.

270 V. Subramanian, E. Wolf and P. V. Kamat, Semiconductor-Metal Composite Nanostructures. To What Extent Do Metal Nanoparticles Improve the Photocatalytic Activity of TiO$_2$ Films?, *J. Phys. Chem. B*, 2001, **105**(46), 11439–11446.

271 A. Wood, M. Giersig and P. Mulvaney, Fermi Level Equilibration in Quantum Dot-Metal Nanojunctions, *J. Phys. Chem. B*, 2001, **105**(37), 8810–8815.

272 P. V. Kamat and B. Shanghavi, Interparticle Electron Transfer in Metal/Semiconductor Composites. Picosecond Dynamics of CdS-Capped Gold Nanoclusters, *J. Phys. Chem. B*, 1997, **101**(39), 7675–7679.

273 S. P. Lim, A. Pandikumar, H. N. Lim and N. M. Huang, Essential Role of N and Au on TiO$_2$ as Photoanode for Efficient Dye-Sensitized Solar Cells, *Sol. Energy*, 2016, **125**, 135–145.

274 F. Zheng and Z. Zhu, Preparation of the Au@TiO$_2$ Nanofibers by One-Step Electrospinning for the Composite Photoanode of Dye-Sensitized Solar Cells, *Mater. Chem. Phys.*, 2018, **208**, 35–40.

275 B. Xu, G. Wang and H. Fu, 23327Enhanced Photoelectric Conversion Efficiency of Dye-Sensitized Solar Cells by the Incorporation of Flower-like Bi$_2$S$_3$:Eu^{3+} Sub-Microspheres., *Sci. Rep.*, 2016, **6**, 1–9.

276 Z. Zolfaghari-Isavandi and Z. Shariatinia, Enhanced Efficiency of Quantum Dot Sensitized Solar Cells Using Cu$_2$O/TiO$_2$ Nanocomposite Photoanodes, *J. Alloys Compd.*, 2018, **737**, 99–112.

277 R. S. Ganesh, M. Navaneethan, S. Ponnusamy, C. Muthamizhchelvan, S. Kawasaki, Y. Shimura and Y. Hayakawa, Enhanced Photon Collection of High Surface Area Carbonate-Doped Mesoporous TiO$_2$ Nanospheres in Dye Sensitized Solar Cells, *Mater. Res. Bull.*, 2018, **101**, 353–362.

278 N. Mir and M. Salavati-Niasari, Effect of Tertiary Amines on the Synthesis and Photovoltaic Properties of TiO$_2$ Nanoparticles in Dye Sensitized Solar Cells, *Electrochim. Acta*, 2013, **102**, 274–281.

279 A. G. Dhodamani, K. V. More, S. M. Patil, A. R. Shelke, S. K. Shinde, D. Y. Kim and S. D. Delekar, Synergistics of Cr(III) Doping in TiO$_2$/MWCNTs Nanocomposites: Their Enhanced Physicochemical Properties in Relation to Photovoltaic Studies., *Sol. Energy*, 2020, **201**, 398–408.

280 R. D. Shannon, Revised Effective Ionic Radii and Systematic Studies of Interatomic Distances in Halides and Chalcogenides, *Acta Crystallogr., Sect. A: Cryst. Phys., Diffr., Theor. Gen. Crystallogr.*, 1976, **32**(5), 751–767.

281 K. H. Eom, T. K. Yun, J. Y. Hong, J. Y. Bae, S. Huh and Y. S. Won, Effect of Nitrogen Doping on the Performance of Dye-Sensitized Solar Cells Composed of Mesoporous TiO$_2$ Photoelectrodes, *J. Nanosci. Nanotechnol.*, 2014, **14**(12), 9362–9367.